NASA CR-175026

NASA

ANALYSIS AND TEST EVALUATION OF THE DYNAMIC RESPONSE AND STABILITY OF THREE ADVANCED TURBOPROP MODELS AT LOW FORWARD SPEED

By
Arthur F. Smith

HAMILTON STANDARD DIVISION
UNITED TECHNOLOGIES CORPORATION
WINDSOR LOCKS, CONNECTICUT 06096

December, 1985

National Aeronautics and Space Administration
Lewis Research Center
Cleveland, Ohio 44135

Contract NAS3-22755

1. Report No.	2. Government Accession No.	3. Recipient's Catalog No.
NASA CR- 175026		

4. Title and Subtitle	5. Report Date
Analysis and Test Evaluation of the Dynamic Response and Stability of Three Advanced Turboprop Models at Low Forward Speed	December, 1985
	6. Performing Organization Code

7. Author(s)	8. Performing Organization Report No.
Arthur F. Smith*	HSER 11055
	10. Work Unit No.

9. Performing Organization Name and Address	11. Contract or Grant No.
Hamilton Standard United Technologies Corp. Windsor Locks, CT. 06096	NAS3-22755
	13. Type of Report and Period Covered
12. Sponsoring Agency Name and Address	Contractor Report
National Aeronautics & Space Administration Washington, D.C. 20546	14. Sponsoring Agency Code

15. Supplementary Notes

Final Report, Project Technical Monitor, O. Mehmed, NASA Lewis Research Center, Cleveland, Ohio 44135

*Now with: Hirock Corporation, 1 Main Road, Granville, MA 01034

16. Abstract

Results of wind tunnel tests at low forward speed for blade dynamic response and stability of three 62.2 cm (24.5 in) diameter models of the Prop-Fan, advanced turboprop, are presented. Measurements of dynamic response were made with the rotors mounted on an isolated nacelle, with varying tilt for non-uniform inflow. Low speed stall flutter tests were conducted at Mach numbers from 0.0 to 0.35.

Measurements are compared with predictions made using beam analysis methods for the model with straight blades, and finite element analysis methods for the models with swept blades. Measured stall flutter stress boundaries are compared to Eigen-solution flutter boundaries.

Calculated 1P stress response agrees favorably with experiment. Predicted stall flutter boundaries correlate well with measured high stress regions.

Stall flutter is significantly reduced by increased blade sweep. Susceptibility to stall flutter decreases rapidly with forward speed.

17. Key Words (Suggested by Author(s))	18. Distribution Statement
Advanced Turboprop Prop-Fan Energy Efficient Structural Response Stall Flutter	[redacted] until December 31, 1987

19. Security Classif. (of this report)	20. Security Classif. (of this page)	21. No. of Pages	22. Price*
Unclassified	Unclassified	106	

* For sale by the National Technical Information Service, Springfield, Virginia 22161

NASA-C-168 (Rev. 10-75)

FOREWORD

This work was accomplished under contract NAS3-22755 for the NASA-Lewis Research Center in Cleveland, Ohio. Mr. Oral Mehmed was the technical monitor for the contract.

All of the testing reported herein was performed by NASA-Lewis personnel in the 10 x 10 wind tunnel at NASA-Lewis. The data were reduced, analyzed and reported by personnel from Hamilton Standard, a division of United Technologies Corporation.

The data reduction was performed by Mr. Donald J. Marshall. The analysis and reporting was performed by Mr. Arthur F. Smith. Mr. Bennett M. Brooks was the Hamilton Standard Project Manager.

TABLE OF CONTENTS

SUMMARY

Stall flutter and dynamic response tests were conducted in the 3 x 3 meter (10 x 10 ft) wind tunnel at the NASA-Lewis Research Center on three Prop-Fan models, in an isolated nacelle installation. These models are designated the SR-2, SR-3 and SR-5, with the blades characterized by increasing sweep, from the unswept (straight) SR-2 blade to the highly swept SR-5 blade. The tests were conducted over flight speed range of 0.0 to 0.35 Mach number, as well as a large range of blade angles and rotational speeds (RPM), including areas of deep stall. Limited testing was conducted for reverse thrust operation. Also, testing was performed with the rotor axis tilted relative to the tunnel airstream to provide angular inflow to the rotor, for many operating conditions. Blade vibratory stress measurements were recorded for all operating conditions. Extensive analysis of these data was performed.

Perhaps the most significant result of the stall flutter testing is that the blades with increased sweep had larger operating regions than the less swept blades and responded with less stress under stalled vibratory conditions. The unswept SR-2 model was the most susceptible to stall flutter, responding with the highest stresses. The moderately swept SR-3 and the highly swept SR-5 models remained stable at increasingly higher blade angles and RPM's than the SR-2, and also responded with lower stresses. It was observed that stressing was significantly reduced with the introduction of forward flight speed, for all of the blade models. As expected, all three models encountered high stressing at the highest blade angles and rotational speeds, which at some conditions was indicative of a forced excitation response due to vortex shedding, or buffeting. Also, high stressing was observed at some reverse thrust (negative or very low blade angle) conditions for the SR-3 and SR-5 models.

Stall flutter calculations were made using a recently developed flutter analysis method that can determine the stability of thin, highly swept blades, such as those used on Prop-Fans. The calculated onset of stall flutter is defined to be at operating conditions for which blade damping goes to zero. Negative damping indicates an unstable condition.

Flutter predictions for the three Prop-Fan models were made and compared to test data. Flutter boundaries were determined from the test data, based on the occurrence of steeply rising stresses with increasing blade angle or rotor RPM, since damping was not measured. The calculations show negative damping occurring at generally the same operating conditions for which high stresses were encountered during test. Very good agreement was seen for the SR-2 and SR-3 models, with less agreement for the SR-5 model which gave only weak flutter indications during test. However, the experimental trend which showed stability to increase with blade sweep was well predicted. The theory predicted that stall flutter will occur primarily in the torsional mode for all three models. This agreed with the SR-2 test data, but not with SR-3 and SR-5 measurements.

Measured blade stress trends for angular inflow operating conditions followed well established trends associated with conventional turboprops. Blade stress increased linearly with rotor tilt angle and consisted almost entirely of 1P response. Stress sensitivity (stress divided by excitation factor) increased with increasing blade angle and RPM, and decreased with increasing Mach number.

Correlation between tested and predicted Campbell diagram modal frequencies was excellent for the important lower modes, for all blade models. This indicates the validity of the structural prediction models.

Increased blade sweep significantly reduced both angular inflow (1P) and critical speed stress responses.

Analytical predictions of 1P blade stress correlate well with measured test data.

SYMBOLS AND ABBREVIATIONS

C_p	Power coefficient = $2\pi Q/\rho n^2 D^5$
D	Prop-Fan Diameter, m
EF	Excitation Factor = $\psi(V_T/644.8)^2\ (\rho/\rho_o)$
F	Centrifugal Force - Newtons
ΔF	Incremental Force - Newtons
K	Stiffness, kg/m
m	Mass per unit length, kg/m
N	Rotational speed, RPM
N_c	Normalized blade chord
n	Rotational speed, revolutions/second
P_N	Normalized load
r	Blade radial station, m
Q	Prop-Fan Torque, Newton - m
SHP	Shaft horsepower
R	Prop-Fan Radius = D/2, m
V_{eq}	Equivalent air speed = $V_T\sqrt{\rho/\rho_o}$, knots
V_T	True airspeed, knots
$\beta_{.75}$	Blade angle at 3/4 radius, degrees
β_{REF}	Reference blade angle, degrees
ρ	Air density (kg/m^3) = 1.2250
ρ_o	Sea level ambient air density (kg/m^3)
σ	Stress, kPa
ψ	Prop-Fan shaft tilt, degrees

SYMBOLS AND ABBREVIATIONS (Continued)

ω	Frequency, Hz
ω_n	Natural frequency, Hz
1P	Frequency = one per propeller revolution, Hz
nP	Frequency = n per propeller revolution, Hz

SI units of measurement used throughout unless specified otherwise.

1.0 INTRODUCTION

The occurrence of fuel shortages, increased fuel cost and the threat of future worsening conditions for air transportation has caused NASA to sponsor studies of new, more efficient, aircraft and propulsion systems. One of the promising concepts established by these studies is the advanced high speed turboprop, or Prop-Fan. This propulsion system differs from existing turboprops. The Prop-Fan has greater solidity than a turboprop, achieved by more blades of larger chord. The turboprop has straight blades with relatively thick airfoil sections; the Prop-Fan has swept back blades with thin airfoil sections to enhance performance and reduce noise. The turboprop cruises at no more than 0.65 Mach number; the Prop-Fan is designed to cruise at 0.7 to 0.8 Mach number. The diameter of the Prop-Fan is about 40 to 50% smaller than that of the turboprop. For maximum performance the Prop-Fan makes use of advanced core engines of the kind being used in modern turbofan engines. Performance is also enhanced by use of a spinner and nacelle aerodynamically contoured to reduce compressibility losses by retarding the high velocity flow through the root sections of the Prop-Fan blades.

Utilizing predicted and measured aerodynamic performance data, weight estimates, and noise projections, several Government sponsored studies by both engine and airframe manufacturers have concluded that a fuel savings of approximately 20 to 40% depending on operating Mach number should be achieved by a Prop-Fan aircraft, as compared with a high bypass ratio turbofan aircraft. With these encouraging results, a research technology effort has been instituted to establish the design criteria for this new propulsion system.

A major objective in the development of Prop-Fan configurations is to insure the structural integrity of the rotor. Since the Prop-Fan is such a significant departure from conventional propellers, with its highly swept, thin blades, the structural demands are substantial. The high speed operation of highly swept blades imparts large forces to the limited material inherent to the thin airfoil sections needed for efficient performance. It is imperative that the rotor be able to absorb the aerodynamic loads at all operating conditions, as well as the centrifugal loads associated with its unique shape and construction. The steady-state dynamic response of the blades must be low and flutter instabilities must be avoided, for safe operation.

As part of the continuing studies of Prop-Fan structural stability and blade dynamic response, static and low speed stall flutter tests, and angular inflow tests were conducted on the SR-2 8-bladed, SR-3 8-bladed, and SR-5 10-bladed model Prop-Fan configurations. These tests were conducted during December 1981 and February 1982 at the NASA - Lewis Research Center. Hamilton Standard, under contract, analyzed the data acquired during these tests.

This report summarizes the results of this stability and dynamic response investigation. Included are trends of the measured blade stress test data with operating conditions for the three models. Total vibratory stress, modal vibratory stress and blade stress frequency spectra were analyzed. In addition, stall flutter stability boundaries and 1P dynamic responses were calculated for comparison to test results. The comparisons were used to evaluate the accuracy of the prediction methods and to recommend improvements to increase their effectiveness as Prop-Fan design tools.

2.0 DESCRIPTION OF EXPERIMENTAL PROGRAM

The tests described in this report were conducted on three Prop-Fan model configurations, mounted on an isolated nacelle, in the NASA-Lewis Research Center 3 x 3 m (10 x 10 ft) wind tunnel. Two types of tests were combined in this study. One test was performed to determine the stall flutter characteristics of the turboprops at static conditions and at low speeds (up to 0.35 Mach number). The second test was performed to determine the effects on dynamic response of rotor tilt relative to the airstream at low speeds (up to 0.35 Mach number).

2.1 Test Models

Each of the three Prop-Fan models is nominally 62.2 cm (24.5 in) in diameter. The Prop-Fan concept incorporates thin airfoils and swept blades to achieve high aerodynamic efficiency with low noise generation. Table 2-I is a summary of some of the Prop-Fan overall design parameters. The model blades are designated SR-2, SR-3 and SR-5, which have respectively increasing tip sweep, as seen in Figure 2-1. The blades and hub for each of the three models were designed and built by Hamilton Standard.

Figure 2-2 shows some of the characteristics used to describe the model blades. Shown are the geometric twist angle, section thickness ratio, chord to diameter ratio, aerodynamic sweep and geometric sweep. The aerodynamic sweep is measured using the local air velocity vector, to account for the flow around the spinner and rotational speed. The geometric sweep is the angle between the tangent to the blade midchord locus and the stacking (pitch-change) axis. The aerodynamic sweep is considered the more important parameter because it describes the movement of each blade section relative to the air.

2.2 Wind Tunnel Facility

The three model Prop-Fans were installed in the NASA-Lewis 3 x 3 m (10 x 10 foot) Supersonic Wind Tunnel. This tunnel is described in Reference 1, and is designed for supersonic testing at Mach numbers from 2.0 to 3.5, but can also be operated for subsonic testing. In the present tests, the Mach range was from 0.0 to 0.35. Conditions in the test section are close to standard sea level conditions. The test section is 12.19 m (40 ft) long and has a cross section of 3.05 x 3.05 m (10 x 10 ft). The test section has two flexible side walls used as a nozzle for adjusting the flow in the supersonic mode. This nozzle was set at the full open position for the subsonic tests, and a set of flow control doors on the downstream end of the test section were used to regulate the tunnel Mach number.

2.3 Propeller Test Rig

Figure 2-3 shows the SR-3 model Prop-Fan blade installed in the wind tunnel test section at NASA-Lewis. The Propeller Test Rig (PTR) is strut-mounted from the ceiling in the tunnel test section with the angle-of-attack (shaft tilt) remotely variable between -2° to +15°. A cutaway view of the PTR is presented in Figure 2-4. The model is driven by a three-stage air turbine utilizing high pressure air at 3.1 x 10^6 newton/m^2 (450 psi) and heated to 366°K (660°R). The turbine is capable of delivering nearly 634 kw (850 hp) to the Prop-Fan model.

A rotating balance which is part of the PTR can be used to measure rotor torque and thrust. Rotor torque only was measured during this test.

2.4 Model Instrumentation

Foil strain gages mounted on the cambered (suction) surfaces of selected blades for each Prop-Fan configuration were used to measure dynamic stresses due to blade vibration.

The blade strain gages were located at points of maximum modal and 1P stresses, based on calculations. These calculations were made at the blade natural vibratory response frequencies, using a beam analysis for the SR-2 model and finite element methods for the SR-3 and SR-5 models. Figure 2-1 shows the relative locations of a full set of strain gages for each model blade. Single element gages were used to measure bending stresses and dual element gages were used to measure shear stresses due to torsion. A full set of gages was applied to opposite blades on each model, while other selected blades were instrumented with either a shear gage, or a shear and a bending gage. These gages were used to determine the relative phasing of strain gage signals between blades. Table 2-II describes the gage locations and functions in more detail. The gage designations correspond to the gage number as shown in Figure 2-1.

The number of strain gage signals that were measured was limited by the number of channels available on a rotary transformer device used to transmit electrical signals from the rotor to the fixed system. The strain gage signals, as well as a once-per-revolution (pipper) signal from the rotor, were recorded on FM magnetic tape for later processing.

2.5 Test Procedures

The tunnel was brought up to speed with the Prop-Fan unpowered. The windmilling rotational speed was dependent on the blade pitch angle setting, which was manually set before tunnel startup. The model rotational speed, at this fixed pitch blade angle and fixed tunnel Mach number, was incrementally increased by increasing the power to the rotor. This was done until an operating limit, such as a blade stress limit, rotational speed limit, rig power limit or vibration limit was reached. The maximum allowable rotational speed was 9000 RPM. This was repeated for different shaft tilt angles. The whole process was repeated for different Mach numbers.

The tunnel had to be shut down in order to change the blade pitch angle (ground adjustable). An inclinometer was used to set the blade pitch angle (reference blade angle) at the reference location prior to tunnel start up. The reference location was 0.78 R for the SR-2 and SR-3 and 0.73 R for the SR-5. A blade/hub collective pitch arrangement allowed a single blade to be used for this procedure.

2.6 Test Conditions

The conditions for these wind tunnel tests were primarily sea level conditions, i.e. (sea level density and temperature). The parameters that were variable for the test were Mach number, Prop-Fan shaft tilt angle, blade angle and rotor RPM. All of these parameters were remotely controllable from the control room except blade angle. A schedule of the blade angles tested can be found in Table 2-III. The RPM range tested was between 2000 and 9000 RPM in 500 RPM increments, and the Mach numbers used are also included in the table. Figures 2-5 through 2-7 show the test envelopes for the SR-2, SR-3 and SR-5 Prop-Fan models. These envelopes show the boundaries of the actual test and include the limits encountered, defined by high stresses, windmilling RPM, maximum RPM and the maximum power available. Also shown are the boundaries of the test envelope for the 15 degree tilt conditions. One set of boundaries is shown for each Mach number.

2.7 Data Reduction

The magnetic tapes which were recorded at NASA-LeRC were processed at Hamilton Standard. The analog tapes were analyzed by obtaining total vibratory stress using peak stress converters and recording the signals on strip charts. As a second step, the output from the magnetic tape was processed using an electronic real time analyzer to produce narrow band spectral analyses. This information was then stored on tape for a permanent record of each case run. The data were then transmitted to a high speed digital computer for processing. At this point, a computer program was used to determine the amplitude of spectral peaks and the associated frequencies. These were then tabulated and printed according to case number and condition. Automatic plot routines were developed that produce Campbell diagrams and curves of vibratory stress vs. RPM for each blade angle. These items are discussed further in the section on test data evaluation.

3.0 ANALYTICAL TECHNIQUES

3.1 Approach

The 1P response theoretical prediction analysis and the stability theoretical prediction analysis used for this project embody different approaches. Both methods, however, require the use of airload computations in order to determine the blade excitations and force derivatives. The stability analysis also requires modal calculations for the mode shapes and frequencies used in the eigen solutions. Figure 3-1 is a flow chart that shows the progression of methods that are used for the computation of stability and 1P response.

The blade definition and operating conditions are used as input for the airloads analyses and the frequency and modes programs, and are also used to set up the grids for the finite element analyses. Two airloads analyses were used, one designated as HS/H045 which uses Goldstein type calculations for the induced flow (see Ref. 2), and the other which uses a skewed prescribed wake method (see Ref. 3) for the induced part of the flow, known as HS/H337. Table 3-I lists the methods and the computer designation of the various analyses discussed in this report.

The next step in the process is to define the blade geometry and its position in space. This includes defining the grid for the finite element methods. These definitions are then used to determine the modal characteristics for the stability analyses.

The blade modal characteristics for the SR-2 blade were determined using the Hamilton Standard beam analysis programs HS/H025 (bending modes) and HS/H027 (torsional modes). The width, sweep, and offset characteristics of the SR-3 and SR-5 blades are such that a simple beam analysis was not adequate to represent the complex behavior observed for these blades. Finite element analyses were required to model the high degree of coupling between flatwise bending, edgewise bending, and torsion modes. The general purpose finite element code MSC/NASTRAN, was used to calculate the modal characteristics for the SR-3 and SR-5 blades.

Blade modal properties were used in the HS/F203 stability analyses. Here, the modal displacement from the frequency and mode calculations are converted to beam type displacements, where each mode is described by two translations and a rotation at each blade section being used. Transformations are made putting the system into the blade chord coordinate system. This is done in order to use linearized aerodynamics and small angle assumptions. The analysis is an energy balance method that provides blade frequency and damping information. The operating condition for which the calculated damping goes through zero is considered the point of flutter onset. Analytical flutter boundaries for the Prop-Fan blades were established by compiling the operating conditions indicating zero damping.

The SR-2 1P dynamic response analysis was performed using the beam analysis code, HS/H026 developed at Hamilton. The SR-3 and SR-5 1P dynamic response analyses were done with the MSC/NASTRAN code using the models developed for the frequency analyses. The blade excitation loads were obtained from the aerodynamic program and used as input to the response analysis, from which blade stresses and bending moments were obtained. Plots of stress per excitation factor were made. Excitation factor is defined as:

$$E.F. = \psi \, (V_{eq}/348)^2$$

where ψ is the inflow angle in degrees and Veq is the equivalent velocity in knots.

3.2 Aerodynamic Loads

A preliminary requirement for the load determination of a Prop-Fan is the knowledge of the flow velocity variations around the disk. Hamilton Standard employs a computer analysis, designated HS/H039, that calculates the flowfield around an aircraft including the fuselage, nacelle and wings. For the present study however, only the features of the nacelle were incorporated to represent the wind tunnel configuration. The analysis uses a three-dimensional potential flow representation of the nacelle. Since the nacelle is at a tilt angle along with the propeller, the cross flow around the nacelle is accounted for, as well as the spreading of the flow around the spinner.

The flowfield, having been determined from the procedure discussed above, is used as input for either one of two Hamilton Standard strip analysis codes, designated HS/H045 and HS/337. These codes determine the time variation of the loads and perform Fourier analyses to get the harmonic components. They both perform a quasi-static lifting line airfoil analysis, using 2D airfoil section data for lift and drag, at a number of azimuthal and radial locations, and are often referred to as multiazimuth strip analyses. A Goldstein type wake analysis is used in HS/H045, and a skewed wake analysis is used in HS/H337 to determine induced effects, via an iterative approach. Refinements have been added to the codes to handle transonic aerodynamics, sweep, compressibility effects, and stall. These codes produce the harmonics of the in-plane and out-of-plane aerodynamic loads at a number of radial locations. These become the input for the beam or finite element structural dynamic analyses.

3.3 Critical Speed Analysis (Beam Models)

The Hamilton Standard beam analysis program HS/H025 gives the natural frequencies, mode shapes, and modal masses for the bending modes of a straight blade acting under the influence of a centrifugal field. Another program, HS/H027, gives the same information for the torsional modes. These decks are limited to the analysis of long, slender, i.e. beam-like, isotropic blades. The accuracy of the codes have been verified over a number of years with correlation of predicted and measured frequencies for many propeller blades. Critical speeds are determined from a Campbell diagram using the HS/H025 and HS/H027 calculated frequencies.

3.4 Critical Speed Analysis (Finite Element Models)

Due to the sweep, offset, and large chords of the SR-3 and SR-5 blades, the beam analyses are not adequate to obtain reasonable approximations of the natural frequencies and the highly coupled mode shapes. Any number of finite element codes could be used to model the blades. For purposes of this contract, the natural frequencies were calculated using the MSC/NASTRAN code (see Ref. 4).

Finite element grids were set up to analyze the bending and centrifugal stresses of the solid blades. The non-linear capabilities of MSC/NASTRAN were used to update the steady load position to the final displaced blade position. The vibratory mode shapes and vibratory modal information are determined about this displaced position. Figure 3-2 shows in schematic form the grid set-up used for the Prop-Fan models. Triangular elements were used in general. However, quadrilateral elements were used on the outer portion of the SR-5, in an attempt to eliminate the bias of the triangular elements in the highly swept tip region.

3.5 1P Analysis (Isolated Nacelle/Beam Blade Model)

A computer code was developed at Hamilton Standard (HS/H026) for the analysis of beam-like blades, (e.g. SR-2) where only 1P response is anticipated. Aerodynamic 1P loads, such as those calculated by the HS/H045 code, and the blade structural properties are used as inputs to the code, which performs an iterative solution for the blade vibratory displacements and stresses. A direct approach to the solution of the equations of motion is used, where the effects of the centrifugal field are taken into account. The effects of differential stiffness and modifications in loading, due to the displacement, are taken into account by iterative techniques.

3.6 1P Analysis (Isolated Nacelle/Finite Element Blade Model)

As in the determination of critical speeds for the SR-3 and SR-5 blades, it was found that a finite element analysis is required to represent the 1P response of these wide, swept blades. There is too much coupling between flatwise, edgewise, and torsional modes to allow the use of a beam representation. For these 1P analyses the MSC/NASTRAN code was used. Finite element models were generated by using quadrilateral (CQUAD4) elements. Figure 3-3 shows a flow chart which outlines the procedure used in the calculation of 1P vibratory stresses. Note that the inclusion of higher order vibrations could easily be incorporated into this procedure.

Aero Loads - Based on previous analyses, it was possible to estimate the steady untwist of the blade at speed. From this estimate of untwist and the initial shape of the blade, a static (zero RPM) position of the blade can be determined, so that the blade angle at speed (initial plus untwist) closely matches the blade angle ($\beta_{.75}$) predicted from the HS/H045 aerodynamic analysis, for the particular operating condition under consideration.

The calculated aerodynamic loads, centers of pressure, and $\beta_{.75}$ are used by the preprocessor code (HS/F194) to distribute the harmonic loads on the finite element grids. The centers of pressure versus span are assumed to be independent of azimuth. They are calculated from the airload analysis with steady state, zero in-flow angle. The aero loads are expressed in terms of in-plane and out-of-plane components. The HS/F194 code converts these to components parallel and normal to any given blade section. The assumption is made that the load parallel to the blade chord (drag) is uniform across the blade. The normal loads (lift) are distributed using an analytical expression:

$$P_N = A(N_c)^B(1-(N_c)^{0.25})^2$$

where N_c is the normalized chordwise position and A and B are chosen to match the total load and center of pressure desired. Figure 3-4, shows typical samples of this distribution function.

Steady State Position - Before the 1P dynamic response analysis could be performed, it was necessary to do an analysis to determine the steady state position and stiffness of the blade. Because of the non-linear effects of prestress (centrifugal stiffening) and large displacements, it is desirable to perform a non-linear analysis of the blade under the influence of centrifugal loading. This portion of the analysis was done using rigid format 64, a geometric non-linear static analysis in MSC/NASTRAN. The solution technique employs a Newton-Raphson iterative scheme to converge on a displaced shape which satisfies the equations of equilibrium. This is a more rigorous approach than the previously used differential stiffness solution (rigid format 4 in COSMIC/NASTRAN). The iteration is done at full RPM. Rigid format 64 in MSC/NASTRAN does account for the centrifugal effects including an update of the load vector with displacement.

It was found during the course of the iterative procedure, that singularities often occurred in the structural stiffness matrix, associated with the lack of plate element stiffness about its own normal. This is a feature of the NASTRAN plate elements. Removal of the singularities can be accomplished by fixing or tying affected degrees of freedom to neighboring nodes (SPCS or MPCS in NASTRAN terminology). It was also found that there exists a procedure within NASTRAN whereby the user may add artificial stiffness to the diagonal of the assembled stiffness matrix. The solution still converges to the correct answer even with an erroneous stiffness matrix. This is a feature of the Newton-Raphson iterative scheme employed. A further feature is that the final solution is a function only of the elemental stiffness matrix and not the assembled global stiffness matrix. Both these fixes were employed during the analyses.

Upon completion of the iteration using rigid format 64 of MSC/NASTRAN, the incremental stiffness matrix is saved on magnetic tape. The incremental stiffness matrix is the stiffness matrix which is used to examine small (linear) perturbations about the steady state deflected position. It includes

the basic elemental structural stiffness and the differential stiffness representing the additional stiffness due to the fact that the blade is in a centrifugal field. However, the matrix output from NASTRAN does not recognize that the magnitudes of the load vectors on the model's mass points change as the points vibrate about the steady state position. This effect can be explained as follows.

Consider an element of mass under the influence of a centrifugal field. There is a radial force acting on this mass equal to $mr\omega^2$, where 'r' is the radius from the center of rotation. If the mass is allowed to deflect outward, then there will be an increase in the centrifugal force due to the increase in radius;

$$\Delta F = m\,\omega^2\,\Delta r.$$

Since the increment in force is in the same direction as the displacement (instead of a restoring force), it is equivalent to a negative stiffness, thus;

$$K_{radial} = -\Delta F/\Delta r = -m\omega^2.$$

It can also be shown that the same effect is present in the tangential direction, hence;

$$K_{tangential} = -\,m\omega^2.$$

The inclusion of these terms in the stiffness matrix is necessary to produce accurate results. Since the new terms are proportional to the mass matrix, just as the inertia terms are in a vibrations problem, it is clear that their importance depends upon the relationship between the frequency of vibration and the rotational speed. The lower the frequency of vibration, the more important these terms are. At high frequencies the inertia terms dominate and the negative in-plane stiffness terms are less important. This negative in-plane stiffness matrix is added to the incremental stiffness matrix generated by MSC/NASTRAN. It is actually added using a program modification (DMAP alter) in rigid format 64, before the stiffness matrix is written to magnetic tape.

Because the stiffness matrix generated from the steady state analysis is based on the shape of the blade after deformation, it was found necessary to save the steady displacements. These displacements are added to the original grid point position and these 'updated' grid cards are used for the dynamic analysis. They could also be used for an eigenvalue analysis. The updated grid cards are checked to verify that the steady state position is near the desired operating condition (i.e. correct $\beta_{.75}$).

Load Distribution - With the calculated dynamic aero loads and centers of pressure as input, the HS/F194 code is used to distribute the loads on the finite element model. This is done in the same manner as for the steady loads, except that the loads are written to different NASTRAN bulk data cards (DAREA instead of FORCE) because the loads are harmonic.

Using the updated grid cards, the aero loads, and the stiffness matrix saved on tape, the dynamic analysis is performed using rigid format 26 in MSC/NASTRAN, Direct Frequency Response. Alternately, the Modal Frequency Response analysis could be used (Rigid Format 30). Note that DMAP alters are required to read the stiffness matrix from tape and effectively replace the stiffness matrix, which would not otherwise have the differential or negative in-plane stiffness effects.

Upon completion of the NASTRAN dynamic analysis the elemental stresses are saved for postprocessing. A computer program has been written which reads the elemental stresses, interpolates for stress at any position and calculates strains for comparison to test. Apparent stress is calculated as the strain in a given direction times Young's modulus. It is to be noted that this postprocessor accounts for the strain gage thickness by increasing the bending, but not membrane strain, to correspond to a location at a distance from the neutral axis which is increased by the gage thickness.

3.7 Aeroelastic Stall Flutter Stability Analysis

The stability of the model Prop-Fan blades was investigated using the HS/F203 stability analysis. This analysis is discussed in detail in Reference 5. For modeling the structure, the mode shapes, frequencies and modal masses are obtained from the results of a finite element analysis run at a particular flow condition. The data are transformed from the finite element coordinate system to the HS/F203 coordinate system using the HS/F214 transformation analysis. The blade is divided into a series of discrete aerodynamic panels with constant properties. Each panel is defined with a plunging and pitching motion about a reference axis along the chord specified by the mode shape displacement definition.

The unsteady aerodynamics are derived from an analysis that was done by Steinman, described in Reference 6. The steady state aerodynamic forces are derived from the results of Hamilton Standard Goldstein performance analysis HS/H444. Only steady-state lift curve slopes are used, as obtained from HS/H444 for the particular operating condition, and are formulated using strip theory. The solution is determined using an eigen solution, or an energy method, where an energy balance is maintained between the energy supplied by the air forces and the strain energy within the structure. The output of this analysis is in the form of response frequency and blade damping. The onset of flutter is determined to be at the point where the damping goes from positive to negative, passing through zero.

3.8 Operating Conditions for Analysis

Some of the operating conditions and ranges of conditions for use with the analysis are shown in Table 3-II. Three specific cases were run for each of the models for the response calculations, and are numbered one through nine. Each case includes a complete run through the flowfield analysis, the multiazimuth analysis including the induced flow calculations and the response analyses, finite element or beam type. Some of the independent parameters

listed are RPM, Mach number, and shaft horsepower. The blade angle at the 75% radius is a dependent variable and has been made to account for the variation in elastic deflection due to the centrifugal and steady airloads. This angle is the result of iteration to a set horsepower, because later correlations become more meaningful when comparing horsepower. This angle was also the angle used for the finite element response calculation with the appropriate deflected shape.

Also included in this table are the operating conditions used for the stability calculations. Two blade angle settings and three RPM's were used for each of the two swept Prop-Fans, the SR-3 and SR-5, to get the frequencies and modes from the finite element method. A range of blade angles at 5 degree intervals was used for the SR-2 blade, since a beam analysis is used to determine the frequencies and mode shapes for straight blades, and it requires a small amount of computer time. The modal frequencies were interpolated between the two blade angles used for the finite element runs on the SR-3 and SR-5. The values of Mach number, blade angle, and rotational speed used in the stability analysis are given for all blades.

3.9 Analytical Results

The calculated natural frequencies resulting from structural analyses are a measure of how well the blade modal properties are represented. The natural frequencies for the SR-2 model Prop-Fan were calculated using HS/H025 and HS/H027. The results are shown in Figure 3-5. The critical speeds for the SR-3 and SR-5 model Prop-Fan are shown in Figures 3-6 and 3-7. The natural frequencies for the SR-3 and SR-5 model blades were computed using the MSC/NASTRAN code. Comparison to test results will be made in a later section.

The results of the 1P vibratory response calculations are shown in Table 3-III for the three model Prop-Fan blades, SR-2, SR-3 and SR-5. The 1P airloads were calculated by either the HS/H045 code or the HS/H337 code, which use a "Goldstein" type momentum analysis and a "Skewed Wake" analysis, respectively. The skewed wake analysis was used for the SR-2 and SR-5. In addition, the Goldstein wake analysis was used for all blades. The stress sensitivity was determined using the HS/H025 & HS/H027 beam analyses for the SR-2 model and the MSC/NASTRAN computer code for the SR-3 and SR-5 models.

Some of the conclusions that can be observed from the calculations shown in Table 3-III are; stress per E.F. decreases somewhat with Mach number, stress per E.F. increases with RPM, the important inboard bending stress per E.F. (gage No. 1) is highest for the SR-2 and lowest for the SR-3, and stress per E.F. increases with increasing blade angle. It is also seen that the skewed wake analysis, used for defining the flowfield induced effects, results in substantially higher stress than the Goldstein analysis.

The stability analysis HS/F203 was run using the modal information generated by the HS/H025, HS/H027 and MSC/NASTRAN codes, and the steady static section lift and moment curve slopes generated by the HS/H444 performance analysis

(see Figure 3-1). Figures 3-8 through 3-10 show the resulting eigen frequencies and damping ratios (damping to critical damping ratio). Sample frequencies and damping plots are shown for the SR-2, SR-3 and SR-5 models, respectively. The operating conditions used are for 9000 RPM and 0.35 Mach number. Since the air forces on the blade can act as a spring, the response frequencies can change with Mach number, blade angle and RPM. These curves show small variations in frequency with blade angle. The total damping is more significantly affected by the air. For all Prop-Fan modes these predicted curves show that the total damping goes negative in the calculated third mode, which is primarily torsional motion. This condition is unstable and the point at which the damping goes through zero can be used to define the onset of stall flutter.

Figure 3-11 consists of summary plots of blade angle vs. RPM showing the calculated stall flutter boundaries, i.e. the locus of points where the damping goes through zero for the SR-2, SR-3 and SR-5 Prop-Fan models at various Mach numbers. These curves show that the stall flutter boundaries occur at higher blade angles with increasing Mach number. At zero Mach number, the higher the sweep, the higher the blade angle at which stall flutter occurs. In general, increasing the blade sweep tends to diminish the amount of area contained within the stall flutter boundaries.

4.0 TEST DATA EVALUATION AND COMPARISON WITH CALCULATIONS

This test program was conducted to study blade stressing due to stall flutter, buffet and tilted flow loading. The stall flutter data were obtained at zero degrees shaft tilt while most of the P-order dynamic response data were obtained at 15° shaft tilt. The tested operating conditions are shown in Figures 2-5 through 2-7.

4.1 Stall Flutter and Buffet

Total vibratory stress values were read from strip charts for each steady state test condition for the six strain gage channels on each model. The stress was determined from the charts by reading the highest amplitude of the stress signals that occur two or more times during the data sample period. This stress is sometimes called the "infrequently repeating peak"*. This total peak stress consists of many frequency components occurring simultaneously on the blade.

Stress vs. RPM - The effect of rotational speed and blade angle on the total stress amplitude for zero forward speed conditions can be observed in Figures 4-1 through 4-3. Here, total vibratory stress for the inboard bending gage is plotted as a function of rotational speed for various reference blade angles. These are given for the SR-2, SR-3 and SR-5 models, respectively. It is seen that the total stress increases with rotational speed, at a rate that is dependent on the reference blade angle. Also, in Figures 4-2 and 4-3 for the SR-3 and SR-5 models, the total vibratory stress increases with reference blade angle up to a blade angle of about 50 degrees, and decreases at higher angles. Similar trends are observed for other gages but will be shown later in other types of plots.

The effect of Mach number on the total vibratory stress is shown in Figures 4-4 through 4-9, where the total vibratory stress is presented as a function of rotational speed for various Mach numbers with zero shaft tilt. Again, these curves were developed for the inboard bending gage for all the blade models. Figures 4-4 and 4-5 are for the SR-2 at blade angles of 31.8 and 35.8 degrees, respectively. The high stresses seem to occur predominantly at zero forward speed conditions, particularly for the higher blade angle. The stress levels at 0.1 Mach number and above remain at about the same magnitude for both blade angles.

Figures 4-6 and 4-7 show a similar stress picture for the SR-3. Here blade angles of 36 and 50 degrees are shown, respectively. Stresses for 0.1 Mach number and above are low. Also, at zero forward speed, stresses for the 50 degree blade angle are much higher than those for the 36 degree blade angle.

---

*The infrequently repeating peak is defined as the maximum stress peak that repeats itself two or three times during the stress data sample period. This value will generally be higher than that derived from any time averaged signal process, such as spectral analysis.

Figures 4-8 and 4-9 show stress vs. RPM for 50 and 60 degree blade angles for the SR-5 model blades. Here also, the stress at zero Mach number is much higher than it is at forward speed, and the data for the two blade angles show similar trends.

SR-2 Contour Plots - The above discussion concerns total (peak) vibratory stresses measured by the inboard gages for each of the three model Prop-Fan blades. A more complete study of the total stresses can be made using contour plots of constant vibratory stress as a function of both blade angle and RPM.

Figures 4-10 and 4-11 are iso-stress contour plots for the SR-2 model operating at Mach numbers of 0.0 and 0.1, respectively. Data for four gages are presented. These are the inboard bending, mid-blade bending, shear and tip bending gages. These are displayed for blade number 1 only, since it was found during data reduction that all the blades showed similar behavior.

The stresses are very high for the bending gages at a blade angle of 50 degrees for all RPM's. For these gages, at zero Mach number (Figure 4-10), the stress contours are parabolic in shape and the stress increases with increasing blade angle and increasing RPM. However, the shear gage shows an entirely different picture. The highest stress shown occurs at 7000 RPM and 36 degrees blade angle. The stress at this point is approximately 62.1 MPa (9000 psi).

In Figure 4-11, for 0.1 Mach number operation, the bending gages show a similar picture as that seen for the zero forward speed data, but with lower stresses. The shear gage, however, shows stress contours that behave more like those for the bending gages.

Figures 4-10 and 4-11 also show the calculated stall flutter boundaries for the SR-2, as were shown in Figure 3-11 for zero Mach number (static) and 0.1 Mach number. The calculated boundary for the static condition includes the region of high stress gradients with RPM and blade angle seen in the shear gage data. There is less correlation between the calculated boundary and the test data for the forward speed condition, although the calculation generally follows the stress increase seen in the data.

SR-2 Spectral Analysis - Time averaged spectral analyses were conducted for some of these SR-2 test data. Figure 4-12 shows plots of the spectral analyses for zero Mach number operation, and represents the output of the inboard bending gage, the shear gage and the tip bending gage. These curves are for operation at 6270 RPM and 39.5 degree blade angle. The bending gages show predominantly high stress in the second bending mode, while the shear gage reflects the torsion mode frequency. Note that the modes are acting independently (uncoupled), since they are at different frequencies. The predominance of the second bending mode, indicates that stall flutter is occurring in this mode, or that possible buffeting is causing the high stresses at the static condition. A discussion of stall flutter and buffeting is presented later in this section.

Figure 4-13 shows spectral analysis plots for the 0.1 Mach number case at 8000 RPM and zero inflow angle. Shown are the inboard bending gage, the shear gage, and the tip bending gage, respectively. The 1-P stress seems to dominate, which is not explained, except that the stresses are relatively low and buffeting could account for this response.

SR-3 Results - Figures 4-14 and 4-15 are total stress contours for the SR-3 model at zero and 0.1 Mach number, respectively. Stress contours are shown for inboard bending, tip bending and shear for blade number 1. The total stresses shown are much lower for the SR-3 than were seen for the SR-2, indicating a benefit of blade sweep. For zero Mach number, the shear gage shows moderate torsion stress while the inboard bending and tip bending gages show high total stresses. A high stress for the inboard bending gage occurs at about a 50 degree blade angle above 4000 RPM. The tip bending gage has a local maximum total stress at a 40 degree blade angle and 5000 RPM and another local maximum at 60 degrees and above 7000 RPM.

At a Mach number of 0.1, the high stresses occur at higher RPM's and higher blade angles than for the static condition. Note that for the forward speed condition, the maximum shear stresses are of the same magnitude as the bending stresses. The calculated stall flutter boundaries, for both the static and forward speed cases, correlate well with the regions of stress rise. This is more clearly seen in the tip gage data than the shear gage data.

Figure 4-16 shows plots of stress spectral analyses for the SR-3 model at a blade angle of 50 degrees and 4000 RPM at zero Mach number for the inboard bending gage, the shear gage and the tip bending gage. For the inboard gage, a response peak occurs at the first bending mode and little else is seen. The shear gage shows response stresses lower than 3000 kPa (434 psi). The tip bending gage shows substantial first mode vibratory stress with some second and fourth mode stress. The placement of the mode frequencies can be extrapolated from the calculated frequencies shown in Figure 3-6.

Spectral plots for another zero Mach number case are shown in Figure 4-17 for the inboard bending, shear and outboard bending gages, respectively. These plots are derived from data taken at a blade angle of 60 degrees and 7500 RPM. Again, the inboard gage shows only first mode stressing while the shear gages show mostly 4th mode stresses. The tip bending shows significant response in all modes up to the 5th. This is indicative of broadband aerodynamic excitation that is a characteristic of a buffeting condition which may occur at these high blade angles, and is probably not associated with stall flutter.

The calculated stall flutter boundaries for the SR-3 model, as obtained from Figure 3-11 for zero Mach number and 0.1 Mach number, respectively, are shown in Figures 4-14 and 4-15. These boundaries are derived from third mode calculations since no stall flutter was calculated for the first and second modes.

SR-5 Results - Figures 4-18 and 4-19 show total stress contours for the SR-5 model Prop-Fan at zero Mach number and 0.1 Mach number, respectively. Both curves display total stress contours for the inboard bending gage, the shear gage and the chordwise bending gage. No stall flutter is apparent on the curves from the lack of any region of steeply rising stress. Only the chordwise bending gage displays total stresses higher than 68,900 kPa (10000 psi), with this occurring at blade angles about 50 degrees above 8000 RPM for zero Mach number. The SR-5 blade seems to be less susceptible to stall flutter and buffet than either the SR-2 or SR-3 Prop-Fan model blades, again indicating an advantage of increased sweep. It is noted that the stress at forward speed is significantly lower than that measured statically.

The calculated flutter boundaries for the SR-5, shown in Figures 4-18 and 4-19 show flutter occurring only at extreme operating conditions. This is supportive of the measured test data, since the SR-5 did not give stall flutter indications during test.

Spectral plots for the SR-5 blade inboard bending gage, the shear gage and the chordwise bending gage are shown in Figure 4-20 for a zero Mach number case at 9000 RPM and a reference blade angle of 40 degrees. Although the stresses are low, all of the gages responded with many modes to an apparent broadband excitation. This may indicate a buffet condition.

Flutter Summary - Operating conditions producing blade aeroelastic instability were determined from test measurements to be those which were accompanied by steeply rising vibratory stresses with a small change of condition. In general, the measured stresses were seen to rise as the blade angle was increased into the stall region, usually between 30 and 45 degrees. Stress also rose with increased RPM in this region. This type of aeroelastic instability occurred in one or two blade structural modes, which is indicative of stall flutter.

At blade angles above 50 degrees, the blade stress response in some cases changed in character, to a lower level of total stress made up of contributions from many blade structural modes. This behavior is indicative of random aerodynamic excitation, known as buffet, which occurs under deep stall conditions.

Forward speed acts strongly to reduce blade stall and resulting stresses. The stresses at 0.1 Mach number and above were considerably below the stresses for static operation.

The SR-3 and SR-5 swept blade models generally showed much lower stress levels than the unswept SR-2 blade model. The straight SR-2 model gave robust flutter indications, while the highly swept SR-5 model gave only weak buffet indications during test. Increased blade sweep increases the operating region free of high stress rises. Stall flutter for the SR-2 and SR-3 models occurred in some bending modes as well as torsional modes. Responses for the SR-5 model occurred in many modes, indicating buffet excitation.

Calculated predictions agreed well with the regions of high stress rise observed during test at zero Mach number. At forward speed conditions agreement was not as good. Flutter was predicted to be in torsional modes for all the blade models, while high stresses were displayed in the bending modes as well. These results are similar to those found for the zero forward speed testing of the Prop-Fan models reported in Reference 7.

4.2 Modal Response Frequencies

As previously discussed in Section 4.1, the spectral analyses of time averaged data were taken from many steady state test runs of the SR-2 and SR-5, and all the test runs of the SR-3 blade model. All of these data were saved on tape. Methods were developed to pick off the stress peaks and to store their amplitude values and frequencies. One important use for these data is the creation of Campbell diagrams, also known as critical speed plots. Experimental critical speed diagrams are shown in Figures 4-21 through 4-23 for the SR-2, SR-3 and SR-5 model Prop-Fan configurations. Also shown on these figures are the calculated blade natural frequencies, discussed earlier.

For the SR-2 model there is good correlation between test data and calculations for the first, third and fourth modes. Some anomalies are noted for the correlations with the other calculated frequencies. The second calculated mode is flanked by two curves of experimental data. There is also another experimental curve just above the third mode but below the fourth. No explanation is offered for this behavior.

The Campbell diagram in Figure 4-22 for the SR-3 model shows that there is excellent correlation between test data and calculations for the first, second and third modes. Again, there occurs an experimental mode which doesn't correlate with calculations and lies between the second and third calculated modes. This mode is comprised of lower level stresses, so it won't significantly affect Prop-Fan operation. It is not known whether this is an extra mode, not predicted by the calculation method, or if the third and fourth mode frequencies are calculated too high.

It should be noted that the SR-3 frequency calculations were done using a blade angle of 55 degrees (measured at the 75% radial station). Two sets of data from the tests are shown, one for a reference blade angle of 32 degrees and the other for a reference blade angle of 50 degrees. The data show little difference between the 32 degree and the 50 degree reference blade angles, even though these tests cover different but overlapping RPM ranges. This is probably due to the fact that the blade is operating in stall for both angles such that there is little change in aerodynamic loading. Also, in structural terms, centrifugal restoring moments in torsion (dumbell effects) generally show little change for variations in blade angle near 45 degrees. It is concluded that data for the 32 degree reference blade angle can be safely compared to the calculated frequencies at a 55 degree blade angle. This reasoning is also used to justify similar comparisons for the SR-2 and SR-5 models, as shown in Figures 4-21 and 4-23.

The Campbell diagram showing the SR-5 model tested and calculated vibration frequencies is given in Figure 4-23. The curves for the SR-5 are similar to those of the SR-3. The first and second experimental modes correlate very well with predictions. However, discrepancies are again seen in the higher modes. The third through the fifth experimental modes are significantly lower in frequency than the calculated modes.

Summary - Comparison of measured and predicted frequencies on the Campbell diagrams for the SR-2, SR-3 and SR-5 models can be summarized as follows. Generally, the lower mode frequencies were well predicted by the theoretical methodology. This is important since good frequency correlation is a necessary indicator of the validity of the structural model. Also, most of the responses observed in test occurred at the lower mode frequencies. Differences between test and theory appear for the higher modes, with these differences appearing to be exaggerated by increased blade sweep. The reasons for this may be that it is more difficult to analytically describe the blade structure to account for sweep. The swept blades may require a finer grid for the finite element analysis, in order to adequately calculate the response at the higher modes.

4.3 Angular Flow Dynamic Response

Total Stress Measurements - Stress measurements were made for all the model blades during wind tunnel tests with the Prop-Fan operating with its drive shaft tilted relative to the tunnel centerline, to provide angular in-flow to the rotor. The results are plotted in Figures 4-24 through 4-26 for the SR-2, SR-3 and the SR-5 model blades, respectively. Here the total stress per excitation factor is plotted as a function of rotational speed for various blade angles. A separate plot is shown for each Mach number tested. All these curves are shown for a tilt angle of $\psi = 15$ degrees.

Excitation Factor (E.F.) is a term that is proportional to Prop-Fan tilt angle and dynamic pressure. It is defined in Section 3.1. E.F. is a useful concept for the study of blade stresses because of its linear dependence on tilt angle. For a uniform, steady inflow to a rotor, theoretically there is no aerodynamic excitation to induce a forced response of the blades. If the rotor shaft is tilted at some angle to this uniform flow, a sinusoidal variation in velocity at the blade will occur with a frequency of 1P. This will induce a 1P response of the blade that is some function of the mean flow velocity and density (dynamic pressure) and the tilt angle.

A typical spectrum of the inboard bending gage signal, for a tilt angle test run of the SR-2 model, is shown in Figure 4-27. It is seen from this curve that the 1P response is the major contributor to the total stress. The 2P and other higher order responses may be due to dynamic response magnification of structural modes by residual higher order aerodynamic excitation from the nacelle or pylon. Also, residual turbulence in the tunnel flow could excite higher blade modes. Note that this 6000 RPM condition is well above the 2P/1st mode critical speed of about 4500 RPM. Away from critical speeds, the total stress is made up of mostly a 1P stress contribution.

The variation of total stress with tilt angle is examined in Figure 4-28. These SR-2 test data were taken at 3000 RPM, well below the 2P crossover. This curve confirms that blade stress is a linear function of tilt angle, and therefore E.F., for constant flight speed. The stress does not go to zero at zero tilt angle, again possibly due to residual tunnel turbulence. There may also be a small angular error in the physical rotor shaft alignment to the tunnel flow.

For most operation conditions of interest, that is, away from critical speeds, it is demonstrated that normalizing blade stress by E.F. is a valid way to account for the effects of tilt angle and dynamic pressure. In fact, this concept has been in use for many years. Another demonstration of this concept for high speed Prop-Fan test data is given in Reference 8. Note that stress divided by E.F. is sometimes known as "stress sensitivity", and these terms are used interchangably.

The total inboard bending stress per E.F. for the SR-2 Prop-Fan blade is shown in Figure 4-24. Stress per E.F. increases with increasing rotational speed and blade angle while decreasing with Mach number. The stress per E.F. increases with blade angle and rotational speed because the blade loading also increases with blade angle and rotational speed. Conversely, the stress per E.F. decreases with Mach number because the loading decreases with increasing Mach number for constant blade angle and rotational speed. This latter effect is due to the reduced section angle of attack accompanying the increasing advance ratio.

Note the first curve in Figure 4-24 which shows SR-2 stress sensitivity at 0.1 Mach number. Here, the stress/E.F. rises rapidly with RPM and has strong peaks near 4500 RPM with some smaller peaks near 2500 RPM. From Figure 4-21 we can surmise that these are the 2P and 3P first mode critical speeds. At the higher Mach numbers, the Prop-Fan windmill RPM is above the 2P crossover speed. Therefore, data are not available at low speeds. However, the 0.1 and 0.2 Mach number conditions show roughly the same magnitude of additional stress sensitivity due to the 2P crossover, and it can be assumed that this behavior can be extrapolated to higher Mach number conditions.

Similar results to those found for the SR-2 model are seen for the SR-3 and SR-5 in Figures 4-25 and 4-26, respectively. Stress sensitivity increases with RPM and blade angle, while decreasing with Mach number. In general, it is observed that stress sensitivity is reduced as the blade sweep is increased, with the highest levels seen for the SR-2 and the lowest levels seen for the SR-5 model. This confirms an advantage of blade sweep in reducing the dynamic structural response to non-uniform inflow.

The high stress sensitivity peaks due to critical speed response are also seen for the SR-3 and SR-5 models in Figures 4-25 and 4-26. For both models the stress peaks are due to 2P/first mode critical speed crossovers. Unlike the SR-2, however, the magnitude of the additional stress sensitivity for the SR-3 and SR-5 decreases somewhat with increasing Mach number. Also, the 2P response follows the trend of decreasing with increasing blade sweep. This indicates that blade sweep is beneficial in reducing inflow induced critical speed response, as well as 1P response.

1P Stress Measurements Comparison to Predictions - Spectral analyses for all models were made for a limited number of test cases of the SR-2 and SR-5 models. Spectral analyses were made for all of the SR-3 steady state runs. The magnitude of the 1P vibratory stresses were read from the spectral data, stored by computer and printed in tables. A typical spectrum is shown in Figure 4-27. The tables will not be presented, but the data are summarized in Figures 4-29, 4-30 and 4-31, where 1P vibratory stress per excitation factor is plotted as a function of shaft power, for the SR-2, SR-3, and SR-5, respectively.

The measured inboard bending stress sensitivity as a function of absorbed rotor power for the SR-2 is shown in Figure 4-29 as dashed lines for 6000 RPM and 8000 RPM. As seen from the data in this figure, stress sensitivity increases with higher power (higher blade loading) for constant RPM. Also, the curve for 6000 RPM is higher than the curve for 8000 RPM. Some calculated points are shown for the skewed wake and Goldstein calculations as obtained from Table 3-III. For 8000 RPM the two calculations bracket the test data such that the skewed wake results are 11% higher than the test data and the Goldstein calculation results are about 10% lower than the test data. For the 6000 RPM case, the skewed wake case coincides with the test data while the Goldstein calculation is 16% lower.

Calculations at 8000 RPM only are available for the SR-3, as shown in Figure 4-30. Here the slope of the test data is greater than the slope of the calculations but the magnitudes fall between those for the skewed wake calculations and the Goldstein calculations. The skewed wake is 9% above the test curve at 112 kilowatts, and the Goldstein calculation is 22% below the test curve at 298 kilowatts.

The SR-5 results are similar to those for the SR-3, as seen in Figure 4-31. At 6000 RPM the Goldstein calculations are 15% lower than the test data. At 8000 RPM the skewed wake calculation is 15% higher than the test results and the Goldstein calculation is 10% below the test results.

It should be pointed out here that the accuracies quoted for the above correlations are based on measurements of moderate stresses. All of the SR-3 and SR-5 stresses discussed above are under 25 MPa, or about 3,500 psi. The SR-2 stresses are below 50 MPa (~ 7000 psi). If the increment between the calculated and tested stress were to remain constant, then at high stress the percentage differences would be smaller, Still, the above correlations indicate that the skewed wake and Goldstein calculations may be confidently used to provide estimates of the upper and lower bounds for 1P stress.

1P Data Trends - The relative stress levels between the three model configurations are shown in Figure 4-32, where stress sensitivity is plotted as a function of blade angle at 8000 RPM and 0.28 Mach number. It is seen that the SR-2 has the highest sensitivity and the SR-5 has the lowest, clearly indicating an advantage of increased blade sweep.

A series of curves shown in Figure 4-33 show 1P vibratory stress sensitivity plotted as a function of Mach number for various rotational speeds for the SR-3 model Prop-Fan blades. The data cover a range of reference blade angles from 24 to 40 degrees. These data are shown for the inboard bending gage. It is seen that the vibratory stress sensitivity increases with blade angle and RPM, but decreases with increasing Mach number for constant blade angle. It should be noted that at constant blade angle, the power also decreases with increasing Mach number. Therefore, these curves do not show the variation with constant power.

An attempt was made to study the effect of power variation through the use of the propeller power coefficient. The power coefficient, defined below, is a non-dimensional function of the dynamic pressure due to rotational speed at the blade tip, and diameter cubed. Everything else being constant, the power the rotor absorbs is proportional to the tip dynamic pressure and diameter cubed. Power coefficient is defined as $C_p = 2\pi Q/\rho n^2 D^5$, where ρ = air density in slugs/ft^3, Q = rotor torque in ft-lbs, n = rotational speed in revolutions/sec and D = the rotor diameter. Use of the power coefficient normalizes the effect of size and RPM in the data.

Figure 4-34 shows the result of cross plotting the plots of 1P stress sensitivity vs. power coefficient for Mach numbers up to 0.35 and rotational speeds up to 9000 RPM. The resulting curves indicate the independence of 1P stress sensitivity from Mach number and rotational speed effects. For blades of similar construction, this family of curves can be useful as a design tool in scaling Prop-Fan blades. Also, they suggest a limit on the power coefficient allowed for each blade angle, to permit safe operation. The fact that these curves are independent of Mach number indicates that for 1P response, aerodynamic compressibility effects are negligible, at least for the relatively low flight Mach numbers considered here. It is not understood why there is a sharp bend in each of these curves.

4.4 Reverse Thrust

One of the operations that a propeller must endure is the reverse thrust condition. Reverse thrust is used on aircraft generally during landing to shorten the ground roll, allowing for more efficient ground operations. The Prop-Fan models were subjected to limited testing in this regime, over a range of operating variables previously discussed. None of the results for the SR-2 model will be discussed, since in the reverse thrust mode no high stresses were observed, except for some moderate stressing at the first mode critical speed.

Figure 4-35 shows total vibratory stress for the SR-3 model plotted as a function of Mach number for various settings of reference blade angle. These curves are shown for blade number 5 shear gage data. The highest total vibratory stress shown occurs at a reference blade angle of -4.0 degrees, zero Mach number and 9000 RPM. The next highest stress occurs at a blade angle of -2.0 degrees for 8000 RPM. Spectral plots are shown in Figure 4-36 for this case, for the three gages on blade number 1. It is seen that the response,

which is higher in level than that for blade 5, is at the third mode natural frequency, which is very close to the 5P critical speed. However, it was observed from oscillograph data at -4 degrees blade angle and 9000 RPM, that the high stress occurs at a frequency of 675 Hz and not at a P-order. For some of the high stress points, strip chart data show the stress amplitude increasing with time at steady state operating conditions. The indications are that this unstable phenomenon is flutter, since the stress amplitude is divergent and the mode is coupled with large torsion and bending responses.

SR-5 data are shown in Figures 4-37 and 4-38. Total vibratory stress is plotted against Mach number for a blade angle of 4.2 degrees and 9000 RPM, for blade number 6 and blade number 1, respectively. Negative blade angle settings were not possible, due to mechanical interference between the ten blades, so small positive angles were set for reverse thrust testing. The data indicate that high stress occurs at zero Mach number and at 0.2 Mach number. The highest stress for blade 1 occurs at Mach = 0.2, and the highest stress for blade 6 occurs at Mach zero. The cause of the differing response for the two blades is not understood.

Figures 4-39 and 4-40 are spectral plots of SR-5 blade stress at the zero Mach number and 0.2 Mach number conditions, respectively, for a 4.2 degree reference blade angle at about 8900 RPM. At zero Mach number, the response is in the second mode and is close to the 2P line (see Figure 4-23). Some of the high stress may be due to magnification caused by the nearness of the response frequency to the critical speed crossover. At the 0.2 Mach number condition, the response is in the first mode with other response peaks observed at exactly twice and three times the first mode frequency. The greatest response is seen at the shear and chordwise bending gages with significantly high stresses.

This phenomenon may be explained by observing the time history waveforms of the strain gage signals for this condition. These are shown in the oscillograph records given in Figure 4-41. Generally, flutter responses are sinusoidal, but these are not. It is speculated that this non-sinusoidal behavior is due to the fact that the steady loads on the blade are negative (net loading on camber side) and may be buckling (oil canning) the blade. If the vibratory loads push the blade into a buckling condition on every cycle, the waveforms shown in Figure 4-41 could be obtained. The time history traces shown could produce the Fourier components of 2X and 3X the fundamental frequency, as seen in Figure 4-40. The buckling of the blade is similar to the bending of a flexible steel carpenter's measuring tape except that the blade is stabilized by centrifugal loads. It is not known if this possible buckling is a result of the flutter, or if this cause-effect relationship is reversed.

5.0 CONCLUSIONS

As a result of the test and analysis program summarized in this report, the following conclusions were obtained regarding the low speed stability (stall flutter), angular flow dynamic response, and reverse thrust response of the SR-2 straight blade, the SR-3 moderately swept blade and the SR-5 highly swept blade Prop-Fan models:

1. Blades with increased sweep respond with lower stresses to stall flutter and buffet.

2. Forward speed acts strongly to reduce blade stall and hence stall flutter stresses. The blade stresses at 0.1 Mach number were reduced considerably below the stresses for static operation.

3. Comparisons were made between tested stall flutter boundaries, based on steeply rising stresses with increasing RPM and blade angle, with calculated boundaries based on zero blade damping. Good agreement between test and prediction was indicated for the SR-2 and SR-3 models, with less agreement for the SR-5 model, which did not give strong flutter indications during test.

4. Stall flutter was predicted to occur in a torsional mode for all of the blade models. During testing, stall flutter was observed for the SR-2 in torsion, as predicted, while for the SR-3 stall flutter was observed primarily in bending modes.

5. During reverse thrust operation, the SR-2 model encountered no high stresses, while high stresses were observed for the SR-3 and SR-5 models at some operating conditions. The SR-5 data gave evidence that the high observed stresses were due to flutter.

6. Correlation between tested and predicted Campbell diagram modal frequencies was excellent for the important lower modes, for all the blade models. Differences between test and theory appear for the higher modes, with these differences increasing with blade sweep.

7. Measured blade stress increased linearly with rotor axis tilt angle. The angular flow stress response, except near critical speeds, consisted almost entirely of the 1P stress contribution.

8. Stress sensitivity (stress divided by E.F.) increased with increasing blade angle and RPM at all Mach numbers tested, and decreased with increasing Mach number.

9. Increased blade sweep significantly reduced both angular inflow (1P) and critical speed stress responses.

10. Stress sensitivity vs. power coefficient was found to be independent of Mach number and RPM, for fixed blade angle, at the low Mach number conditions examined. Stress sensitivity was strongly dependent on power coefficient at low blade angles, and only weakly dependent on power coefficient at high blade angles.

11. For Mach numbers up to 0.35, the theoretically based 1P stress sensitivity calculations agreed very well with measured values. The skewed wake analysis and the Goldstein analysis may be confidently used to provide estimates of the upper and lower bounds for 1P stress, respectively.

6.0 RECOMMENDATIONS

1. Stall Flutter

The results from this test program indicate that stall flutter is not a problem for the swept blades. However, the model blade designs are of solid metal construction and are considered very stiff. It is not known how full scale composite blades with lower relative stiffnesses will behave. Thus, the following recommendations are offered regarding improvement of the stall flutter prediction methods.

a. Non-linear theoretical methods should be developed to predict blade stress and limit amplitude, rather than the linear methods used which estimate stall flutter onset boundaries based on damping. It is thought that stall flutter can exist at very low limit amplitudes and stresses. Therefore, it would be more useful to compare calculated stresses to measured stresses.

b. Develop and improve empirical prediction methods and acquire improved test data for unsteady airflow effects. Perform oscillating NASA 16 series airfoil tests in a wind tunnel to study their stalling characteristics. Buffeting as well as stall flutter conditions should be included in this test program.

c. Continue current unsteady airflow theoretical research into stall flutter. Extend the effort to include buffeting.

d. Correlate new analyses with existing tests, not necessarily restricted to Prop-Fan tests.

e. Measure rotating blade unsteady pressure distributions in stalled regions.

2. Angular Flow Response

Efforts should be made to improve the accuracy of the 1P response prediction methods. This should include study of the effects of varying the induction calculation method, in addition to other aspects of the aerodynamic analysis.

3. Reverse Thrust

Attempts should be made to determine the cause of the reverse thrust high stresses observed for the swept blades. The initial effort should include a wind tunnel flow visualization test to determine the nature of the flow field behavior. This will provide guidance for future theoretical/empirical analysis studies.

7.0 REFERENCES

1. Aiello, Robert A.; "NASA Lewis 10-by-10 foot Supersonic Wind Tunnel", NASA TM X-71625, Nov. 1974.

2. Goldstein, S.; "On the Vortex Theory of Screw Propellers", Proceeding of the Royal Society of Aviation, Vol. 123, 1929.

3. Egolf, T. A. and Landgrebe, H.A.; "A Prescribed Wake Rotor Inflow and Flowfield Prediction Analysis - User Manual and Technical Approach", NASA CR-165894, June, 1982.

4. MacNeal, R. H.; "The Nastran Theoretical Manual" (Level 15.5), MacNeal - Schwendler Corp., December 1972.

5. Turnberg, J.; "Classical Flutter Stability of Swept Propellers", Report No. 83-0847 CP, AIAA/ASME/ASCE/AHS 24th Structures, Structural Dynamics and Materials Conference. May 2-4, 1983/Lake Tahoe, Nevada.

6. Steinman, D. B.; "Aerodynamic Theory of Bridge Oscillations", American Society of Civil Engineers, Transactions, Paper No. 2420, October, 1949.

7. Smith, A.F.; "Analysis and Test Evaluation of the Dynamic Stability of Three Advanced Turboprop Models at Zero Forward Speed", NASA CR-175025, December 1985.

8. Bansal, P., Arseneaux, P., Smith, A., Turnberg, J. and Brooks, B.; "Analysis and Test Evaluation of the Dynamic Response and Stability of Three Advanced Turboprop Models", NASA CR-174814, August 1985.

TABLE 2-I. PROP-FAN MODEL SUMMARY

	SR-2	SR-3	SR-5
NO. BLADES	8	8	10
MATERIAL	STEEL	TITANIUM	TITANIUM
DIAMETER	24.5 IN	24.5 IN	24.5 IN
3/4 CHORD	3.57 IN	4.53 IN	4.10 IN
AIRFOIL (NACA)	16 SERIES	16 SERIES	16 SERIES
DESIGN C_L	0.084	0.214	0.271
A F (TOTAL)	1632	1880	2100
A F (PER BLADE)	204	235	210

TABLE 2-II. STRAIN GAGE DESIGNATION PROP-FAN MODEL TESTS

BLADE	DESCRIPTION	RADIAL STATION, IN.	GAGE DESIGNATION									
			BLADE NO 1	2	3	4	5	6	7	8	9	10
SR-2	INBOARD BENDING	5.0	BG1-1	*	*	*	BG5-1	*	*	*	*	*
SR-2	MID-BLADE BENDING	7.0	BG1-2	*	*	*	BG5-2	*	*	*	*	*
SR-2	SHEAR-V GAGE	7.5	BG1-3	BG2-3	*	*	BG5-3	BG6-3	*	*	*	*
SR-2	TIP BENDING	10.0	BG1-4	*	*	*	BG5-4	*	*	*	*	*
SR-3	INBD. BENDING	4.4	BG1-1	*	*	*	BG5-1	*	*	*	*	*
SR-3	SHEAR-V GAGE	9.6	BG1-4	BG2-4	*	*	BG5-4	BG6-4	*	*	*	*
SR-3	TIP BENDING	10.7	BG1-6	BG2-6	*	*	BG5-6	BG6-6	*	*	*	*
SR-5	INBD. BENDING	5.3	BG1-1	BG2-1	BG3-1	*	*	BG6-1	BG7-1	BG8-1	*	*
SR-5	CHORDWISE BENDING	8.9	BG1-5	*	*	*	*	BG6-5	*	*	*	*
SR-5	SHEAR-V GAGE	10.4	BG1-3	*	*	*	*	BG6-3	*	*	*	*

TABLE 2-III. VARIATION OF TEST PARAMETERS FOR THE NASA-LeRC MODEL PROP-FAN TESTS IN 10 X 10 WIND TUNNEL

MODEL	REF. BLADE ANGLE (DEG.)*
SR-2	-14.5 -13.5 -12 -8 -4 12 16 20 24 28 32 36 40 50 60 70 80
SR-3	-8 -6 -4 -2 0 12 16 20 24 28 32 36 40 50 60 70 80
SR-5	4.2 5.5 6.0 8.2 12 16 20 24 28 32 36 40 50 60 70 80
MACH NO. (ALL MODELS)	0.0 0.1 0.2 0.28 0.35
RPM (ALL MODELS) TILT ANGLE (ALL MODELS)	2000 TO 9000 RPM, 500 RPM INCREMENTS 0.0 DEG. AND 15.0 DEG. (AND OTHER SELECTED TILT ANGLES)

*REFERENCE BLADE ANGLE(βREF) TO BLADE ANGLE AT 3/4 RADIUS STATION (β3/4) CONVERSION

$\beta_{REF} = \beta_{3/4} - 0.8$ (FOR SR-2 AND SR-3)

$\beta_{REF} = \beta_{3/4} + 0.5$ (FOR SR-5)

TABLE 3-1. HAMILTON STANDARD COMPUTER PROGRAMS

DESIGNATION	PURPOSE
MSC NASTRAN	Finite element analysis used to predict vibratory mode shapes and frequencies for swept, thin structures.
H025	Beam type analysis used to predict vibratory bending mode shapes and frequencies.
H026	Beam type analysis used to predict 1-P vibratory response.
H027	Beam type analysis used to predict vibratory torsional mode shapes and frequencies.
H039	Three-dimensional potential flow field analysis used to determine the influence of the nacelle on rotor inflow.
H045	Goldstein analysis with azimuthal variations (see H444).
H337	Skewed wake blade aerodynamic loads lifting line analysis, with vortex wake representation and azimuthal variations.
H444	General Goldstein-type performance strip analysis for Prop-Fans. Provides power, thrust, section force data and angles of attack. Section lift and moment slopes are determined for use in the stall flutter analysis, F203.
F194	Distributes steady or unsteady airloads to finite element nodes for use in MSC NASTRAN.
F203	Eigen-solution modal stability analysis. Calculates damping and frequency using unsteady aerodynamics.
F214	Transposes all coordinate system motions into the blade section coordinate system, in order to take advantage of small angle assumptions for stability analysis.
MODES	Converts mode shapes from finite element or beam analyses to form used by the F203 stability analysis.

TABLE 3-II. OPERATING CONDITIONS FOR THE MODEL BLADE CALCULATIONS

1P RESPONSE CALCULATIONS (15 DEG INFLOW ANGLE)

CASE	MODEL	RPM	MACH NO.	SHAFT HORSE POWER (HP)	BLADE ANGLE FOR FINITE ELEMENT (DEG)
1	SR-2	6000	0.28	150	43.6
2		8000	0.28	300	38.2
3		8000	0.28	450	42.8
4	SR-3	8000	0.28	150	32.5
5		8000	0.28	300	38.4
6		8000	0.28	400	41.9
7	SR-5	8000	0.35	300	42.3
8		8000	0.28	300	39.8
9		6000	0.28	150	45.3

STABILITY CALCULATIONS		
A. FINITE ELEMENT MODEL	BLADE ANGLE (DEG.)	RPM
SR-2	-20 IN 5 DEG 55 INCREMENTS	5000, 7000, 9000
SR-3	15 55	5000, 7000, 9000
SR-5	15 55	5000, 7000, 9000
B. STALL FLUTTER (ALL MODELS) MACH NO. 0.0 0.1 0.2 0.3 0.35 BLADE ANGLE -20 DEG TO 70 DEG 5 DEG INCREMENTS ROTATIONAL SPEED 5000, 7000 AND 9000 RPM SEA LEVEL CONDITIONS		

TABLE 3-III. MODEL PROP-FAN CALCULATED VIBRATORY STRESS FOR 15 DEGREE SHAFT TILT

PARAMETER	INDUCTION TYPE	GAGE NO.	CASE NO.	1	2	3	4	5	6	7	8	9
MODEL TYPE				SR-2	SR-2	SR-2	SR-3	SR-3	SR-3	SR-5	SR-5	SR-5
RPM				6000	8000	8000	8000	8000	8000	8000	8000	6000
MACH NO.				0.28	0.28	0.28	0.28	0.28	0.28	0.35	0.28	0.28
BLADE ANGLE (DEG)				43.6	38.2	42.8	32.5	38.4	41.9	42.3	39.8	45.3
SHAFT POWER (kW)				112	224	336	112	224	298	224	224	112
				STRESS/EF*, PA/DEG								
GOLDSTEIN		1		8274	8474	10460	3337	4454	5130	4448	4937	5240
GOLDSTEIN		2		7564	6378	7991	441	793	945	476	531	641
GOLDSTEIN		4		2200	1434	1889	662	559	607	207	110	469
SKEWED WAKE		1		10005	10460	13252	4185	5590	-	-	6171	-
SKEWED WAKE		2		9074	7840	10129	552	993	-	-	724	-
SKEWED WAKE		4		2627	1793	2448	862	759	-	-	207	-

*E.F.$=\psi\left|\frac{V_{EQ}}{348}\right|^2$, WHERE ψ IS THE TILT ANGLE IN DEG AND V_{EQ} IS THE EQUIVALENT VELOCITY AT THE OPERATING CONDITION

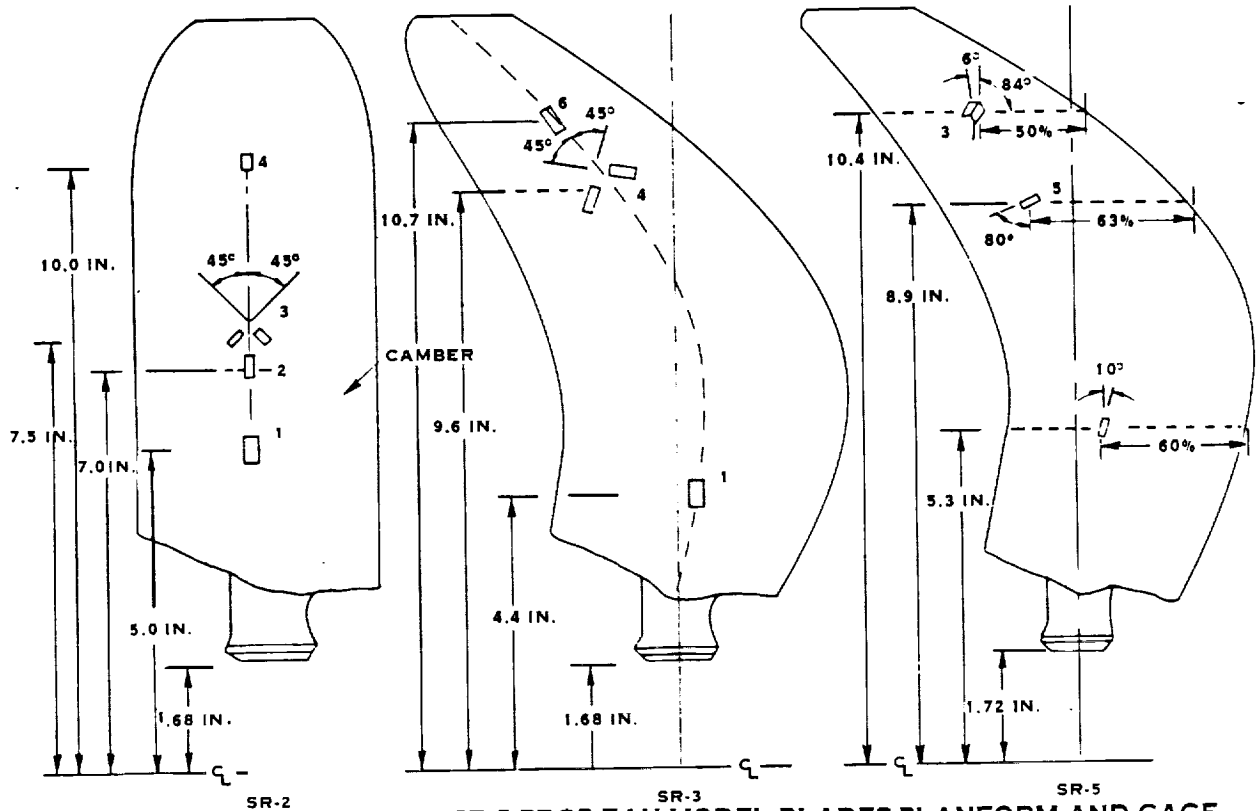

FIGURE 2-1 SR-2, SR-3, AND SR-5 PROP-FAN MODEL BLADES PLANFORM AND GAGE LOCATION-CAMBER SIDE

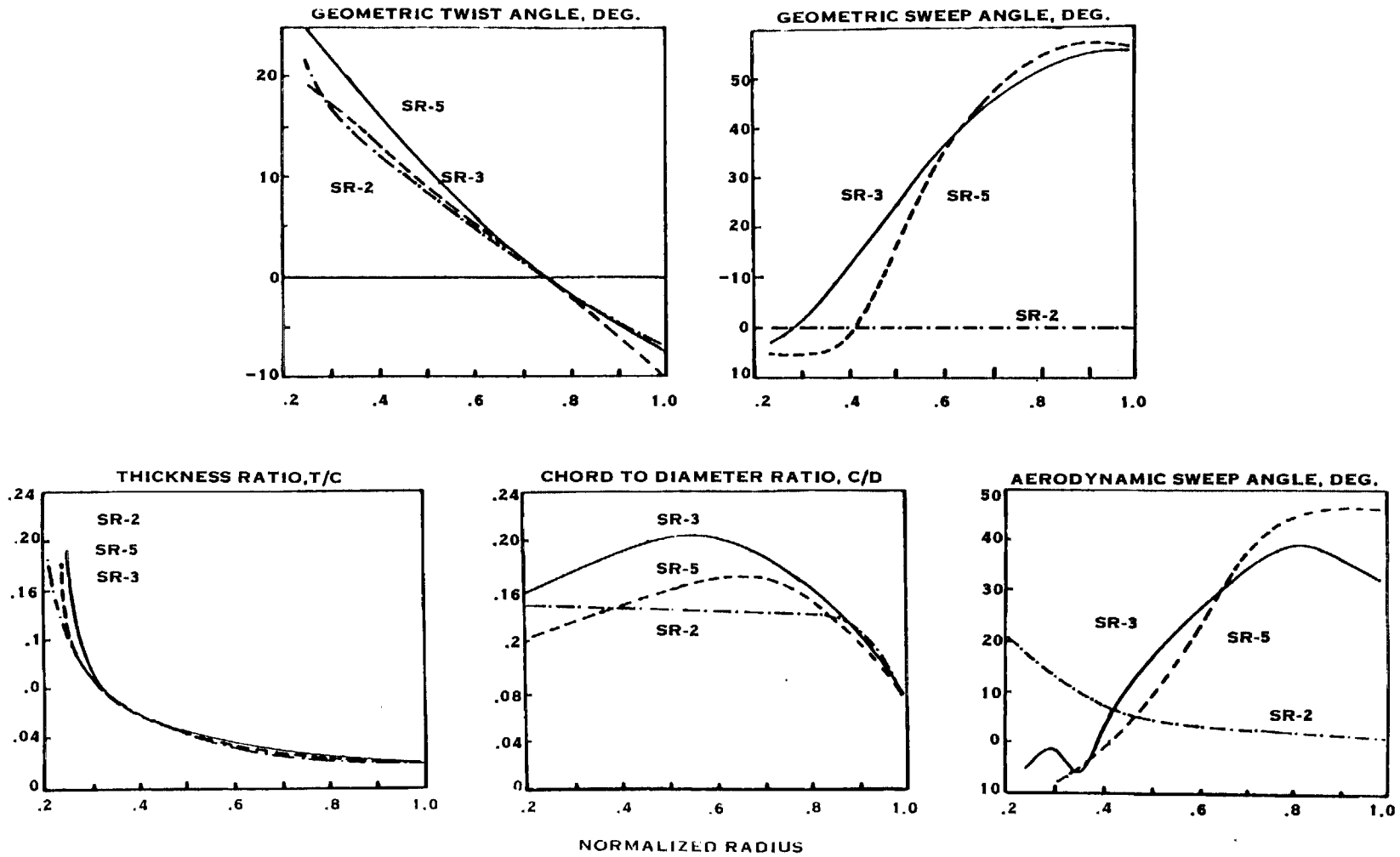

FIGURE 2-2. MODEL CHARACTERISTICS

FIGURE 2-3. INSTALLATION OF THE SR-3 MODEL PROP-FAN IN THE NASA LEWIS SUPERSONIC WIND TUNNEL

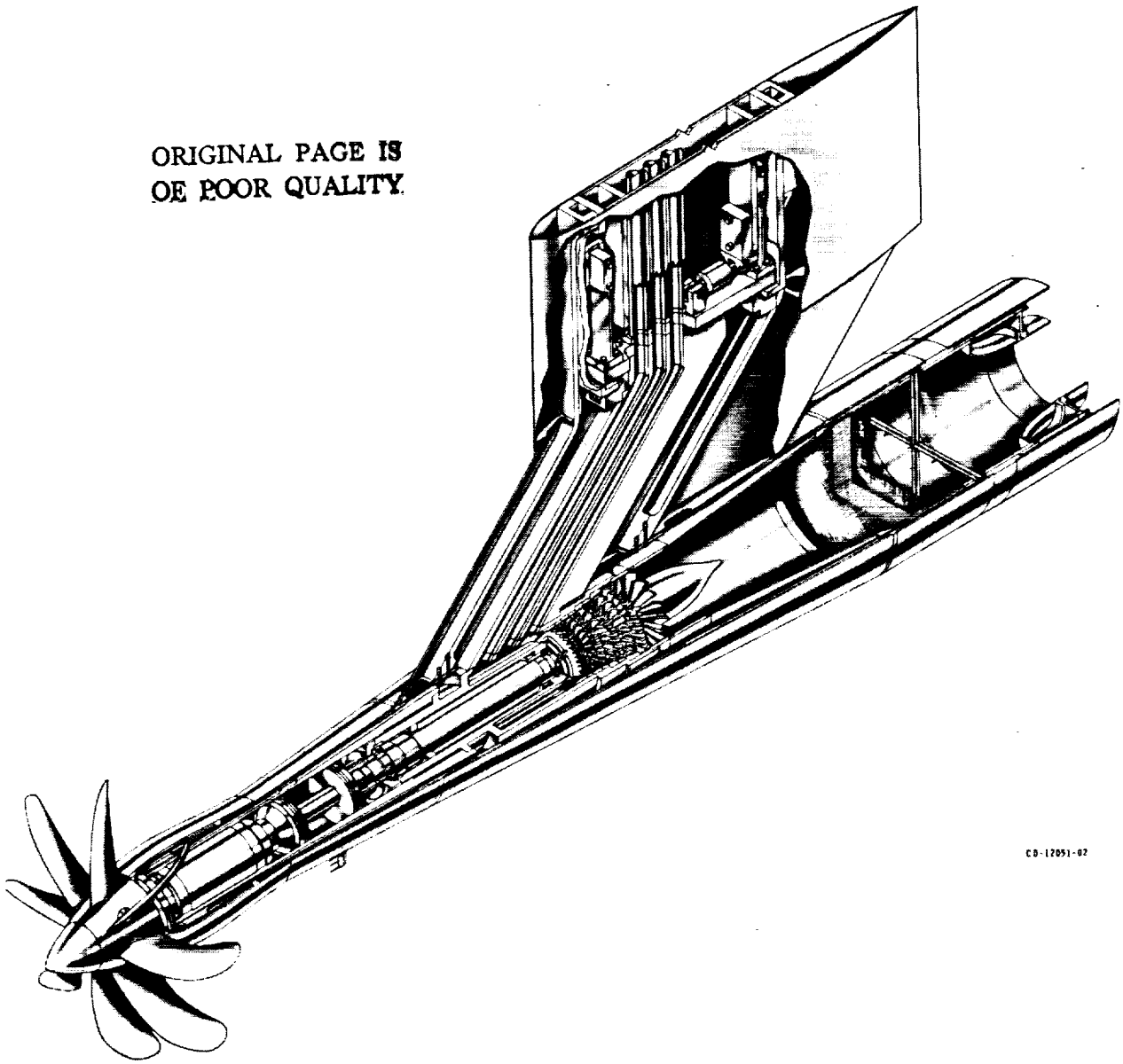

FIGURE 2-4. CUTAWAY VIEW OF THE PROPELLER TEST RIG

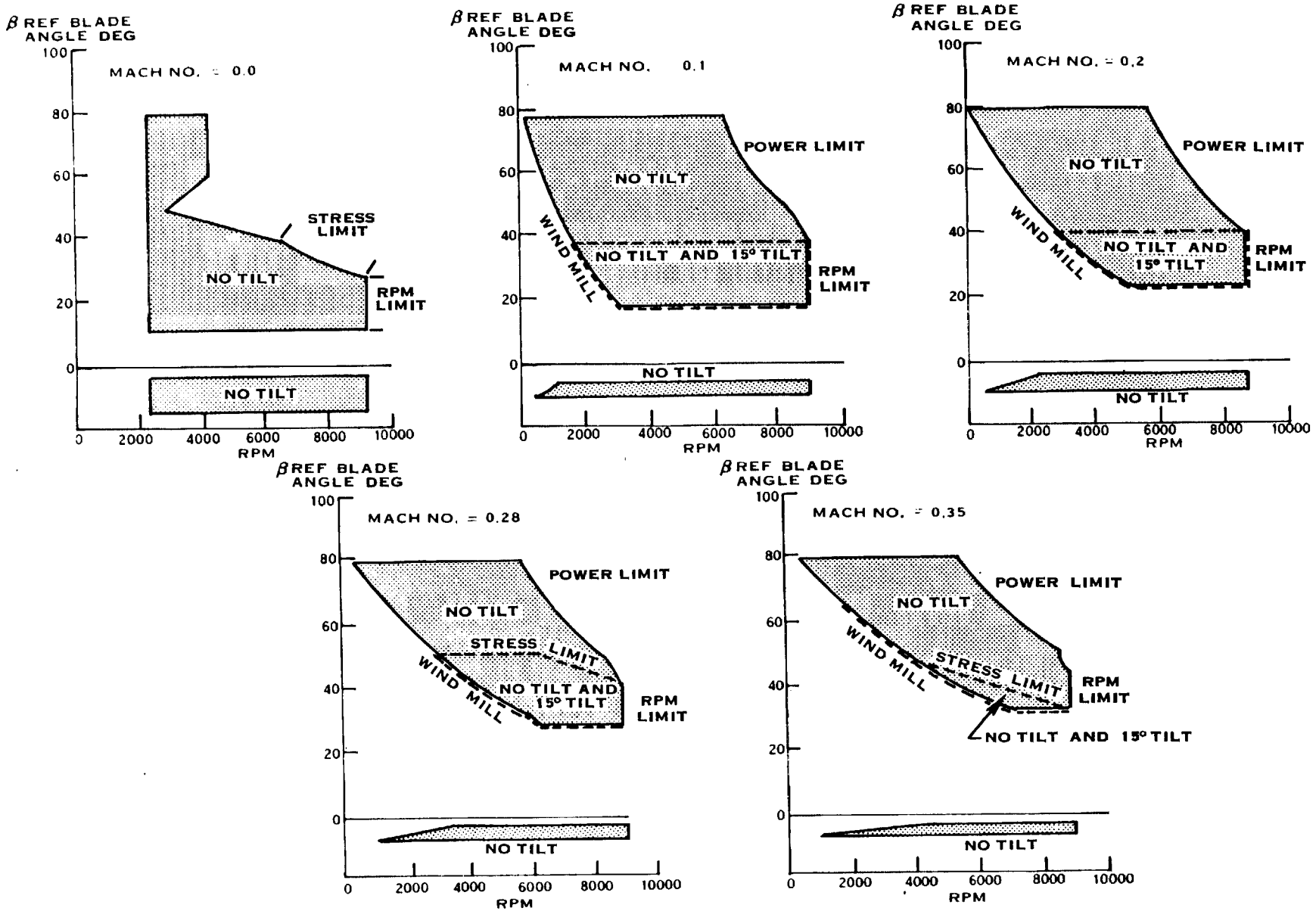

FIGURE 2-5. SR-2 MODEL PROP-FAN NASA-LEWIS 10 X 10 LOW-SPEED WIND TUNNEL TEST TEST ENVELOPES

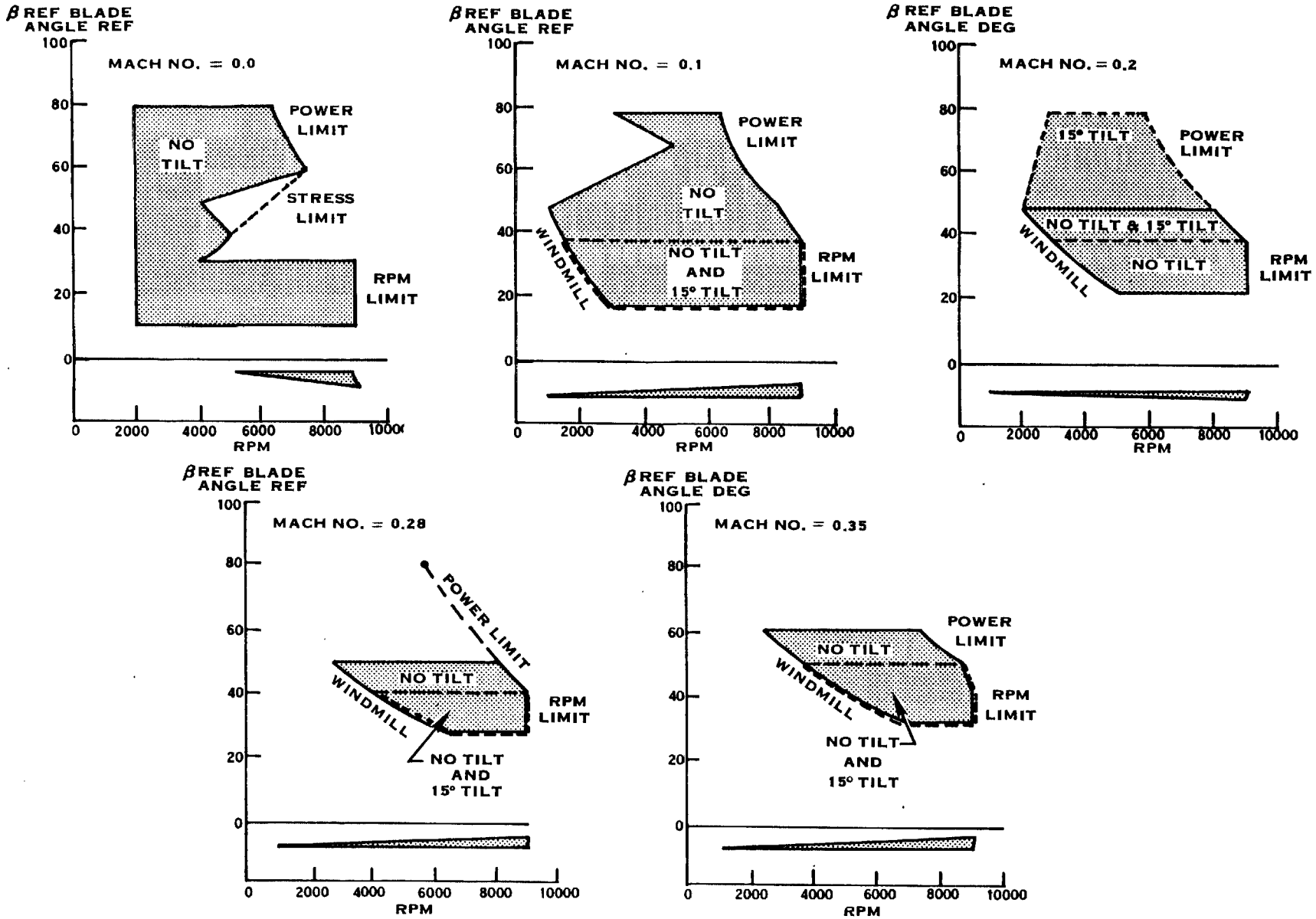

FIGURE 2-6. SR-3 MODEL PROP-FAN NASA-LEWIS 10 X 10 LOW-SPEED WIND TUNNEL TESTS TEST ENVELOPES

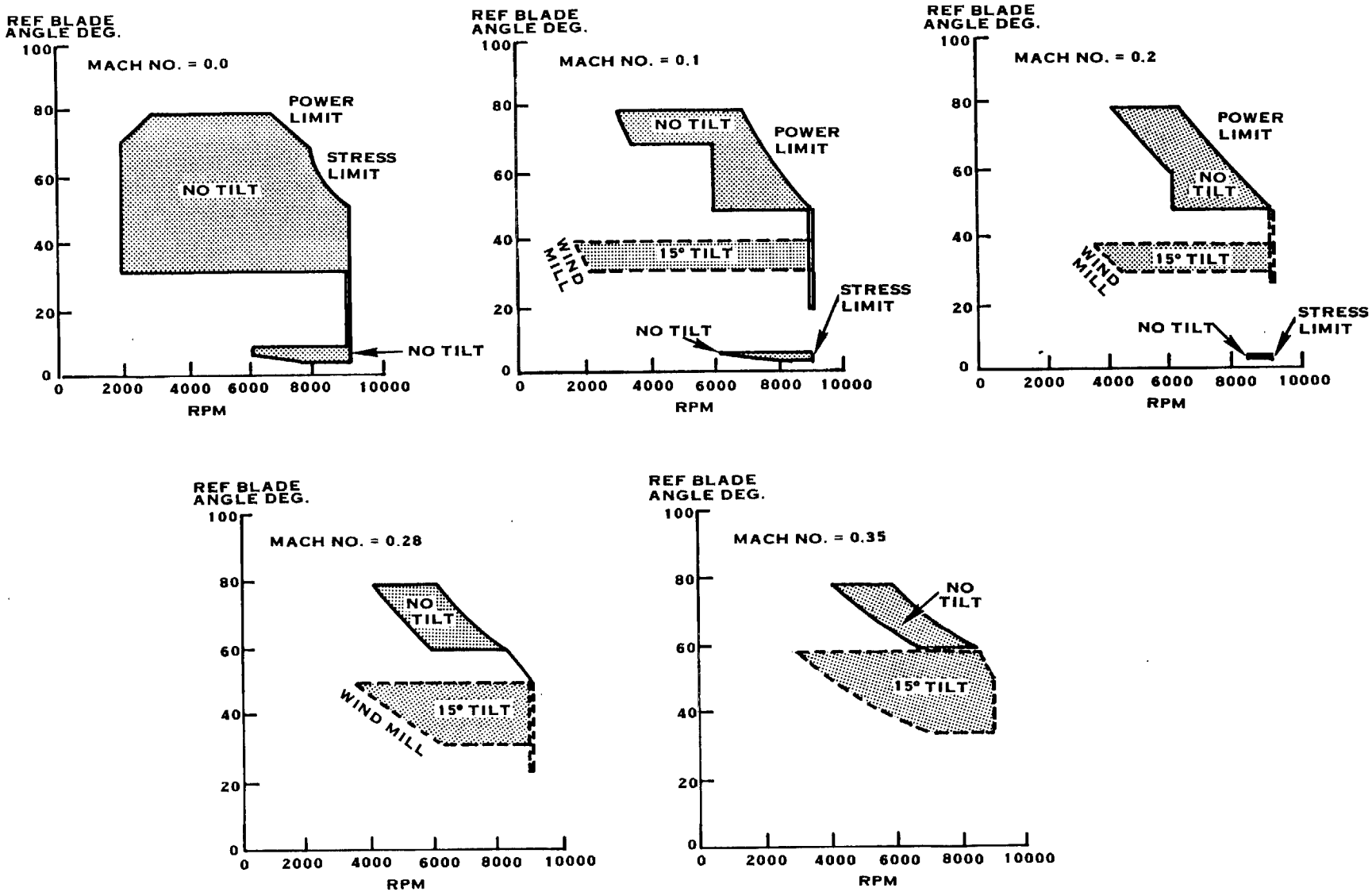

FIGURE 2-7. SR-5 MODEL PROP-FAN NASA-LEWIS 10 X 10 LOW-SPEED WIND TUNNEL TESTS TEST ENVELOPES

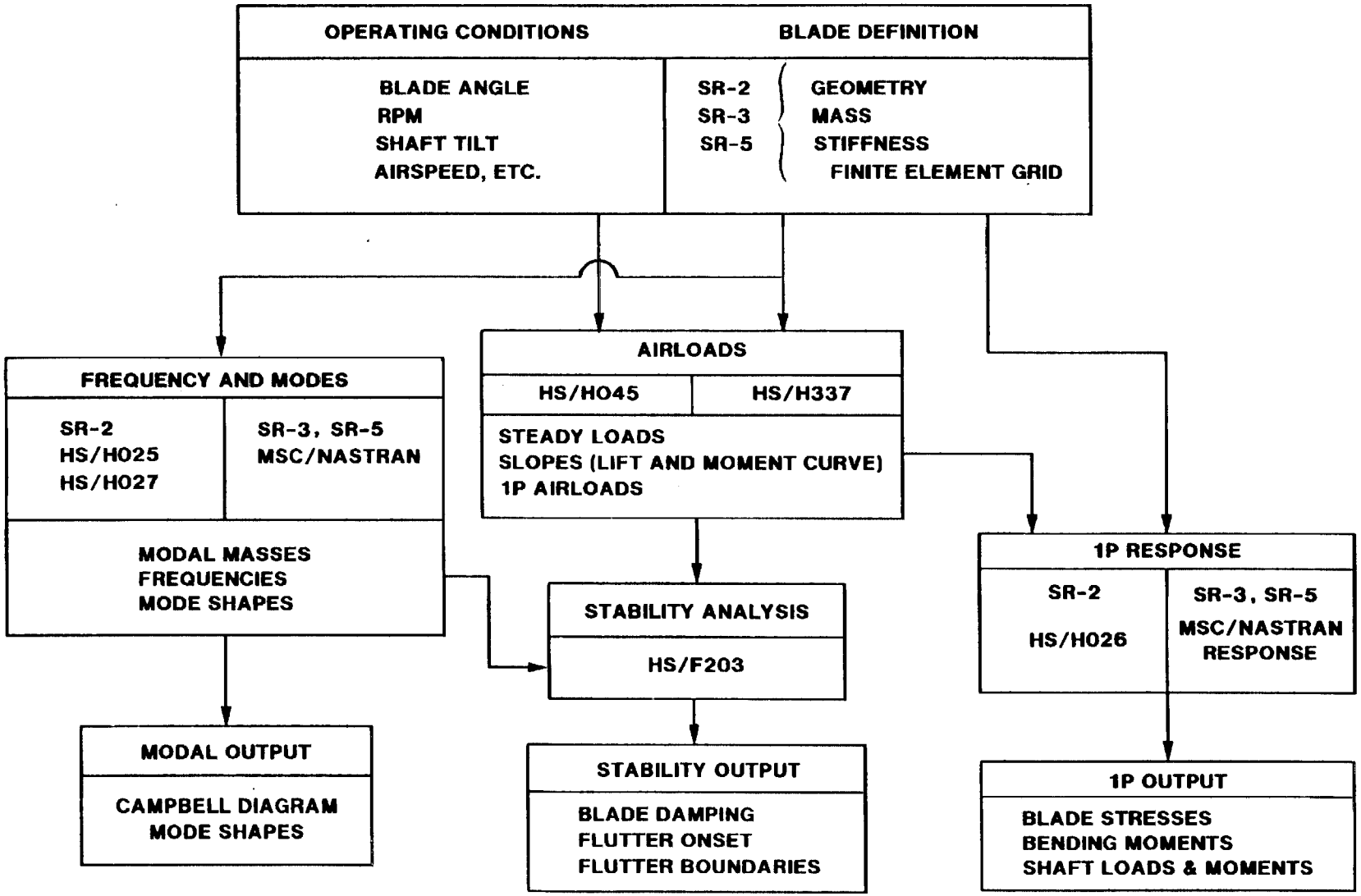

FIGURE 3-1. FLOW DIAGRAM FOR ANALYTICAL PROCEDURES

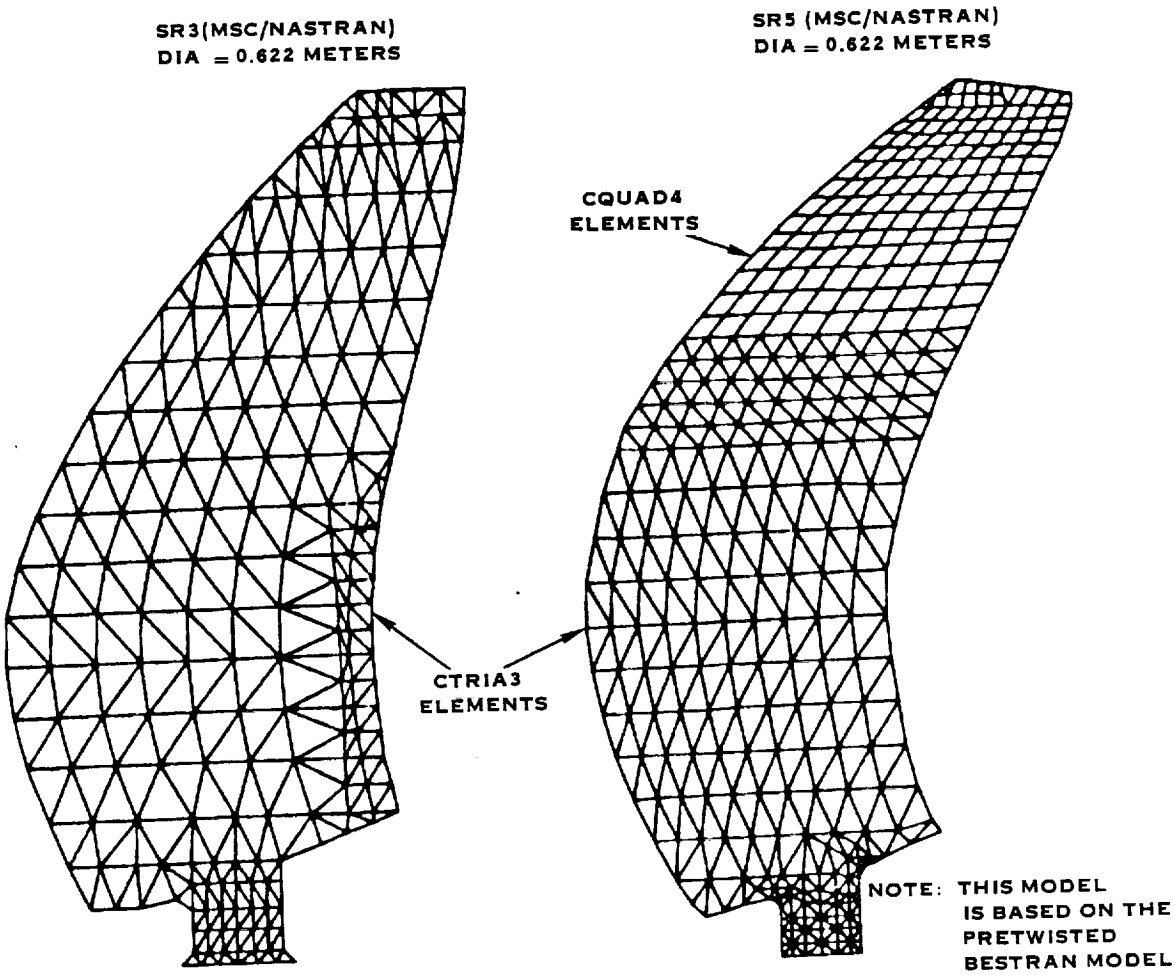

FIGURE 3-2. PROP-FAN ANALYTICAL MODELS USED FOR 1P RESPONSE PREDICTIONS

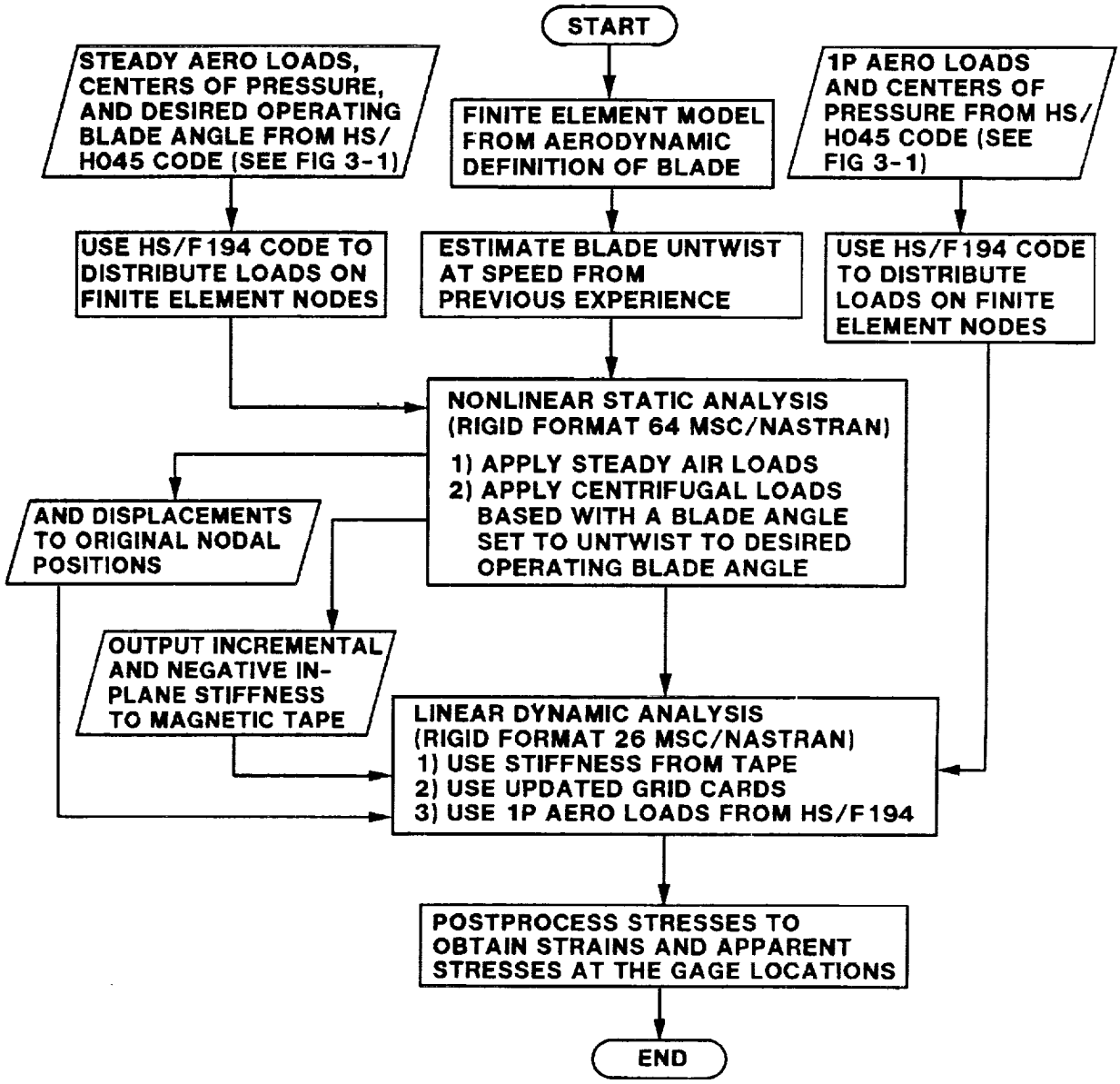

FIGURE 3-3. PROP-FAN MODEL BLADE ANALYSIS-1P DYNAMIC ANALYSIS USING MSC/NASTRAN

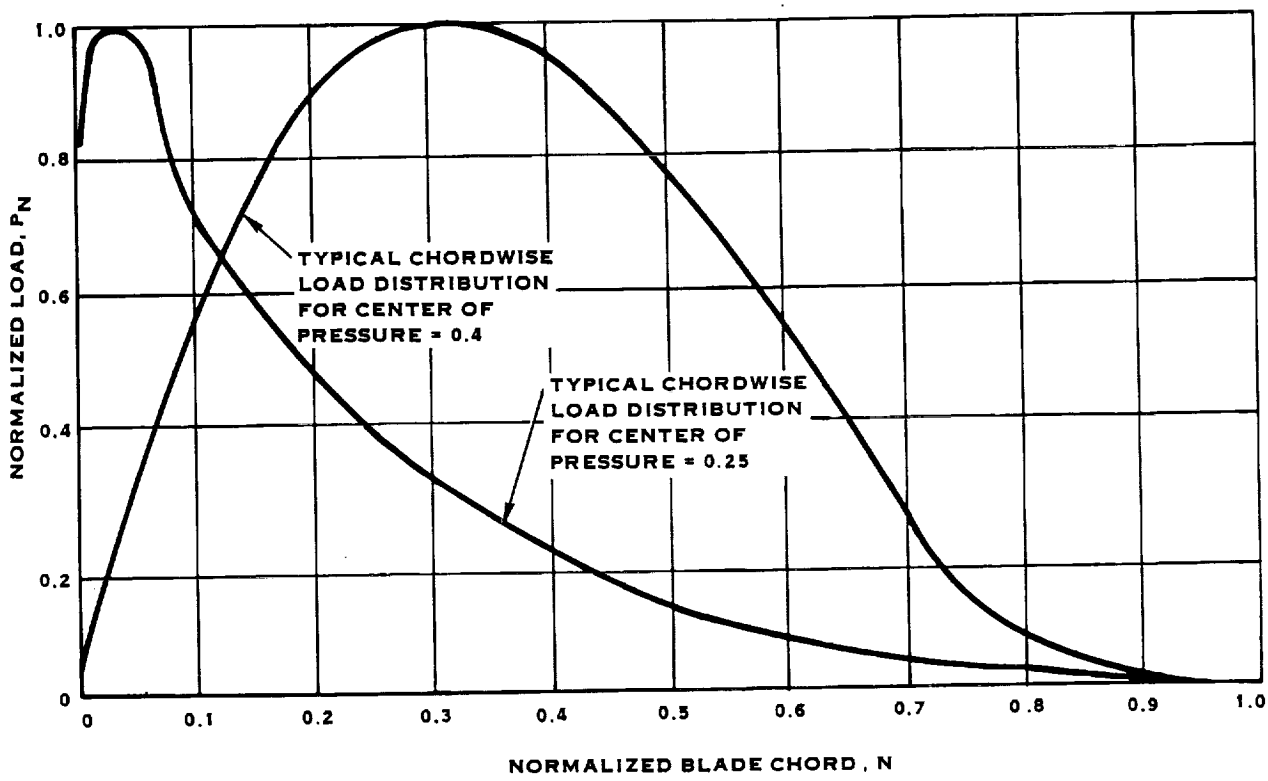

TYPICAL CHORDWISE 1P LOAD DISTRIBUTION BASED ON THE ANALYTICAL FUNCTION $P_N = A(N_C)^B (1-(N_C)^{.25})^2$ WHERE N_C IS THE NORMALIZED BLADE CHORD AND A AND B ARE CHOSEN TO GIVE THE CALCULATED TOTAL LOAD AND TO MATCH THE CALCULATED CENTER OF PRESSURE.

FIGURE 3-4. SR-3 AND SR-5 MODEL PROP-FAN 1P ANALYSES

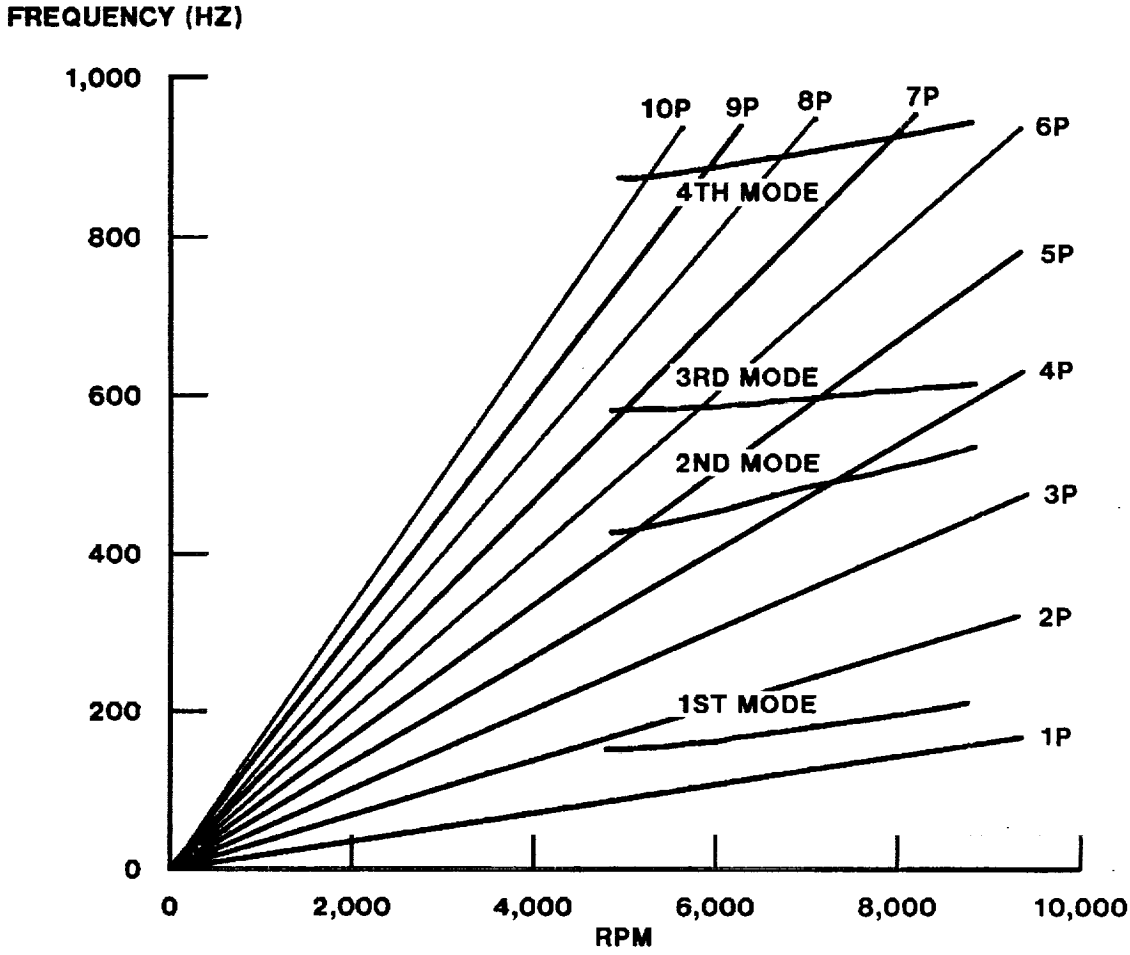

FIGURE 3-5. SR-2 PROP-FAN MODEL BLADE HO25 & HO27 RESULTS BLADE ANGLE = 55°

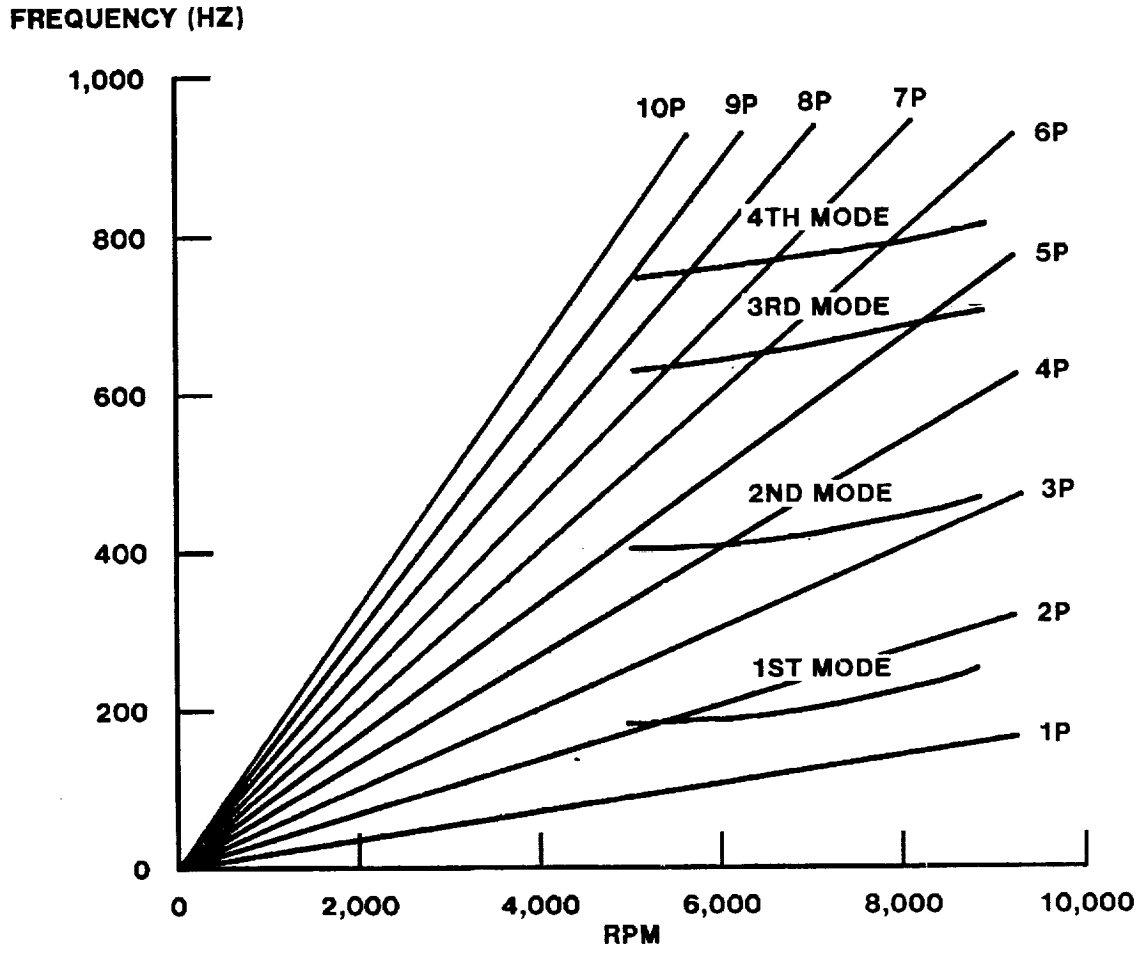

FIGURE 3-6. SR-3 PROP-FAN MODEL BLADE MSC/NASTRAN RESULTS BLADE ANGLE = 55°

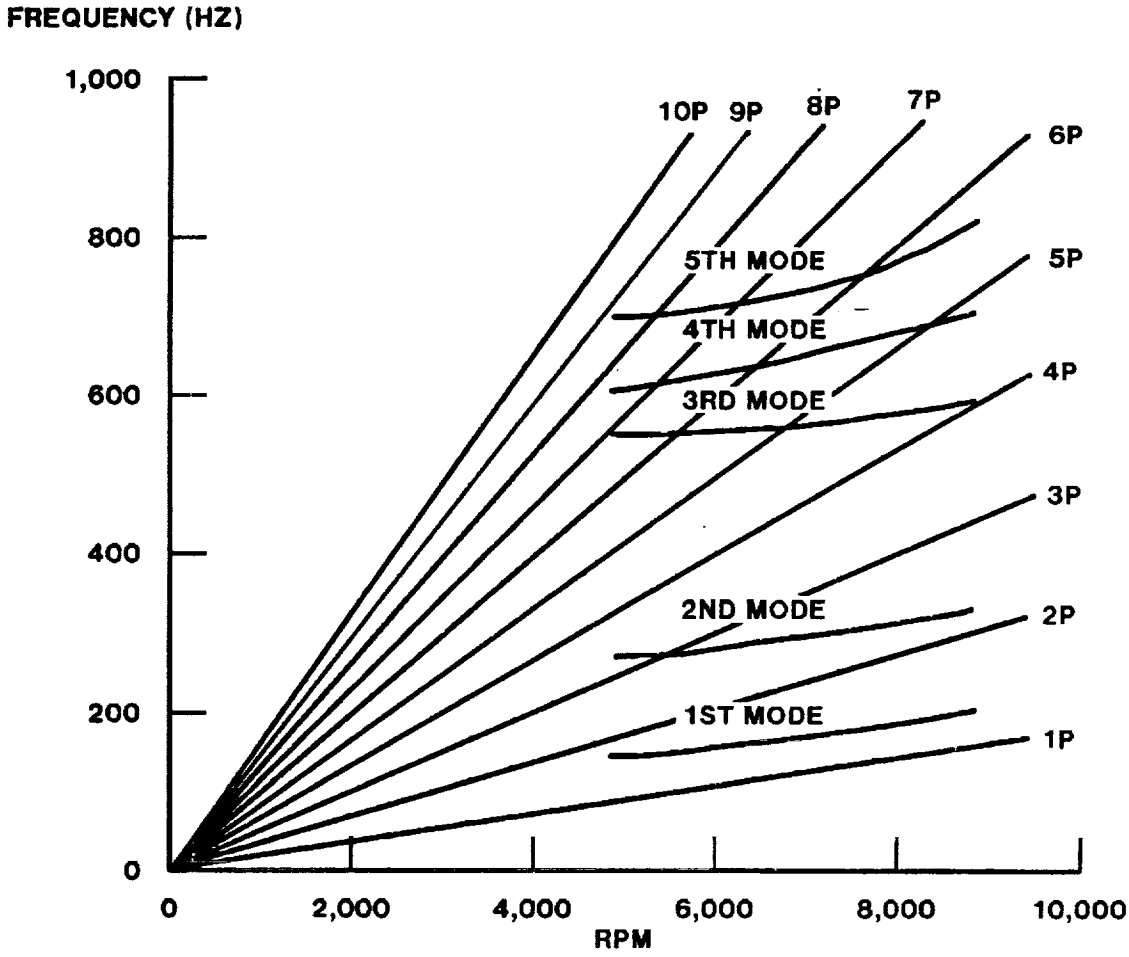

FIGURE 3-7. SR-5 PROP-FAN MODEL BLADE MSC/NASTRAN RESULTS BLADE ANGLE = 55°

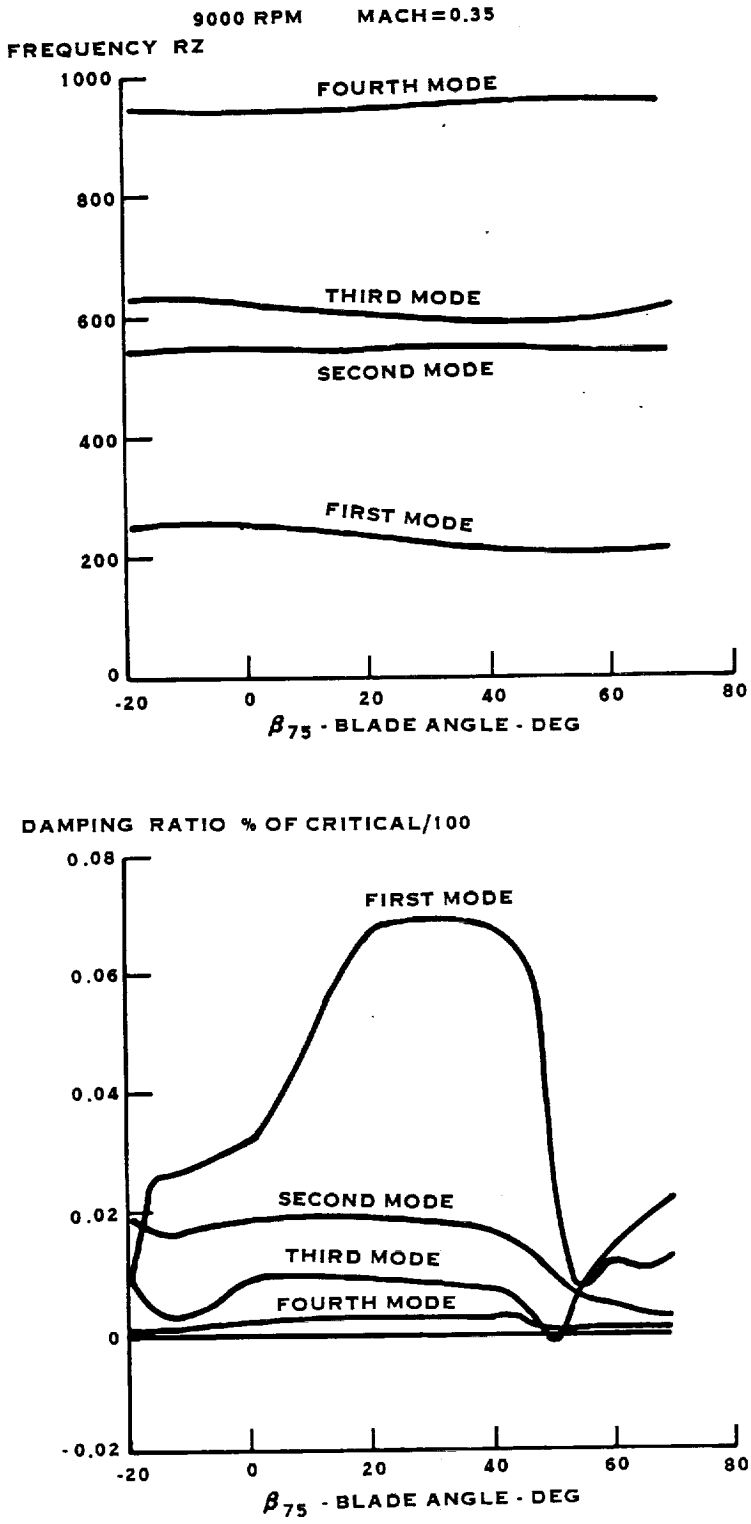

FIGURE 3-8. CALCULATED BLADE FREQUENCIES AND DAMPING RATIO'S FOR THE SR-2 PROP-FAN MODEL USING THE F203 ANALYSIS

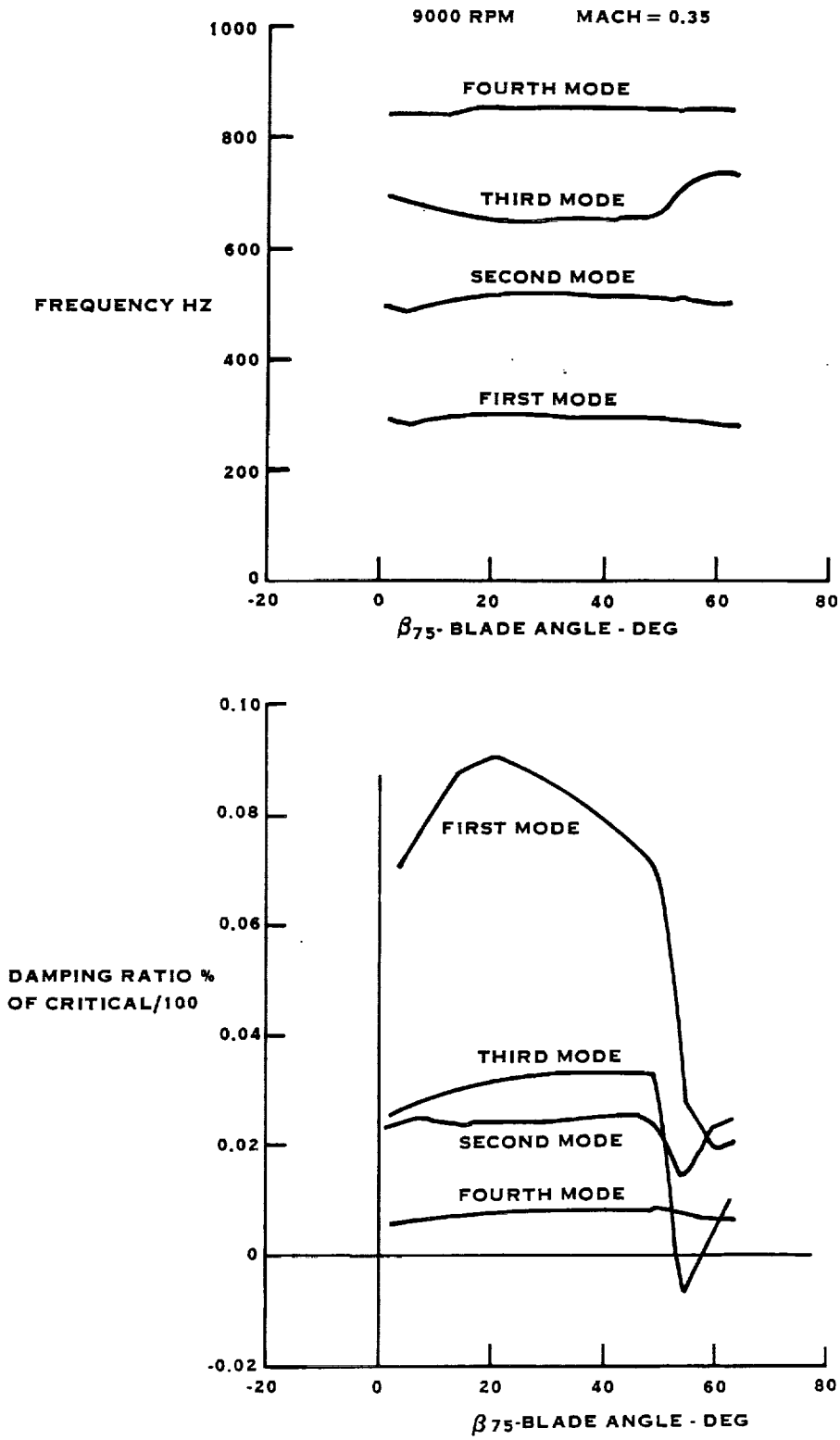

FIGURE 3-9. CALCULATED BLADE FREQUENCIES AND DAMPING RATIOS FOR THE SR-3 PROP-FAN MODEL USING THE F203 ANALYSIS

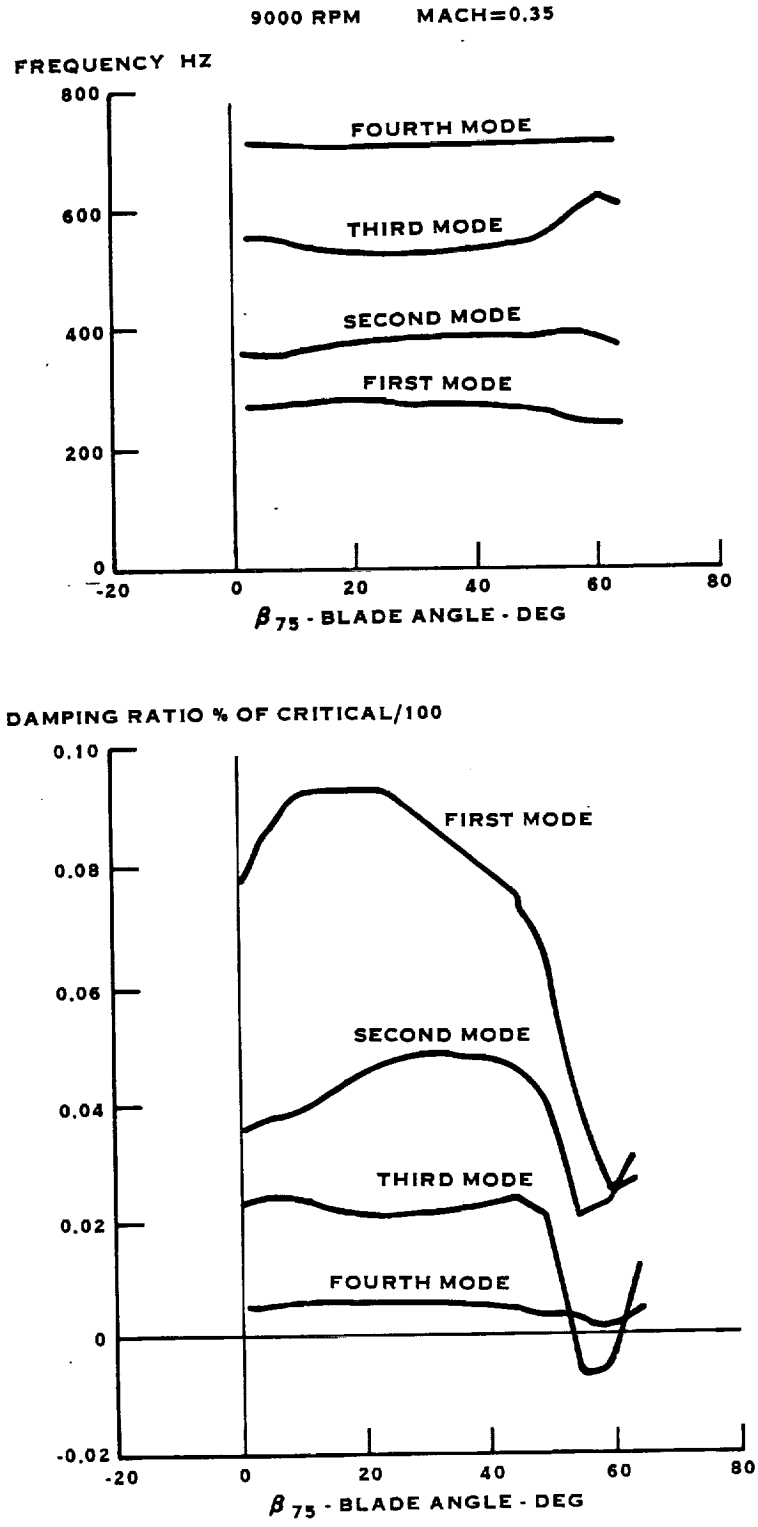

FIGURE 3-10. CALCULATED BLADE FREQUENCIES AND DAMPING RATIO'S FOR THE SR-5 PROP-FAN MODEL USING THE F203 ANALYSIS

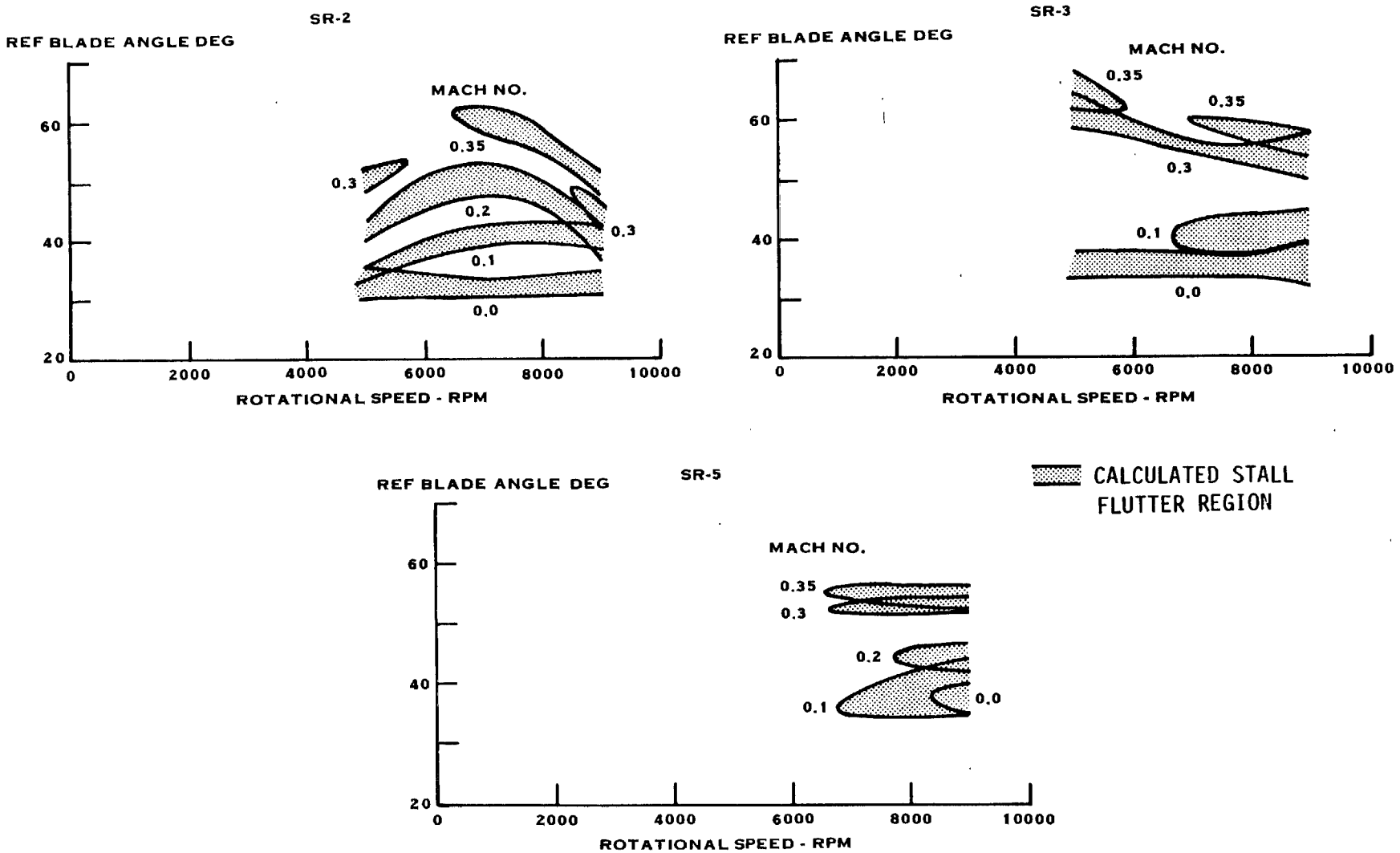

FIGURE 3–11. PROP–FAN 10 X 10 LOW SPEED WIND TUNNEL TESTS AT NASA–LEWIS THIRD MODE CALCULATED FLUTTER BOUNDARIES. (NO STRUCTURAL DAMPING)

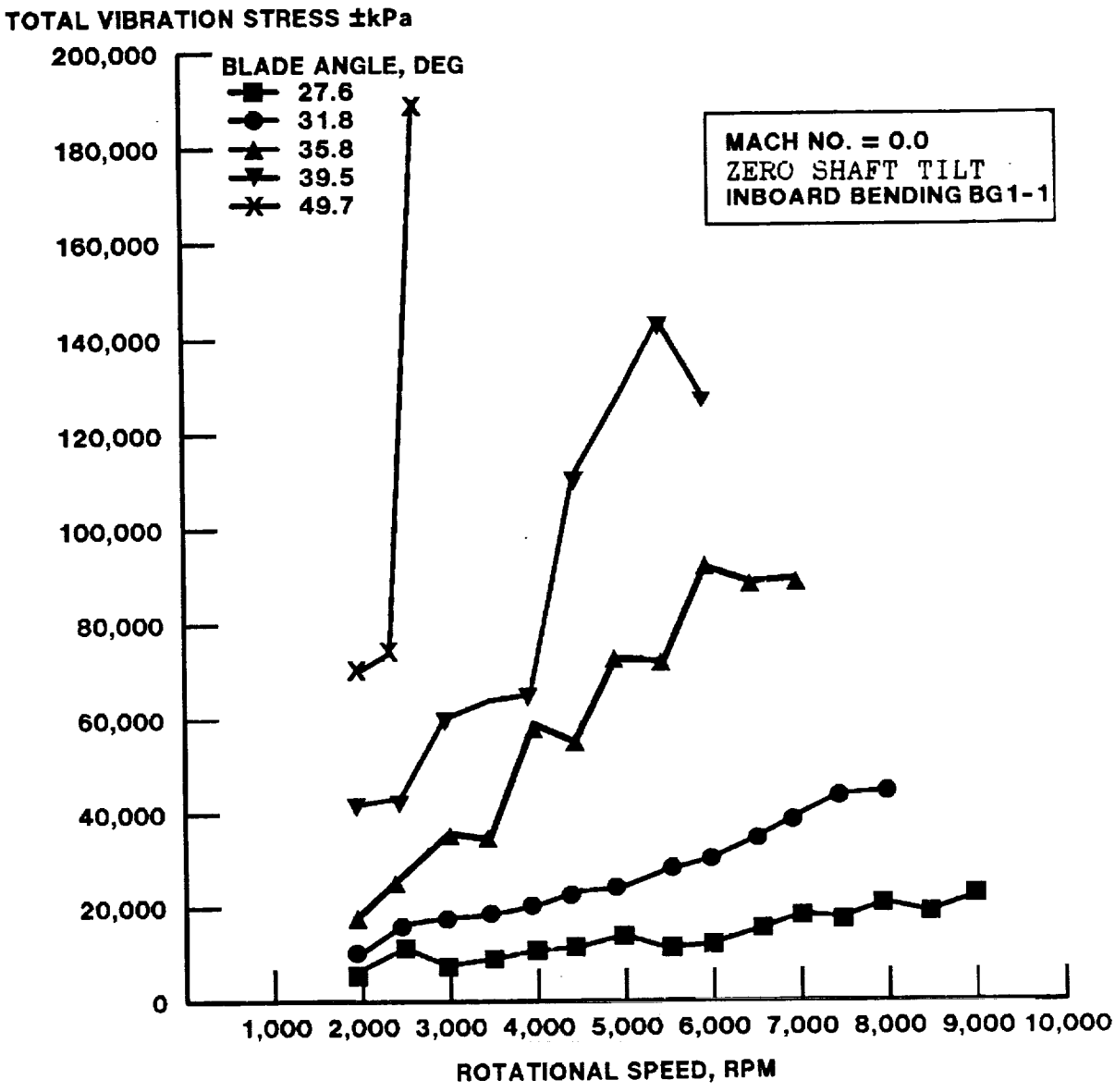

FIGURE 4-1. SR-2 MODEL BLADE 10 X 10 LOW SPEED WIND TUNNEL TESTS AT NASA LEWIS

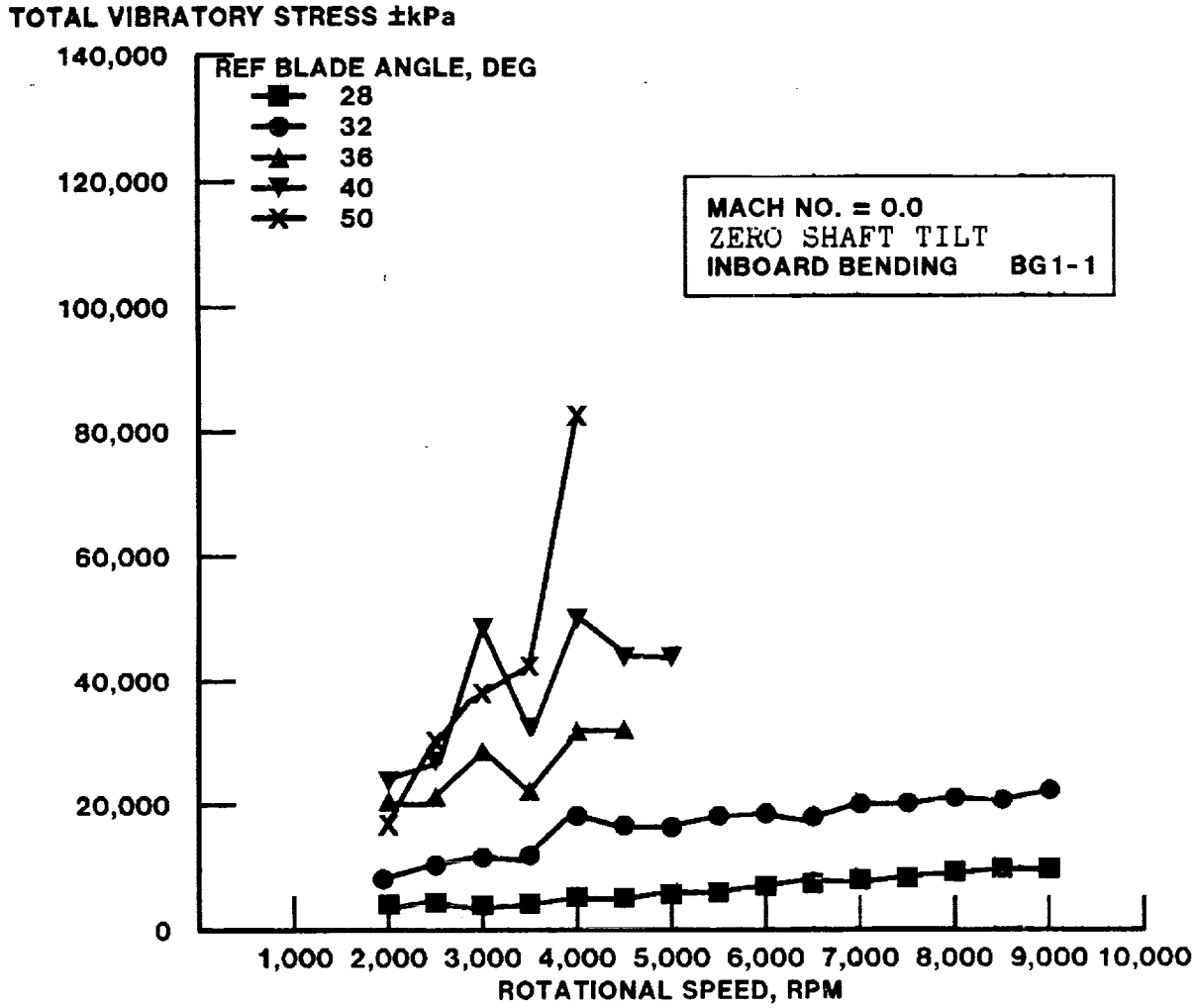

FIGURE 4-2. SR-3 MODEL BLADE 10 X 10 LOW SPEED WIND TUNNEL TESTS AT NASA LEWIS

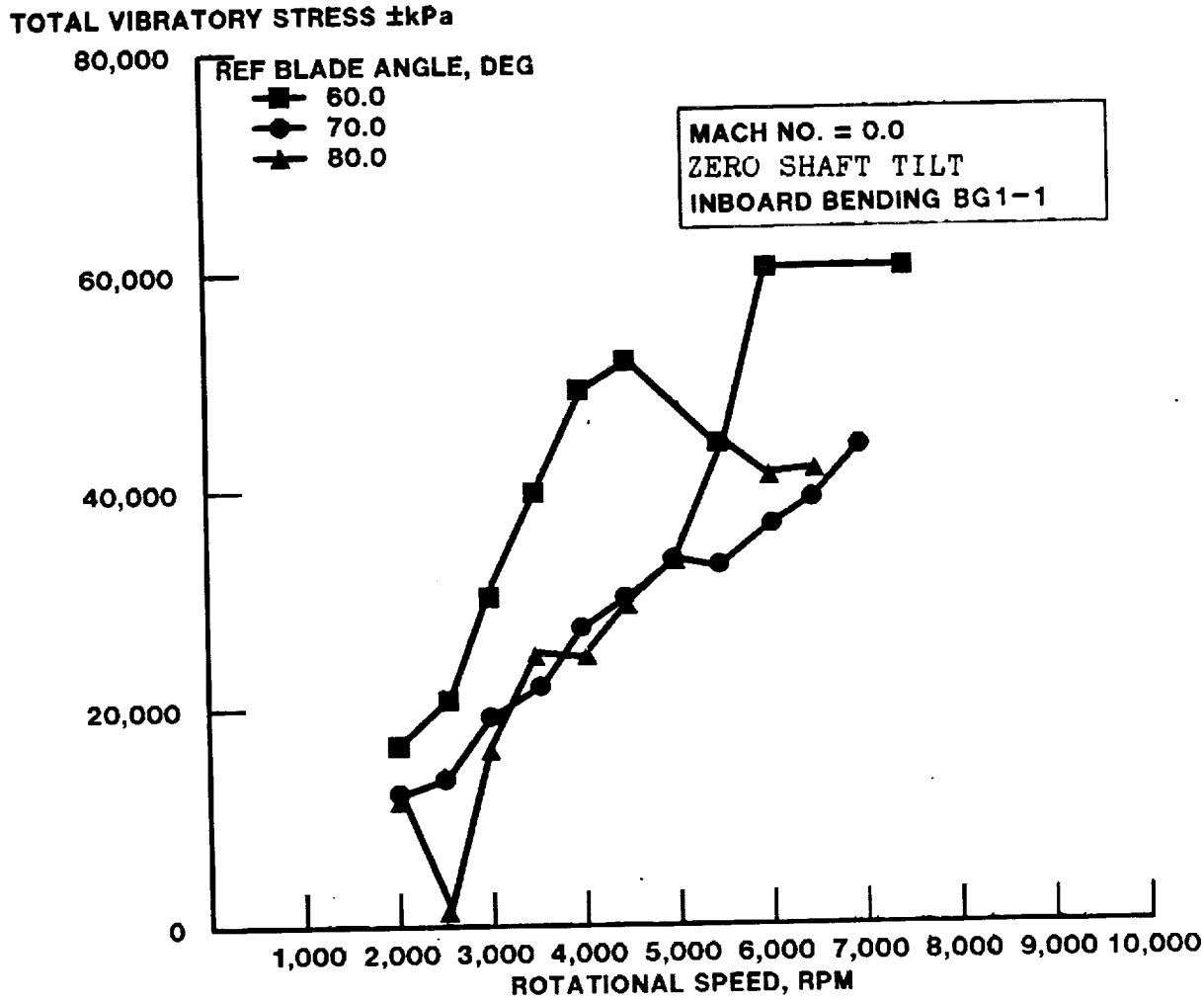

FIGURE 4-2. (CONTINUED)

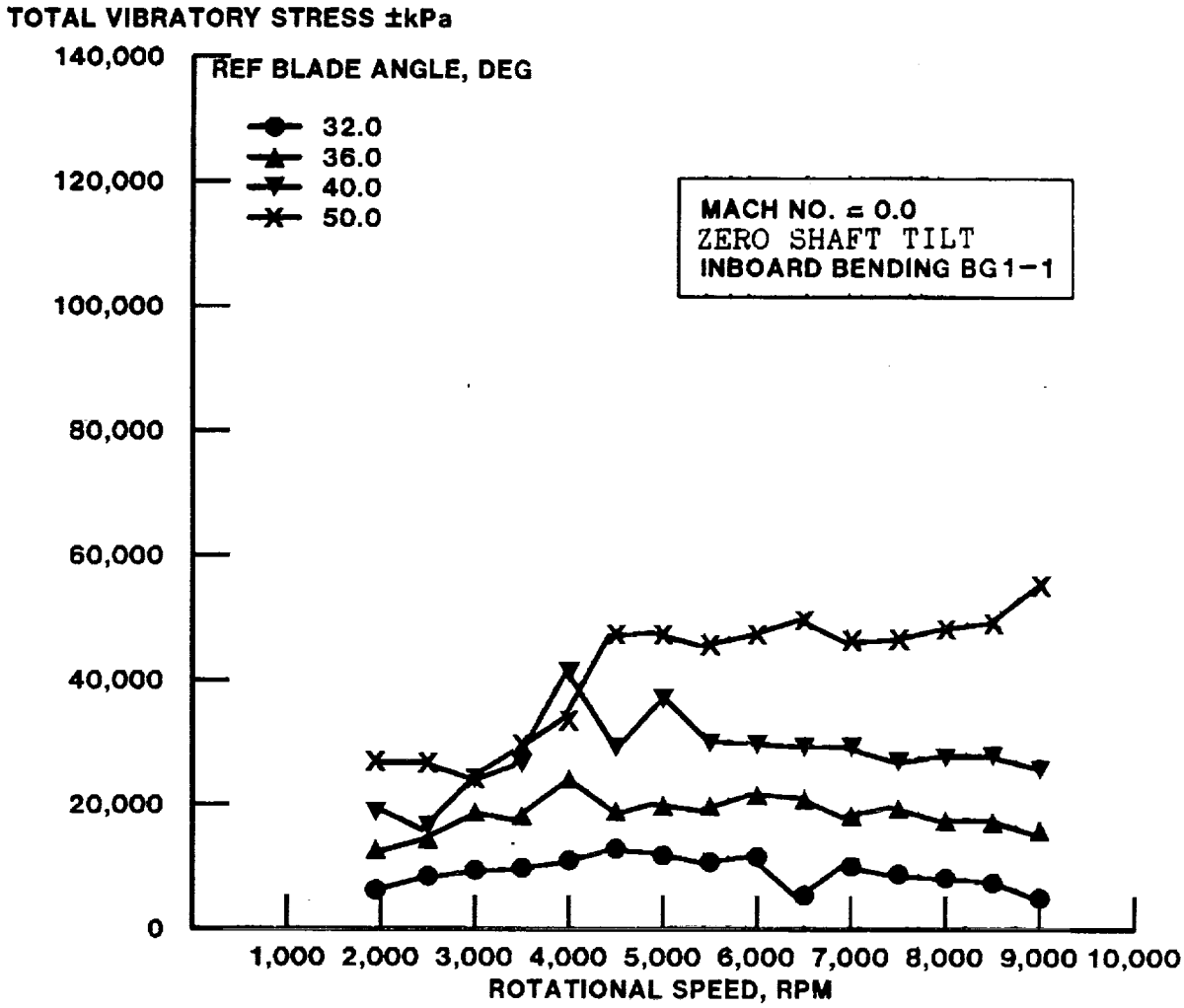

FIGURE 4-3. SR-5 MODEL BLADE 10 X 10 LOW SPEED WIND TUNNEL TESTS AT NASA LEWIS

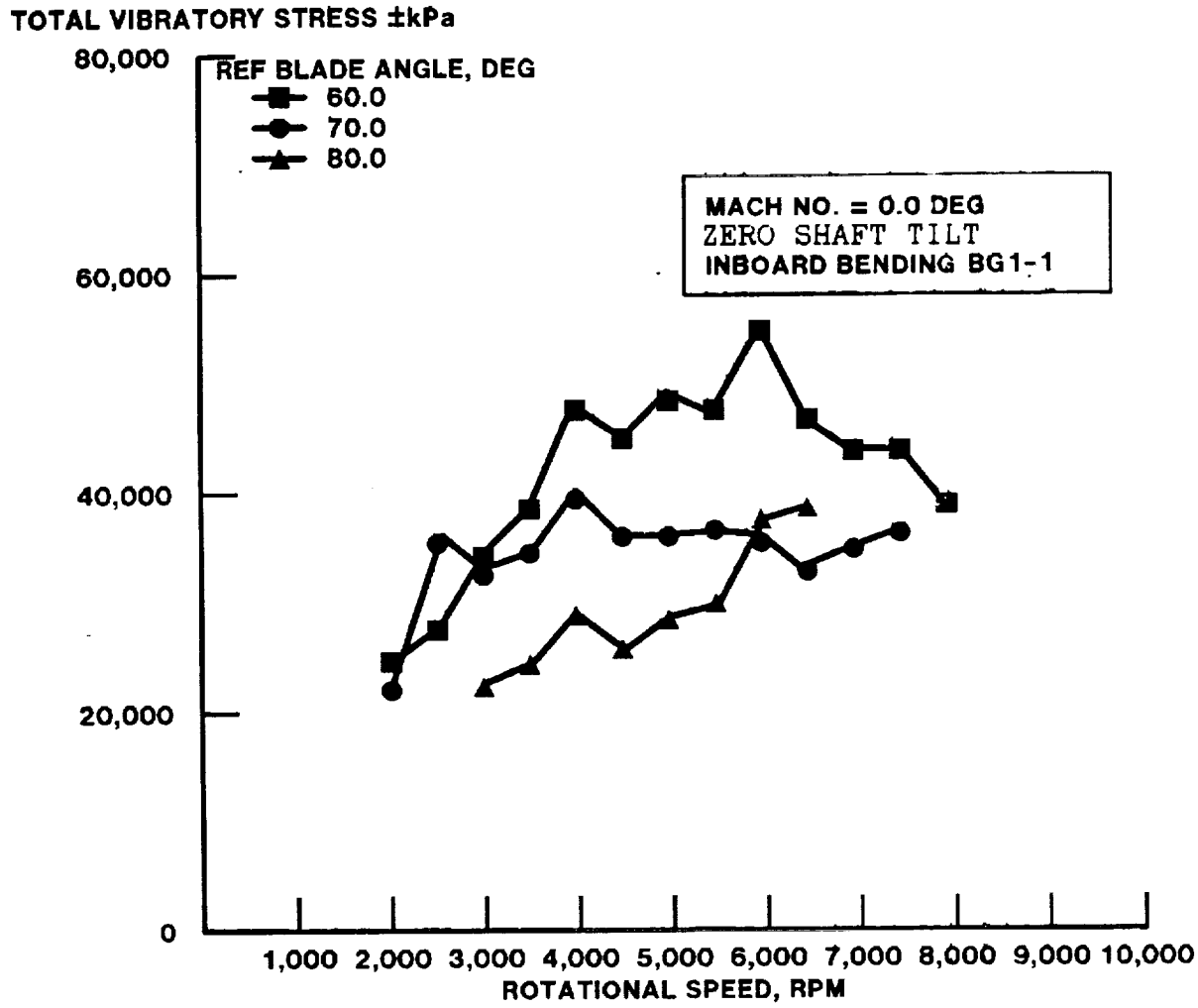

FIGURE 4-3. (CONTINUED)

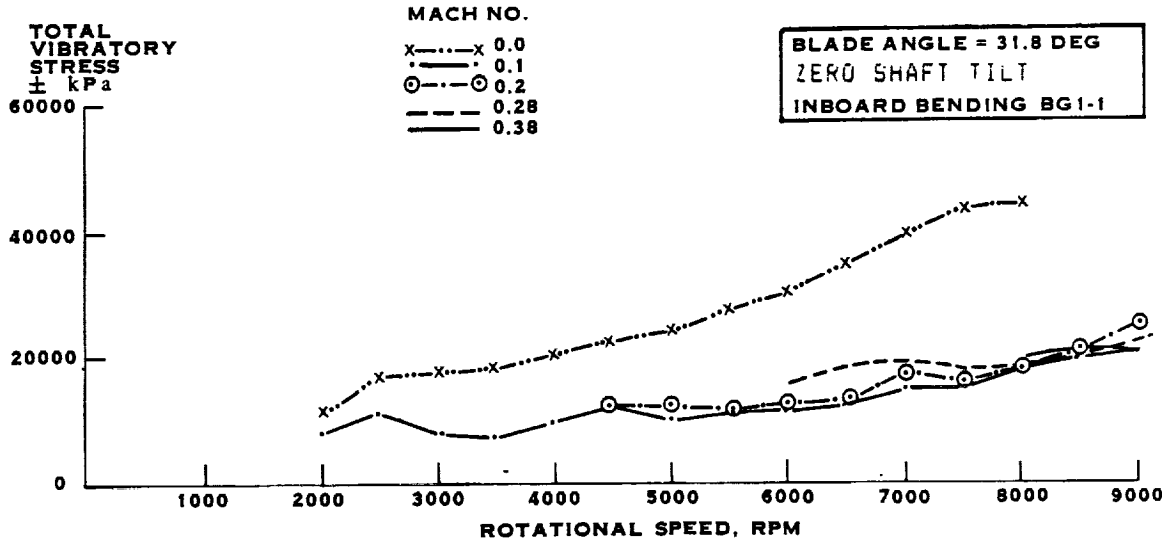

FIGURE 4-4. SR-2 MODEL BLADE 10 X 10 LOW SPEED WIND TUNNEL TESTS AT NASA LEWIS

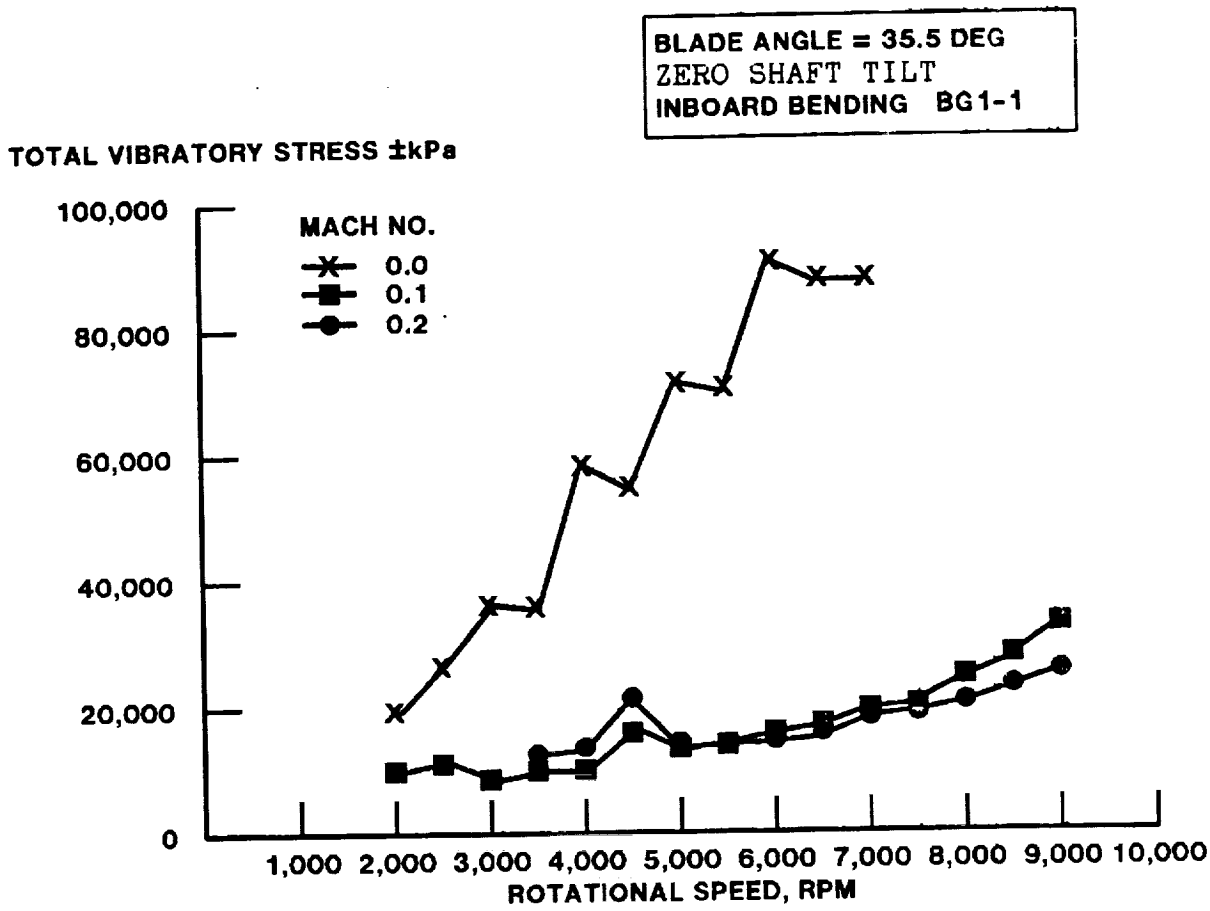

FIGURE 4-5. SR-2 MODEL BLADE 10 X 10 LOW SPEED WIND TUNNEL TESTS AT NASA LEWIS

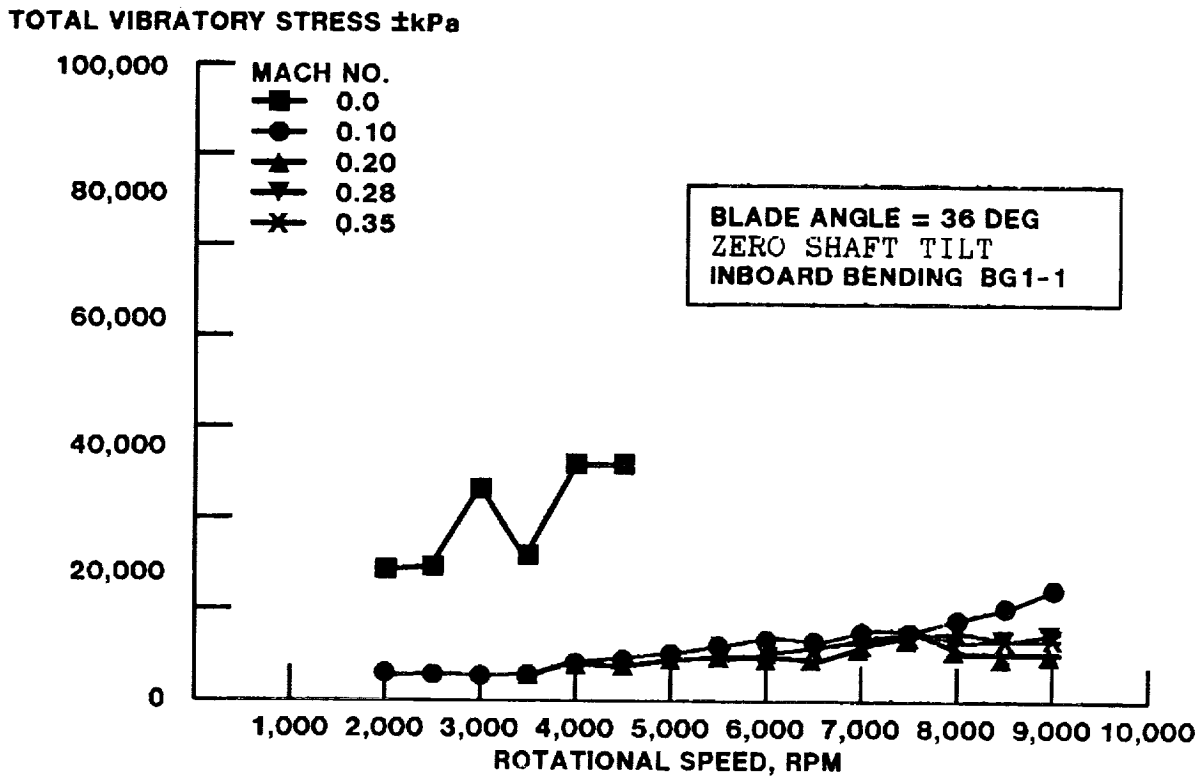

FIGURE 4-6. SR-3 MODEL BLADE 10 X 10 LOW SPEED WIND TUNNEL TESTS AT NASA LEWIS

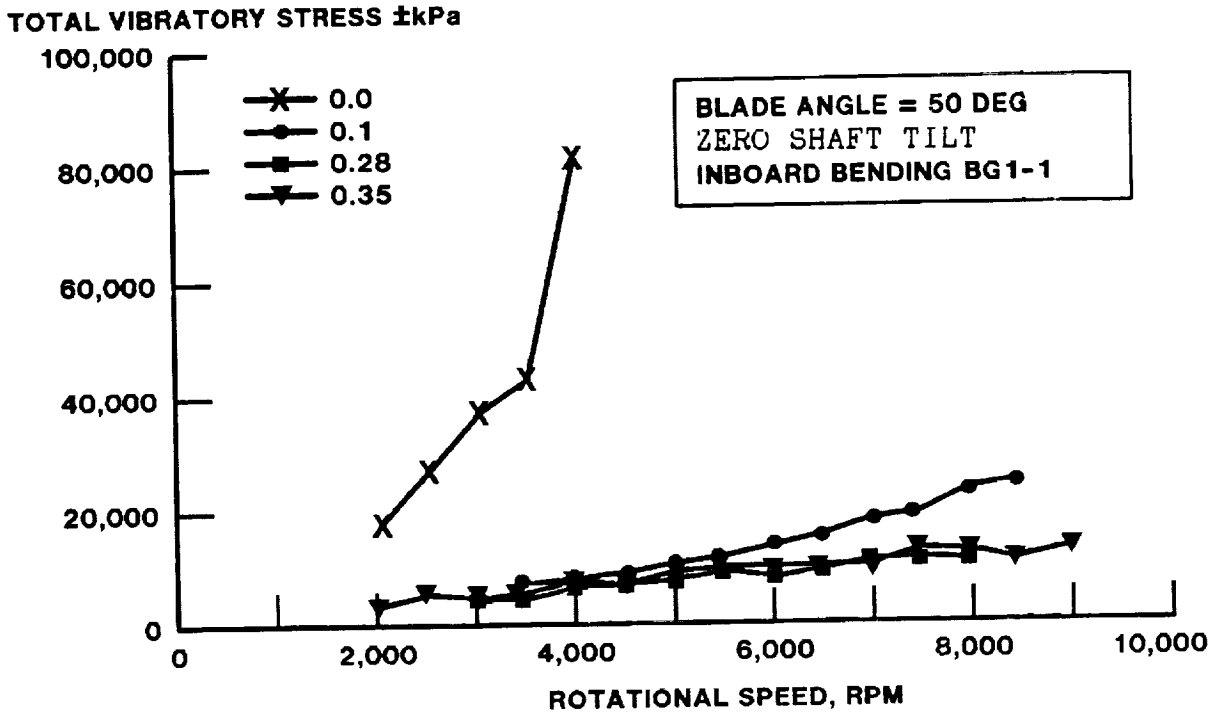

FIGURE 4-7. SR-3 MODEL BLADE 10 X 10 LOW SPEED WIND TUNNEL TESTS AT NASA LEWIS

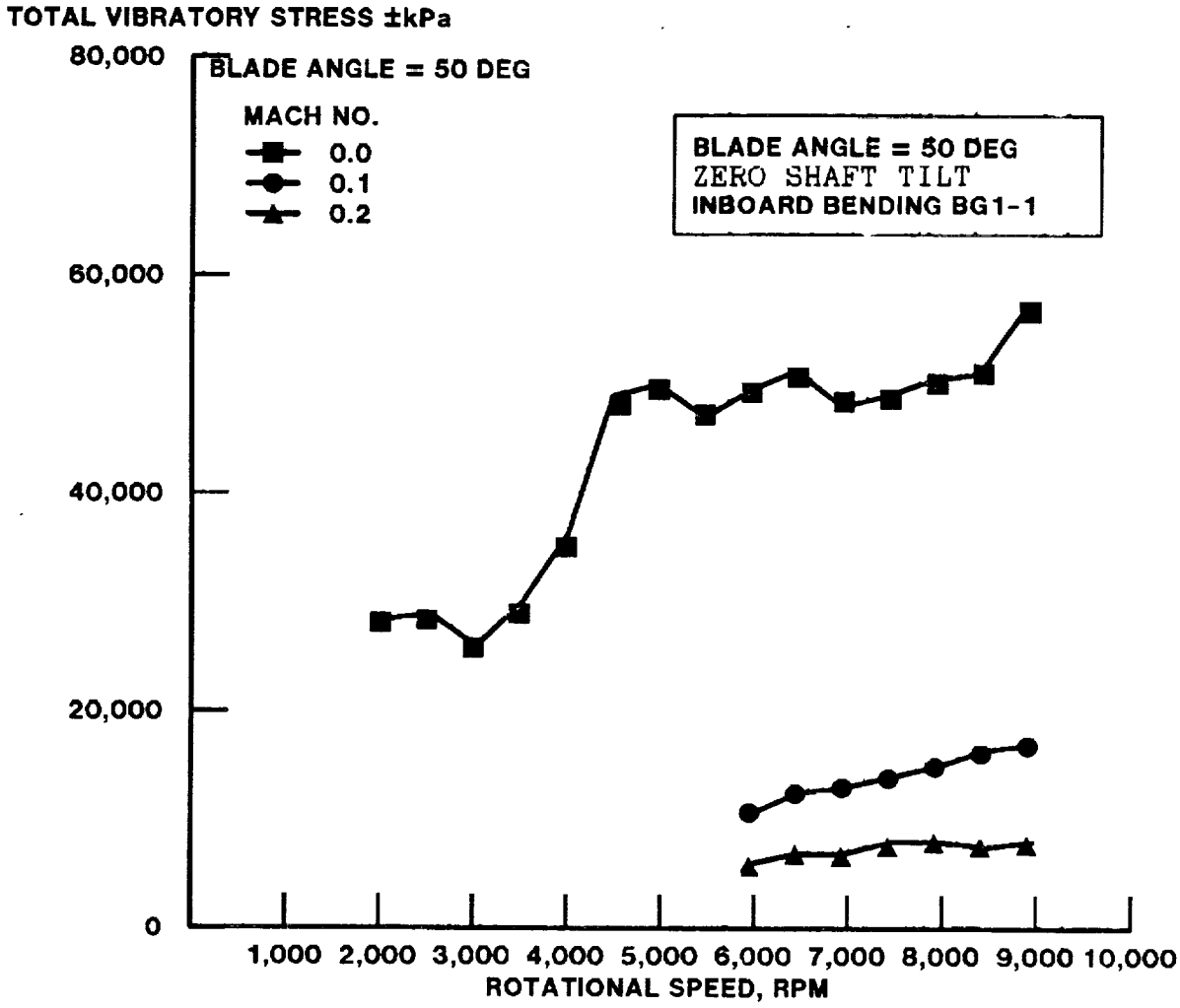

FIGURE 4-8. SR-5 MODEL BLADE 10 X 10 LOW SPEED WIND TUNNEL TESTS AT NASA LEWIS

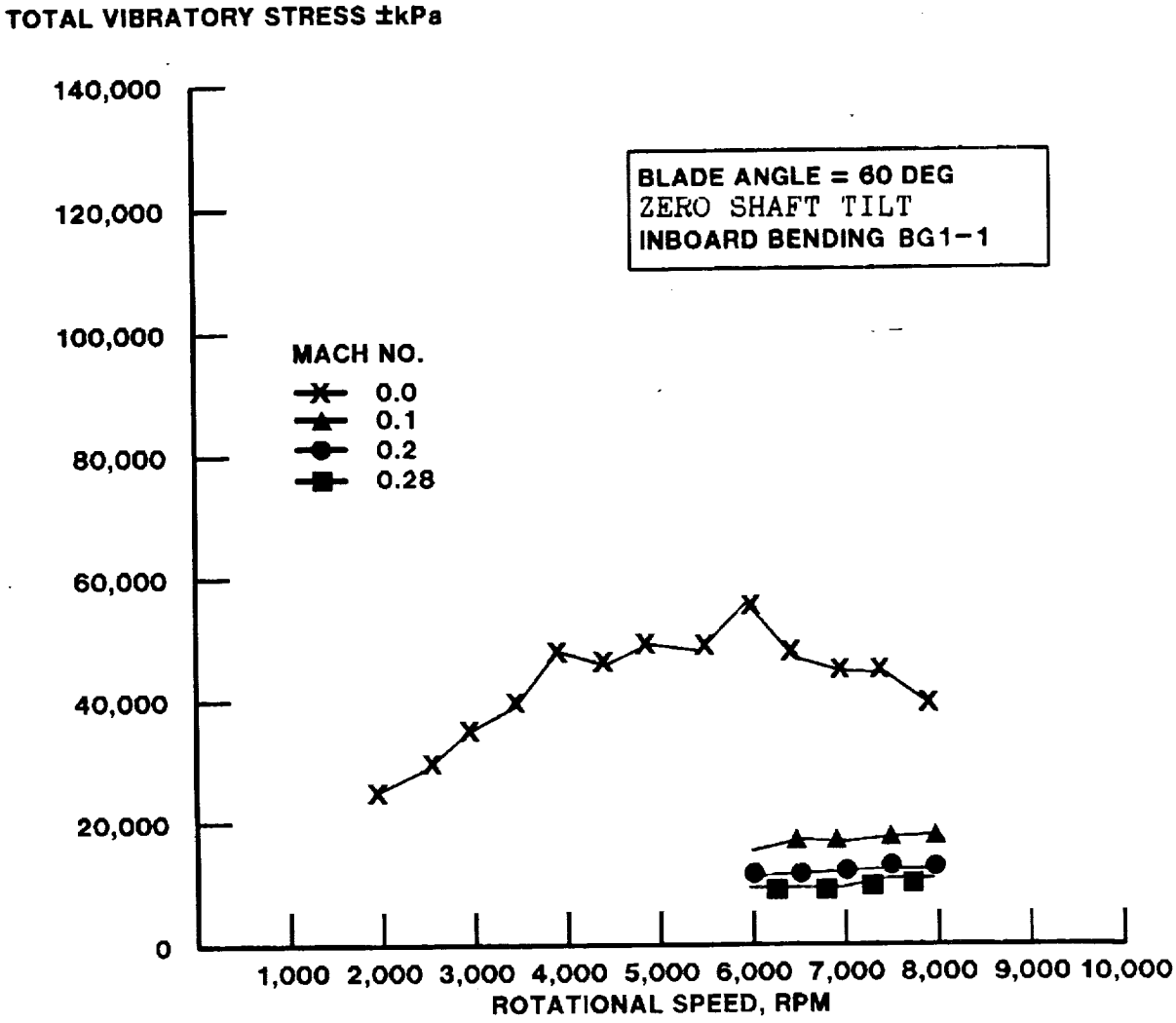

FIGURE 4-9. SR-5 MODEL BLADE 10 X 10 LOW SPEED WIND TUNNEL TESTS AT NASA LEWIS

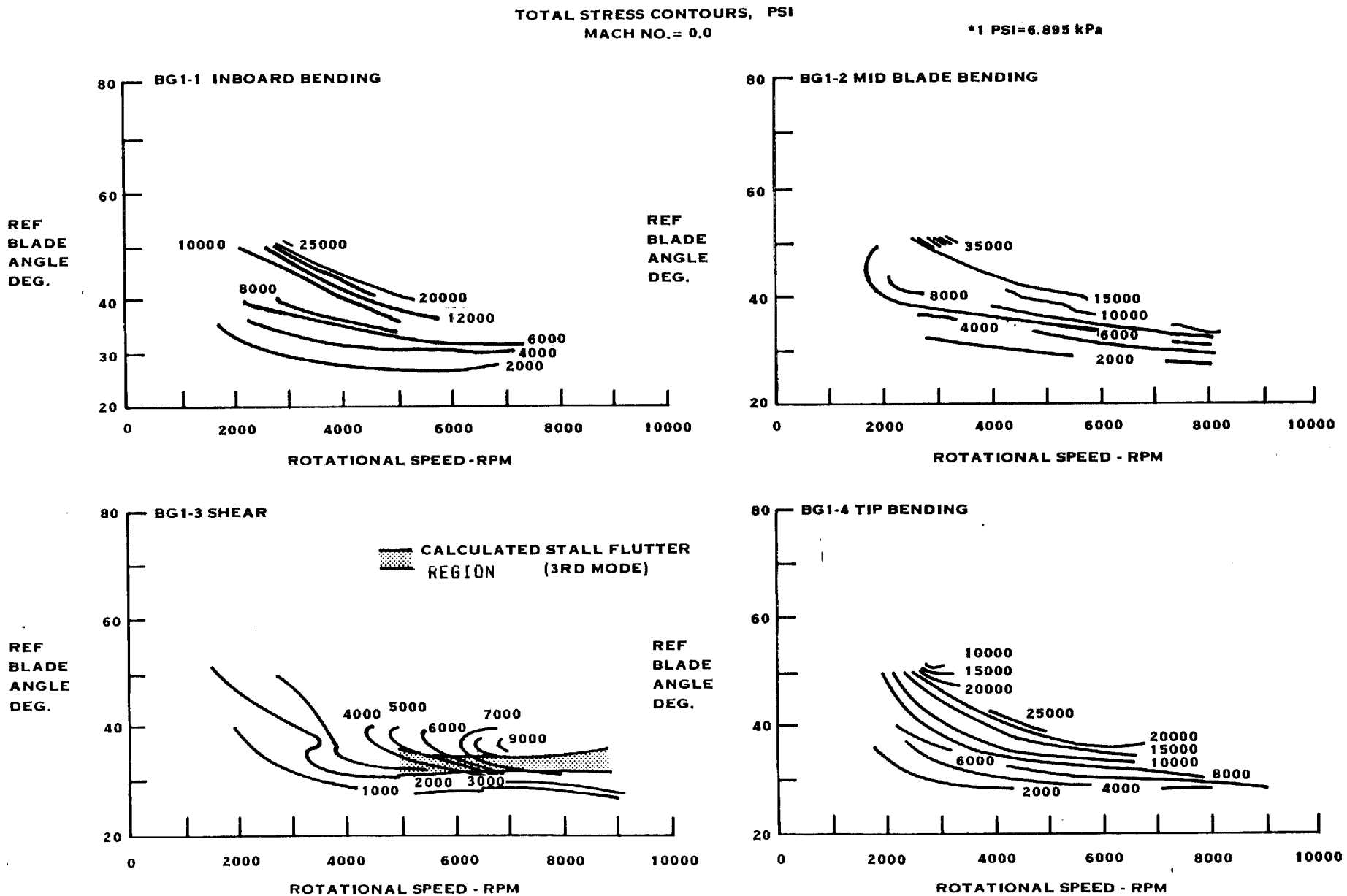

FIGURE 4-10. SR-2 MODEL PROP-FAN 10 X 10 LOW SPEED WIND TUNNEL TESTS AT NASA-LEWIS

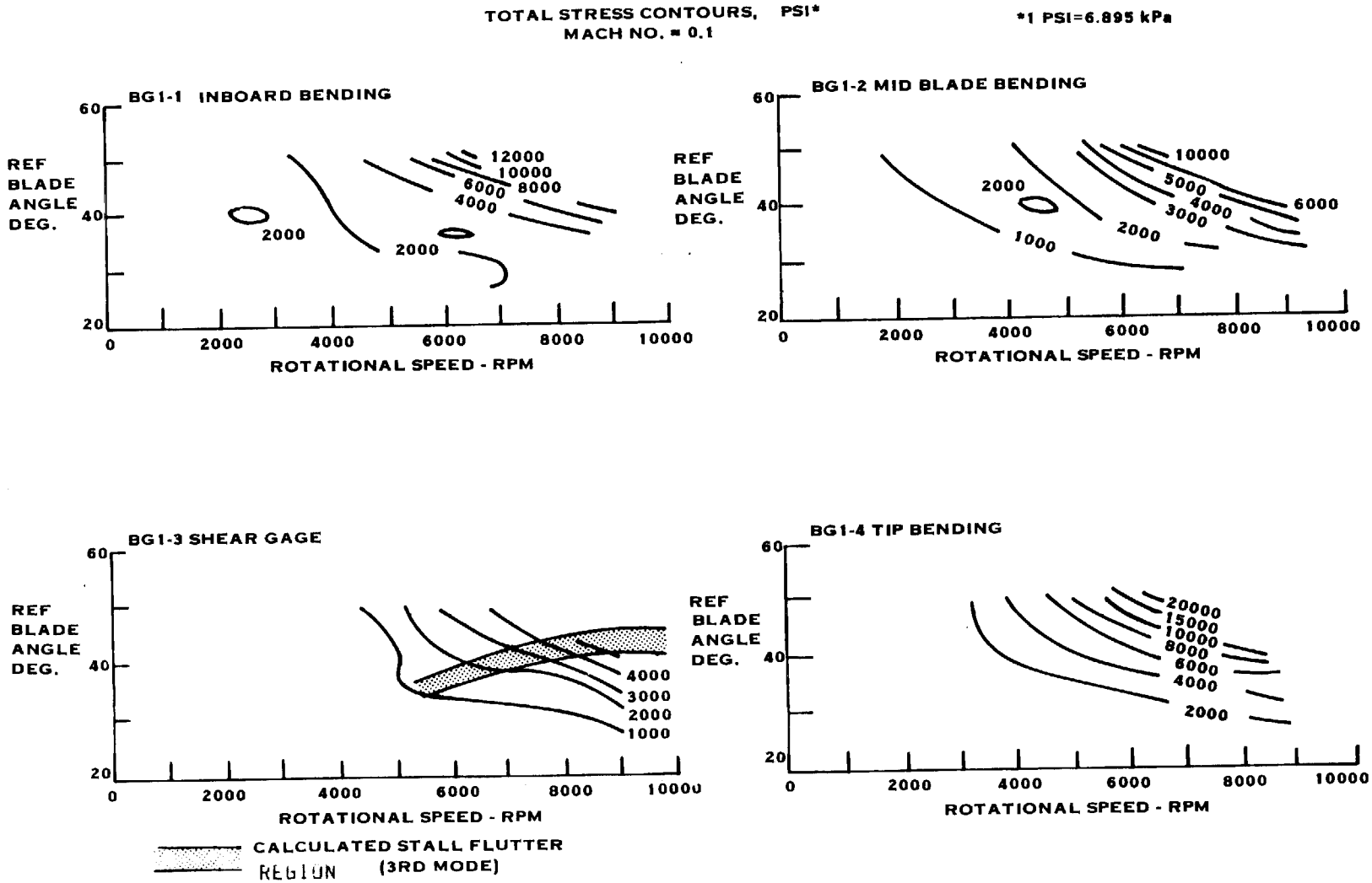

FIGURE 4-11. SR-2 MODEL PROP-FAN 10 X 10 LOW SPEED WIND TUNNEL TESTS AT NASA-LEWIS

MACH NO. = 0.0
RPM=6270
BLADE ANGLE = 39,5°
NO TILT

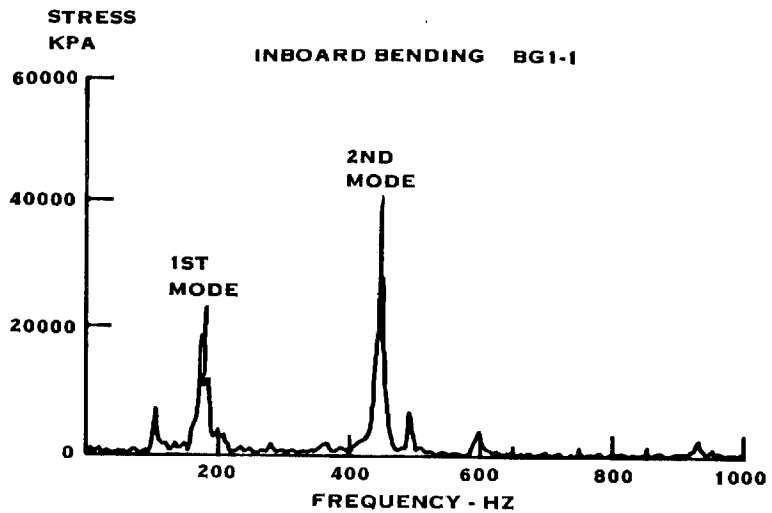

MODE	(bω/V).8
1	.307
2	.750
3	1.014

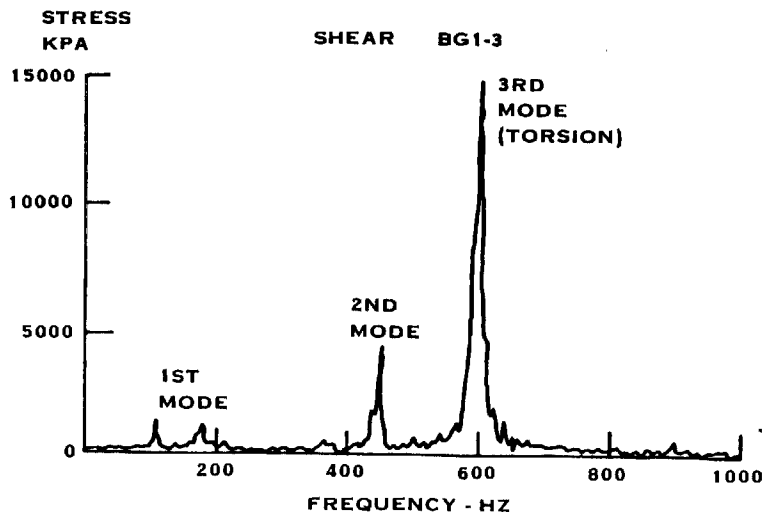

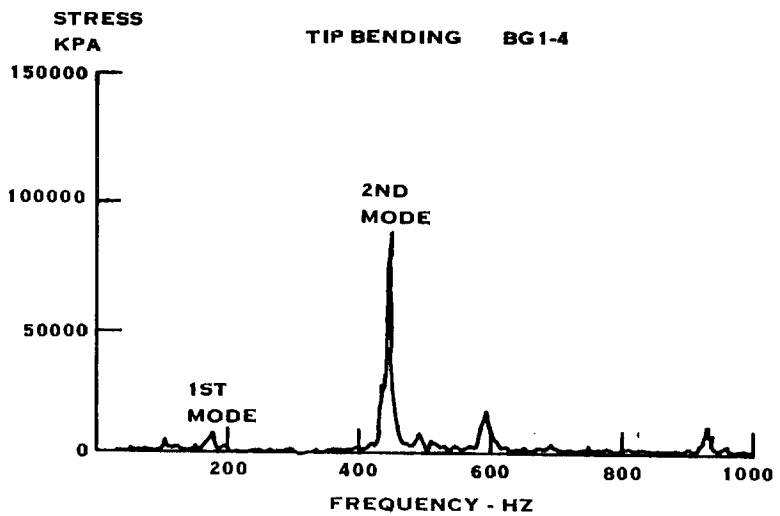

MACH NO. = 0.1
8000 RPM NO TILT
BLADE ANGLE = 31.8

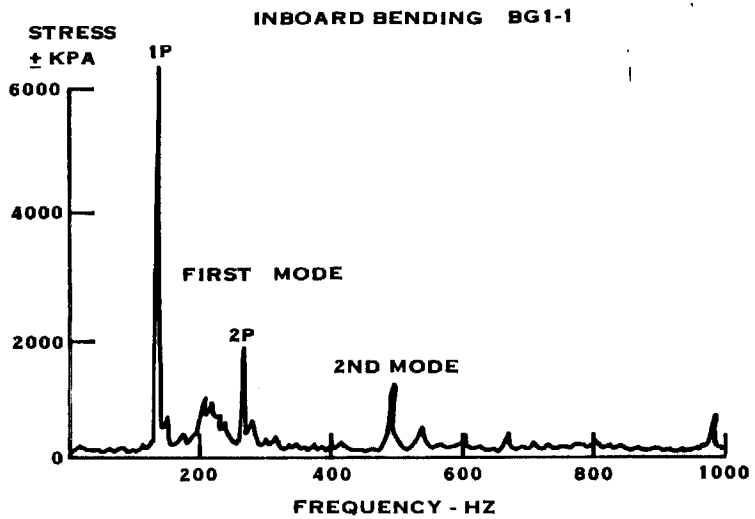

MODE	(bω/V).8
1	.272
2	.642
3	.778

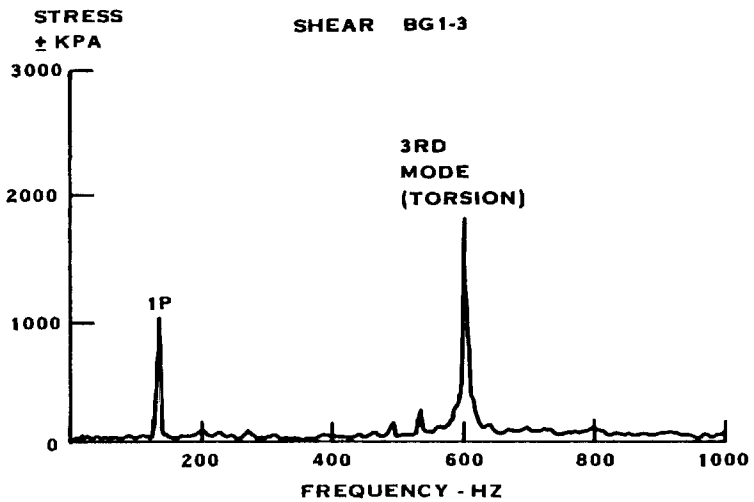

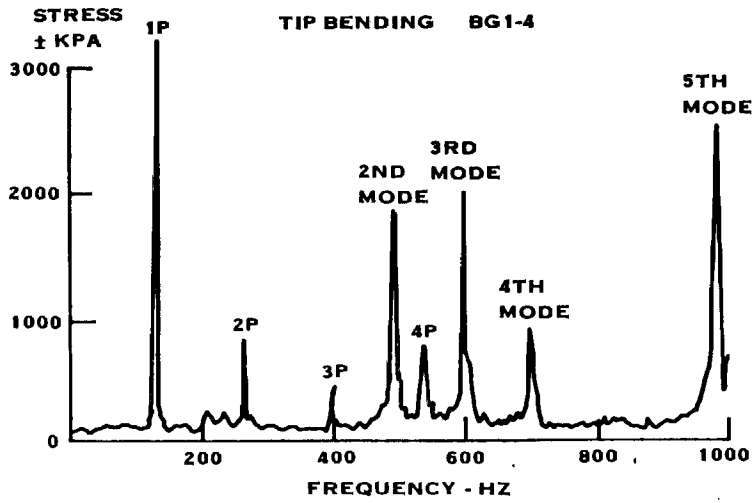

FIGURE 4-13. SR-2 PROP-FAN NASA-LEWIS 10 X 10 WIND TUNNEL TESTS

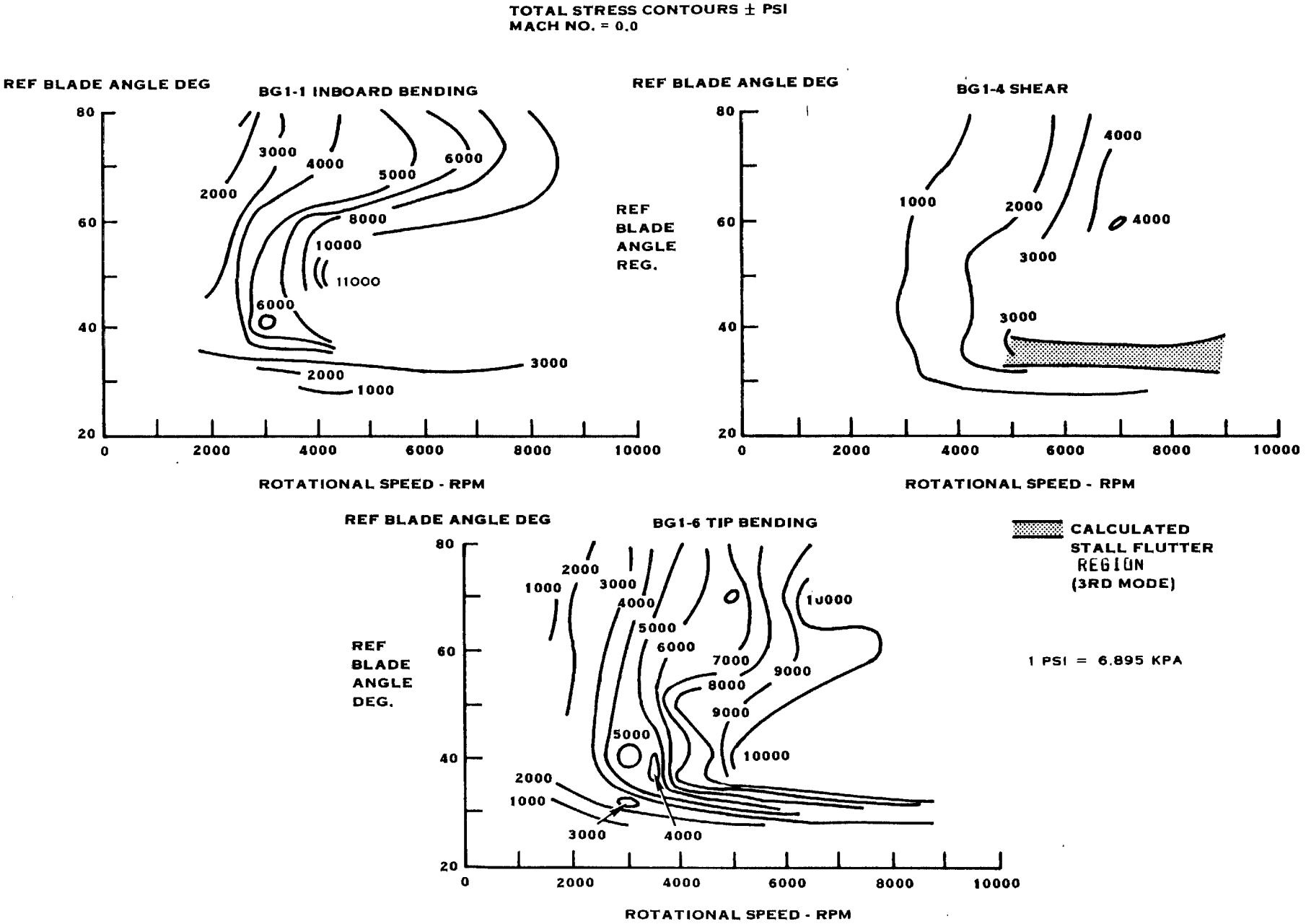

FIGURE 4-14. SR-3 MODEL PROP-FAN 10 X 10 SPEED WIND TUNNEL TESTS AT NASA-LEWIS

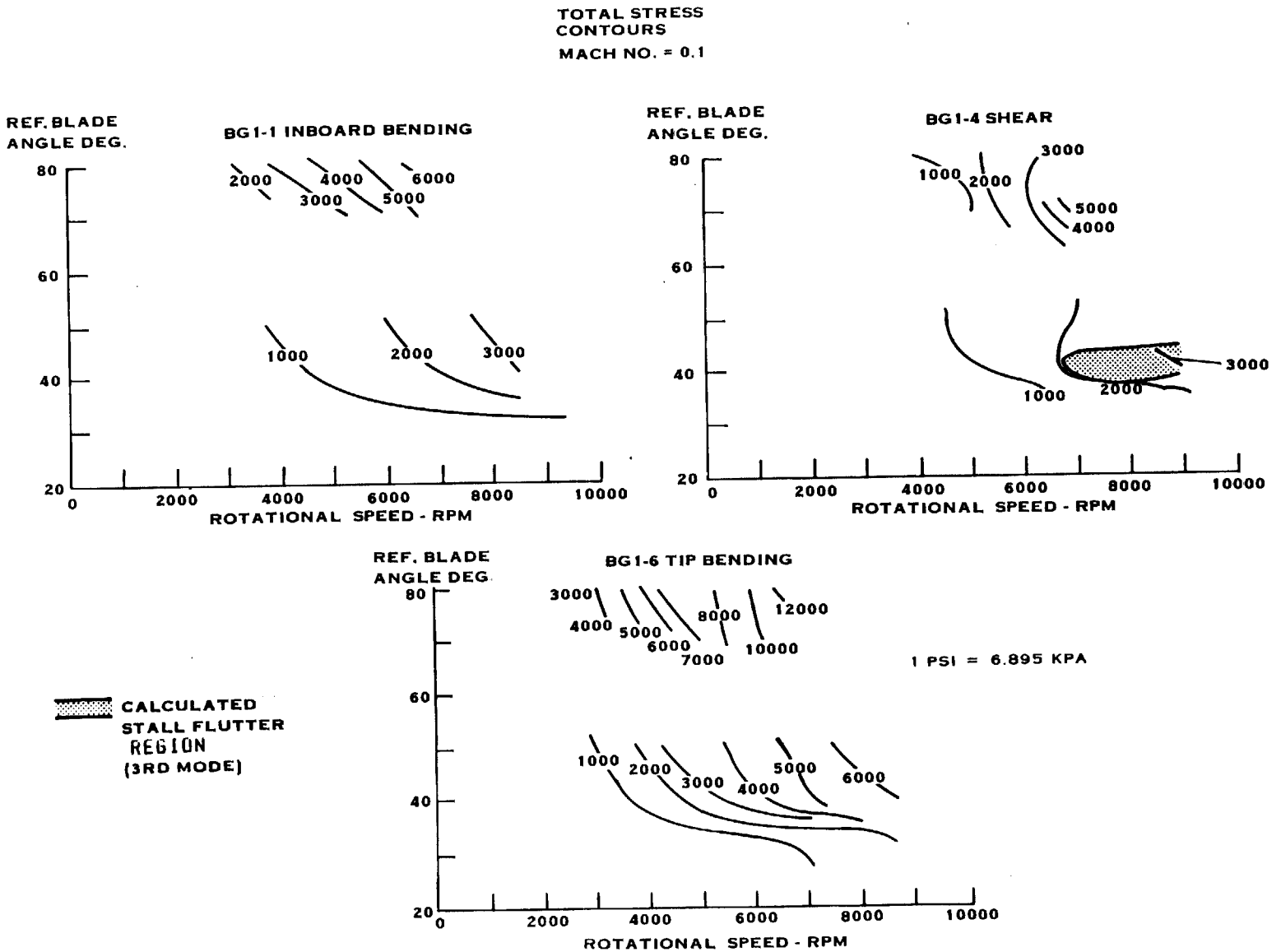

FIGURE 4-15. SR-3 MODEL PROP-FAN 10X10 LOW SPEED WIND TUNNEL TESTS AT NASA-LEWIS TOTAL STRESS CONTOURS, ±PSI MACH NO. = 0.1

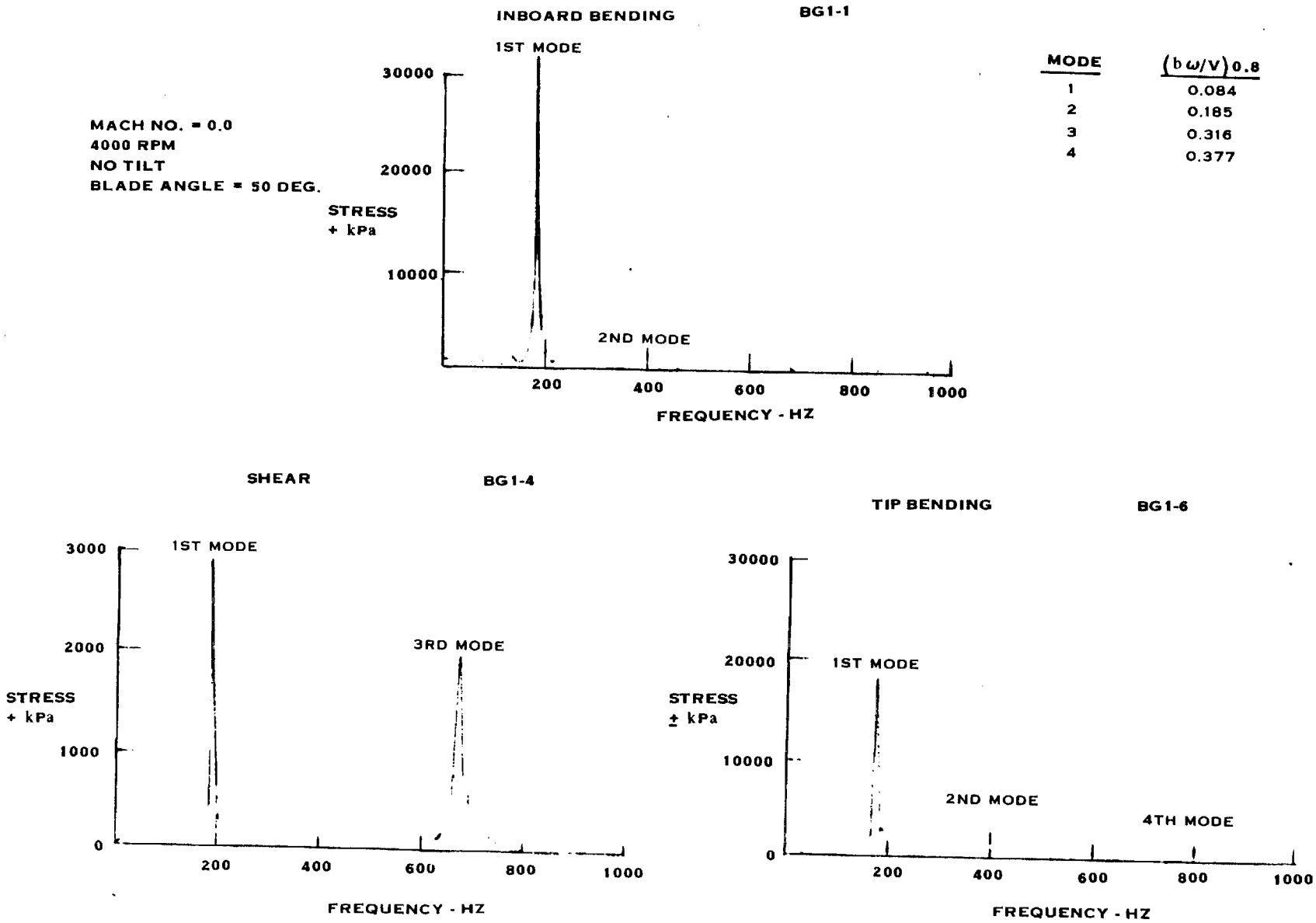

FIGURE 4-16. SR-3 PROP-FAN NASA-LEWIS WIND TUNNEL TEST

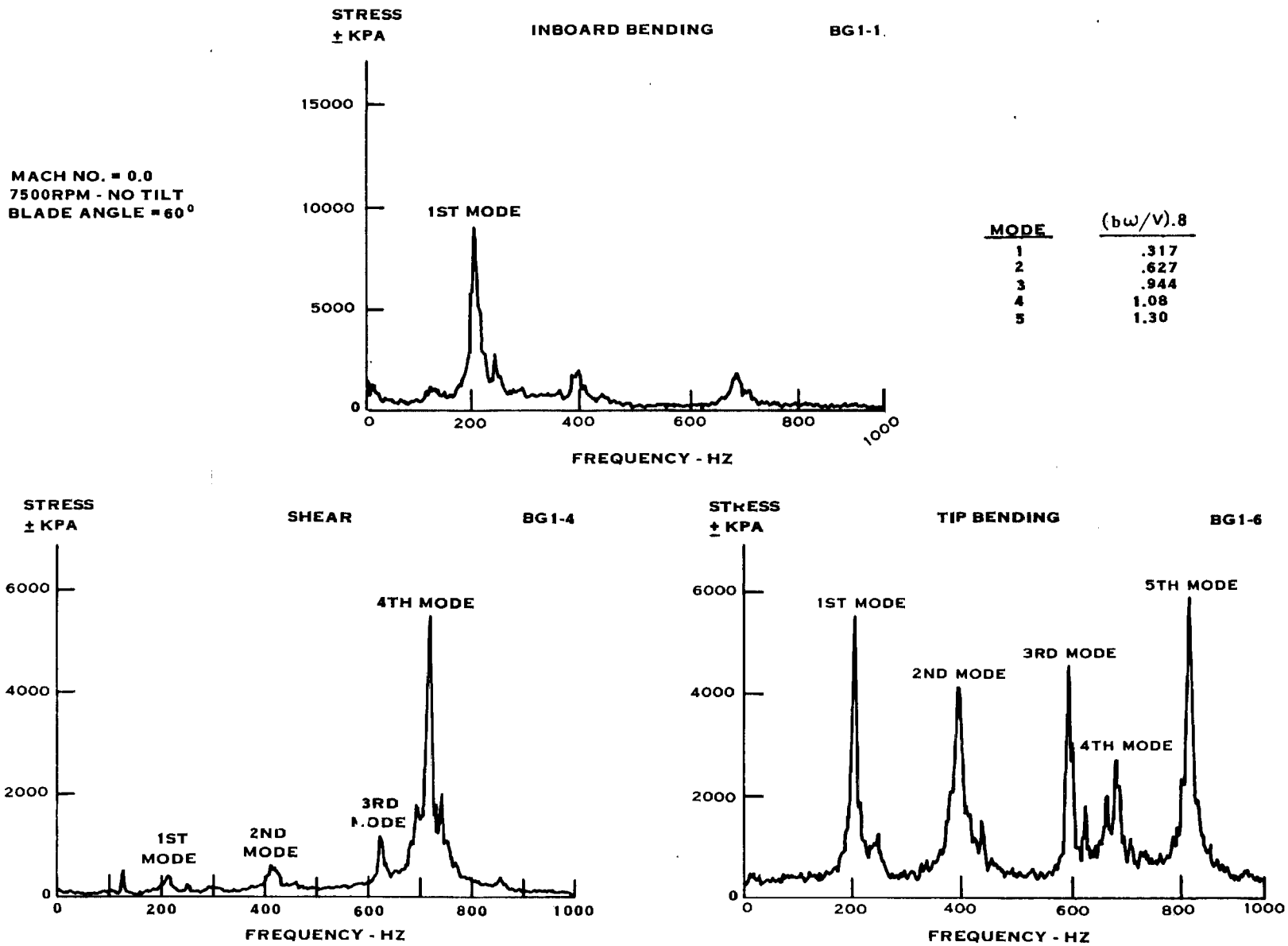

FIGURE 4-17. SR-3 PROP-FAN NASA-LEWIS 10 X 10 WIND TUNNEL TESTS

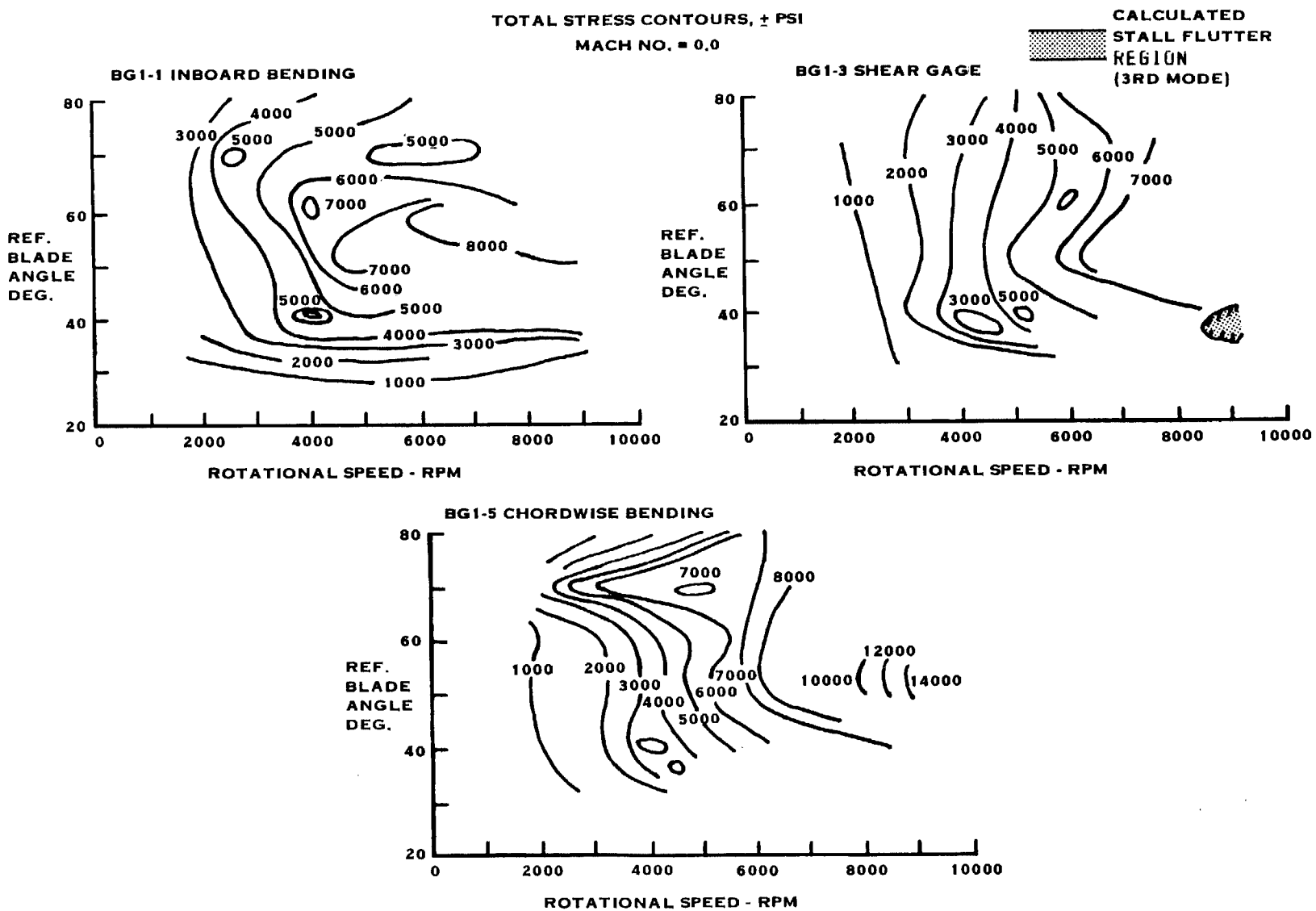

FIGURE 4-18. SR-5 MODEL PROP-FAN 10 X 10 SPEED WIND TUNNEL TESTS AT NASA-LEWIS TOTAL

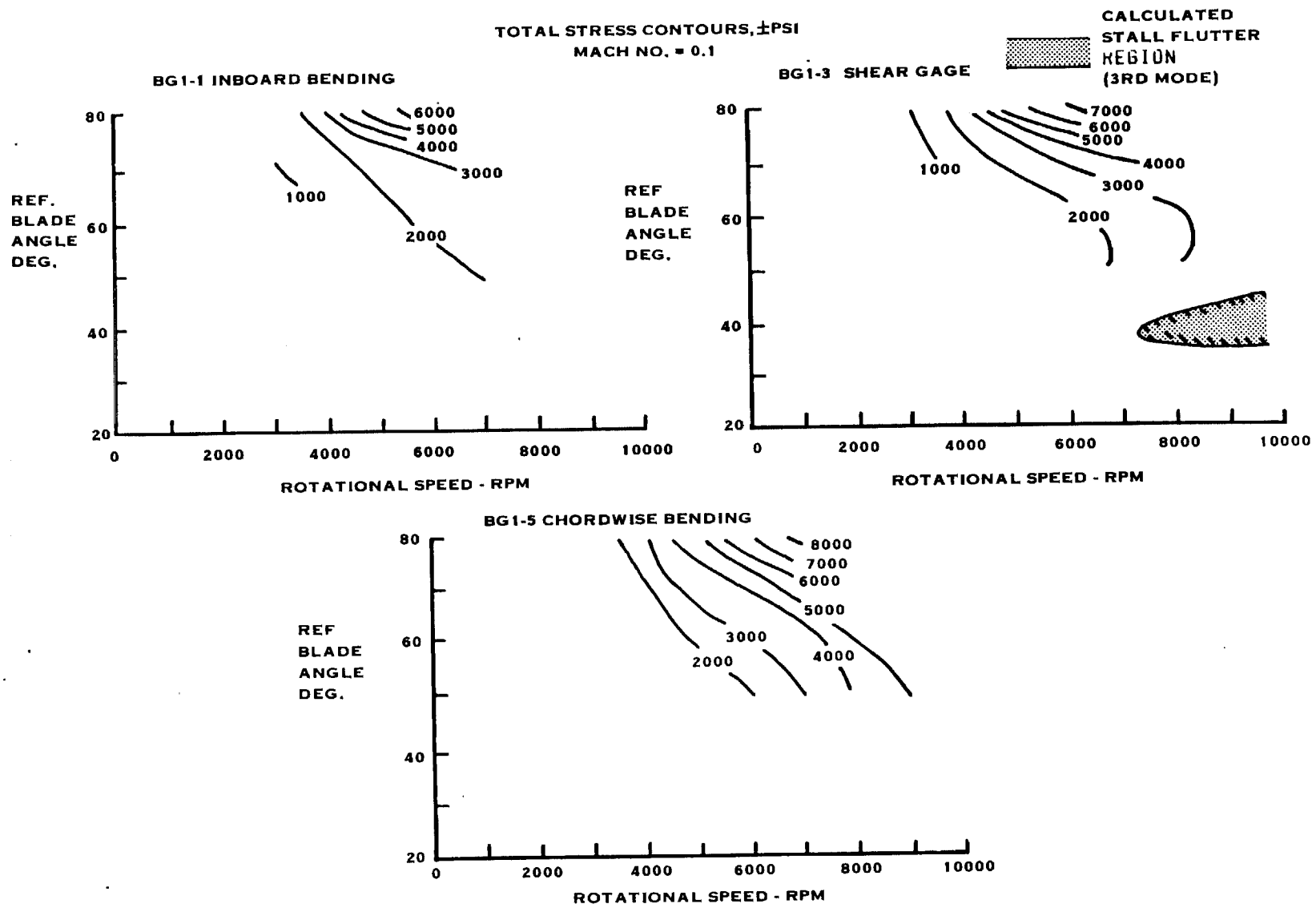

FIGURE 4-19. SR-5 MODEL PROP-FAN 10X10 LOW SPEED WIND TUNNEL TESTS AT NASA-LEWIS

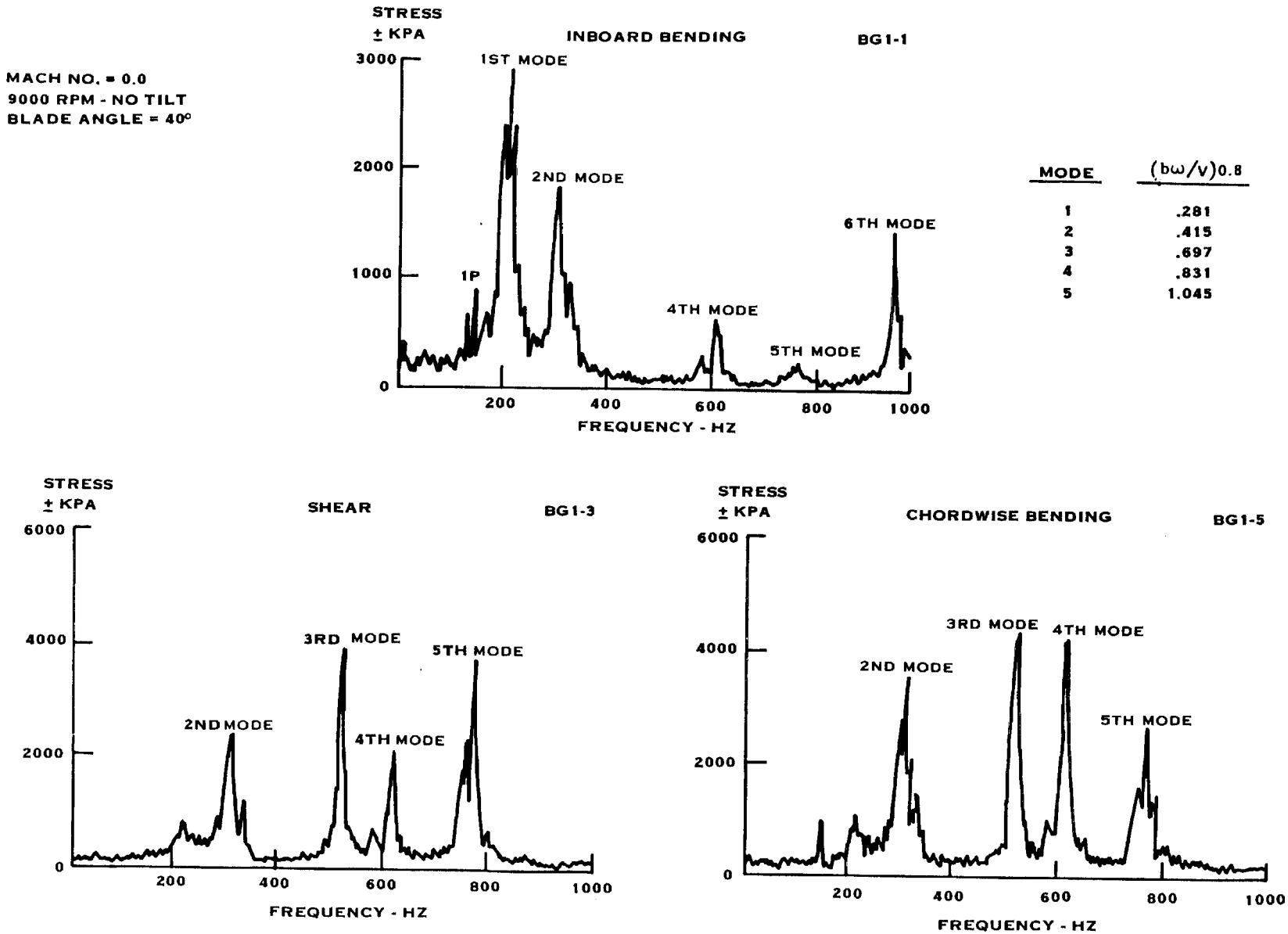

FIGURE 4-20. SR-5 PROP-FAN NASA-LEWIS 10 X 10 WIND TUNNEL TEST

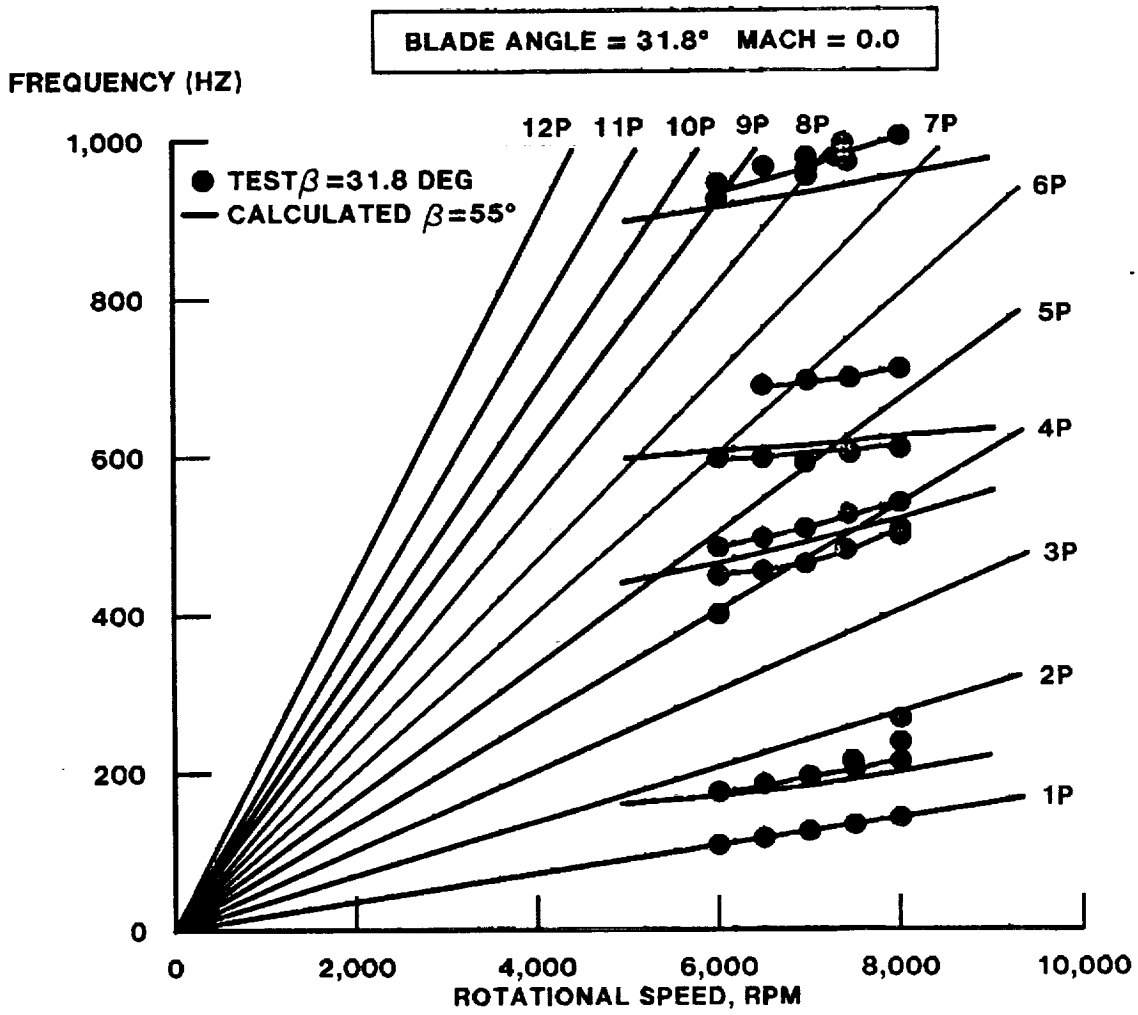

FIGURE 4-21. SR-2 MODEL PROP-FAN

MEASURED AND CALCULATED NATURAL FREQUENCIES

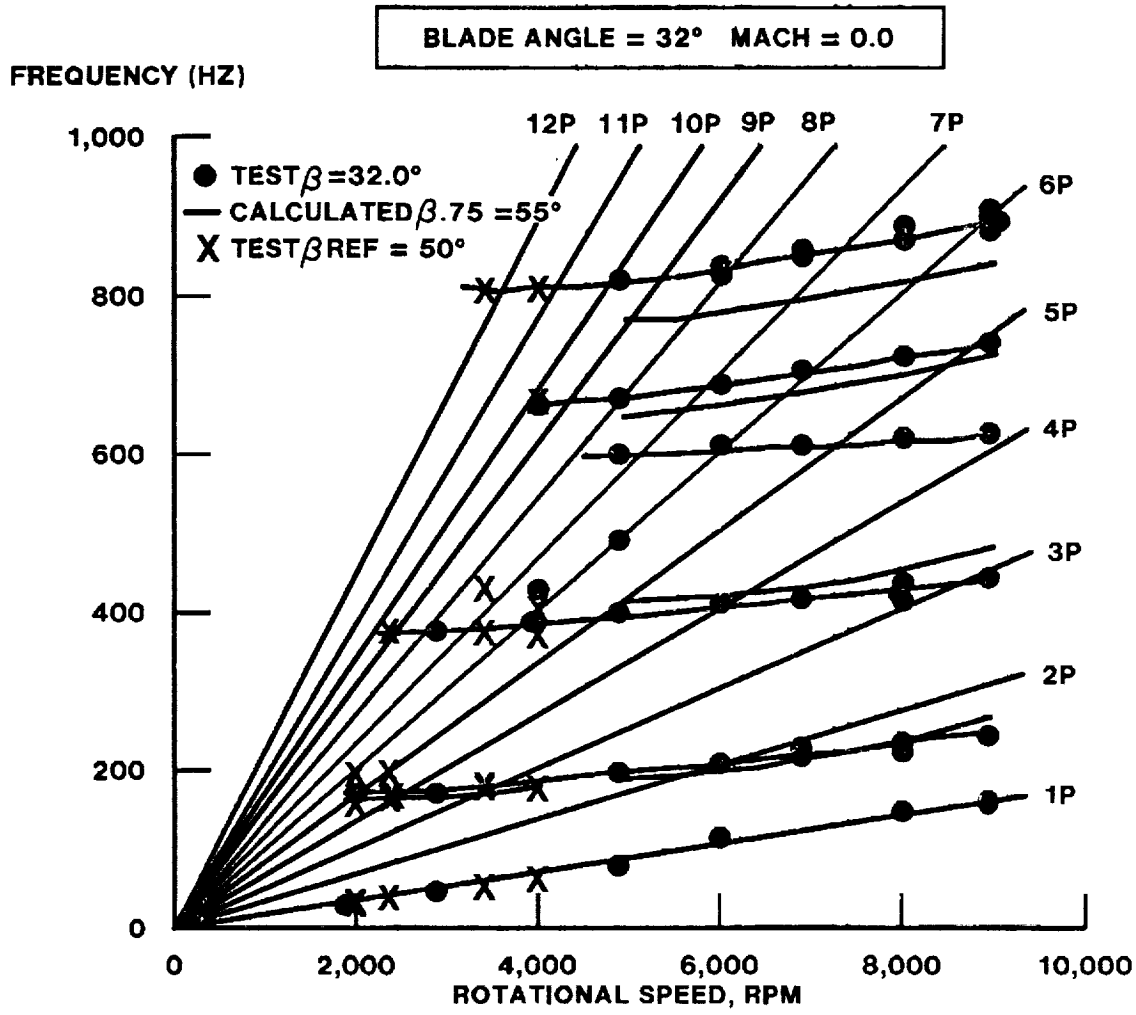

FIGURE 4-22. SR-3 MODEL PROP-FAN
MEASURED AND CALCULATED NATURAL FREQUENCIES

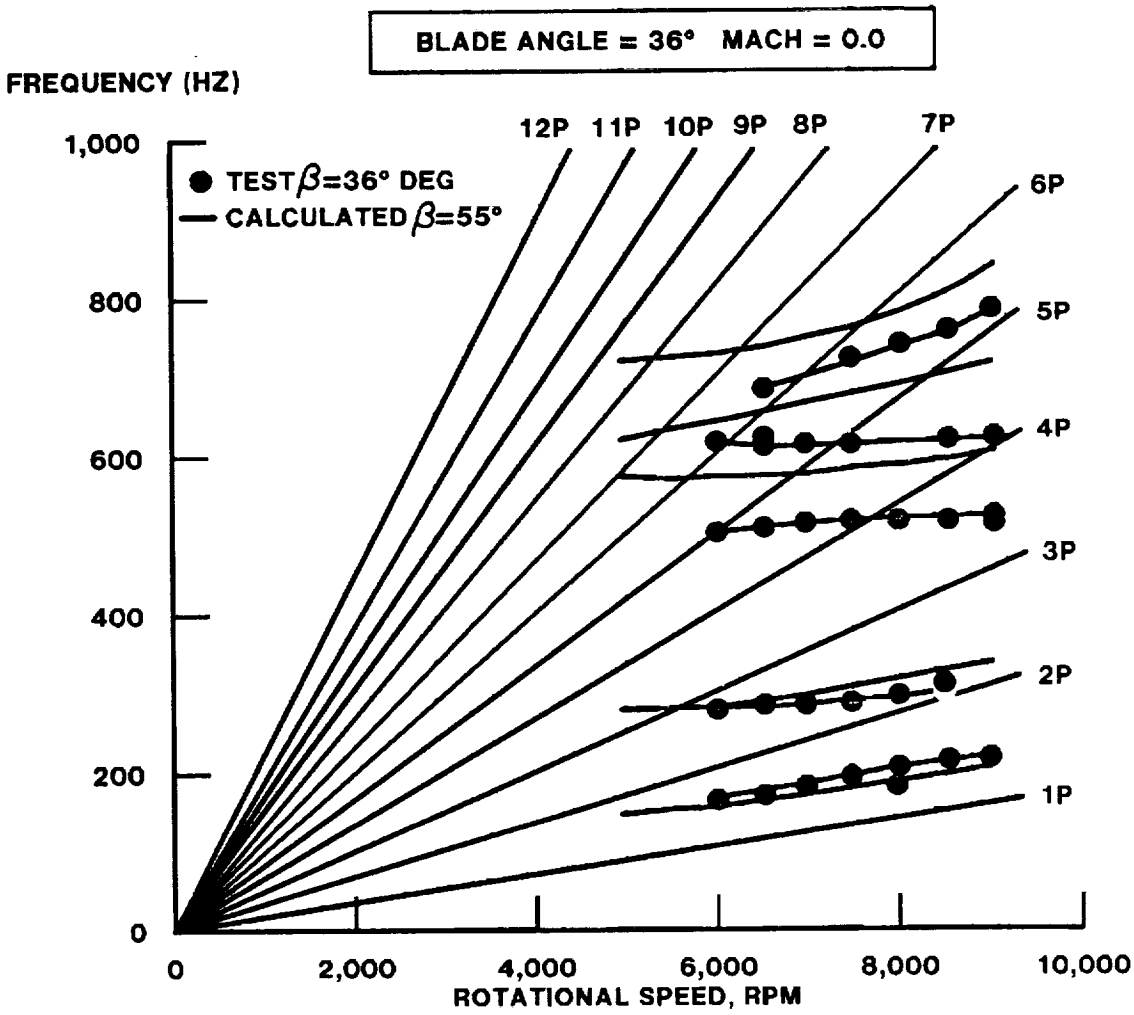

FIGURE 4-23. SR-5 MODEL PROP-FAN

MEASURED AND CALCULATED NATURAL FREQUENCIES

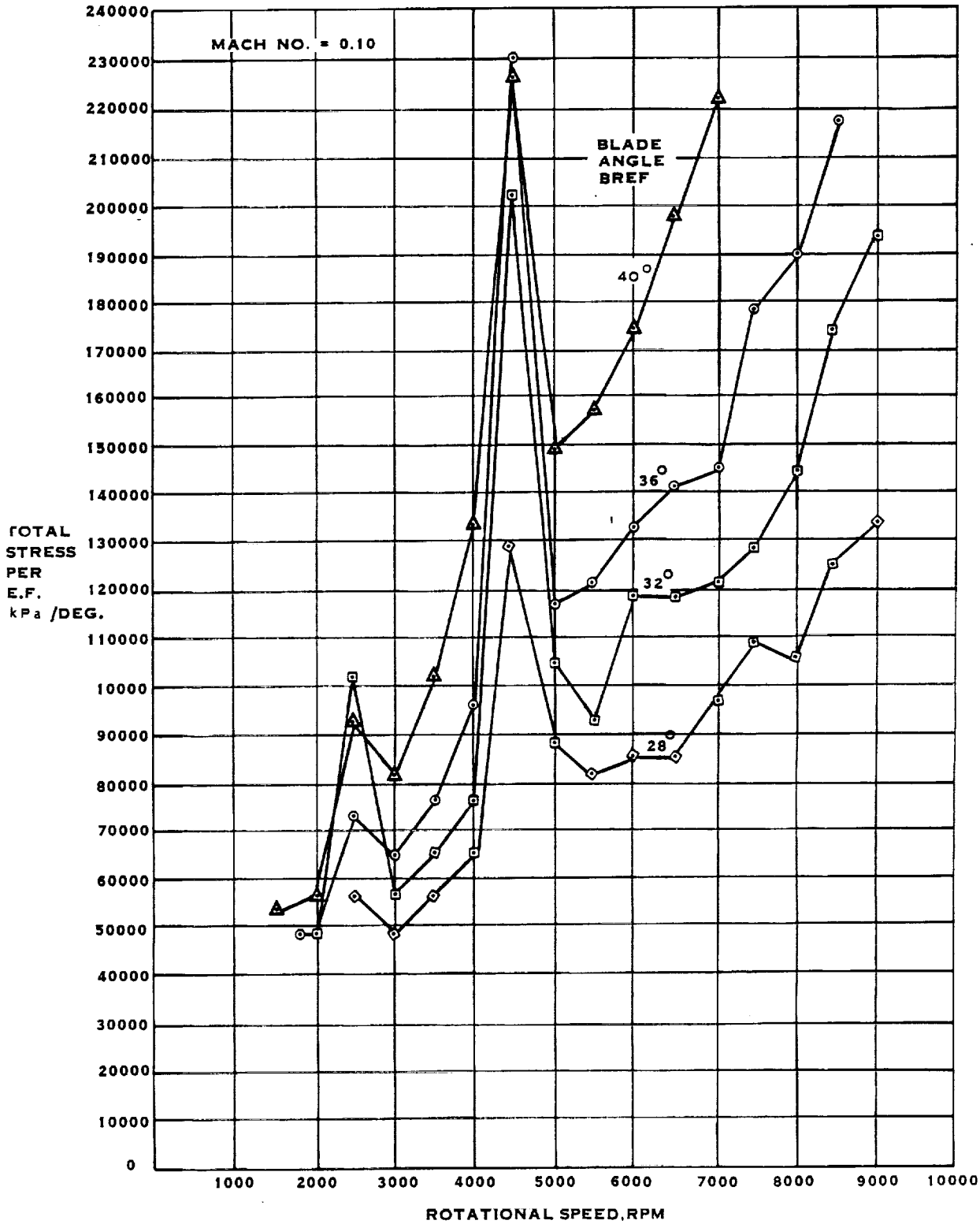

FIGURE 4-24. SR-2 MODEL BLADE 10 X 10 LOW SPEED WIND TUNNEL TESTS AT NASA LEWIS
BG1-1 TILT= 15 DEG.

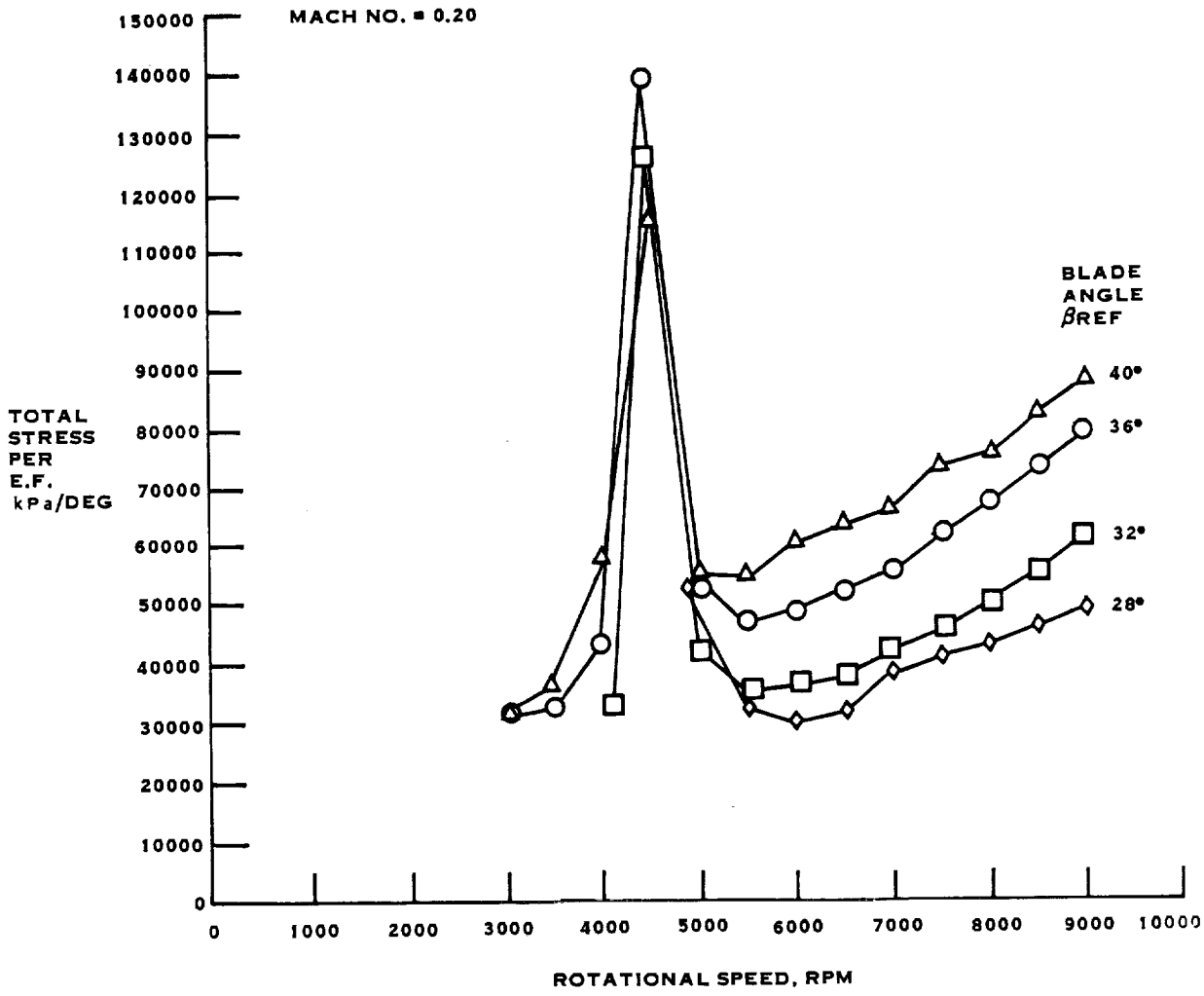

(FIGURE 4-24. CONTINUED) SR-2 MODEL BLADE

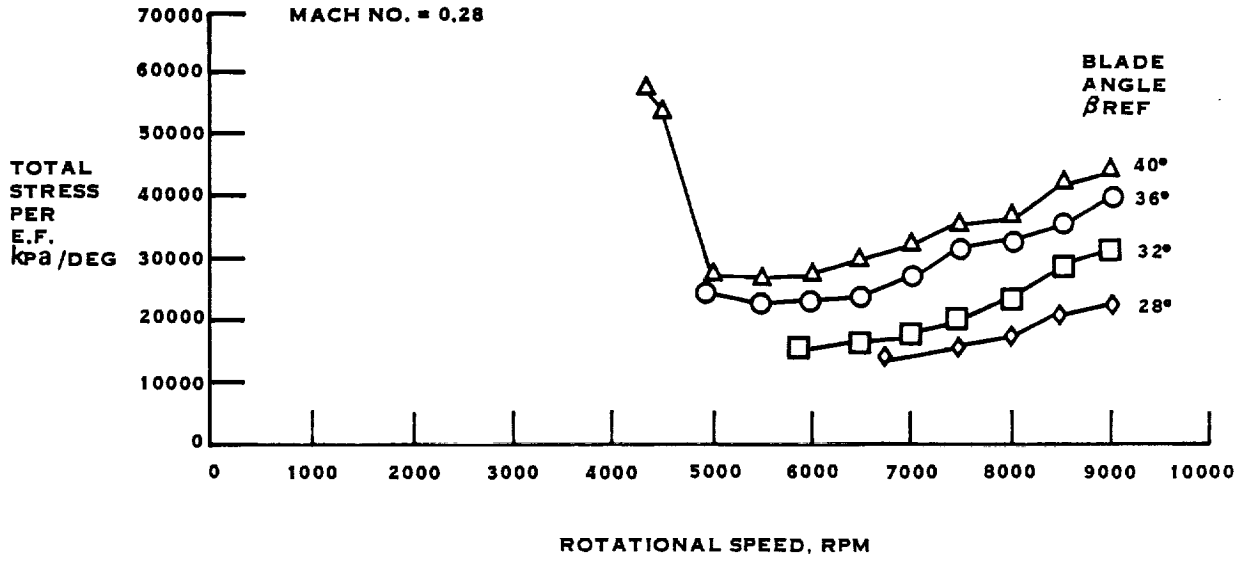

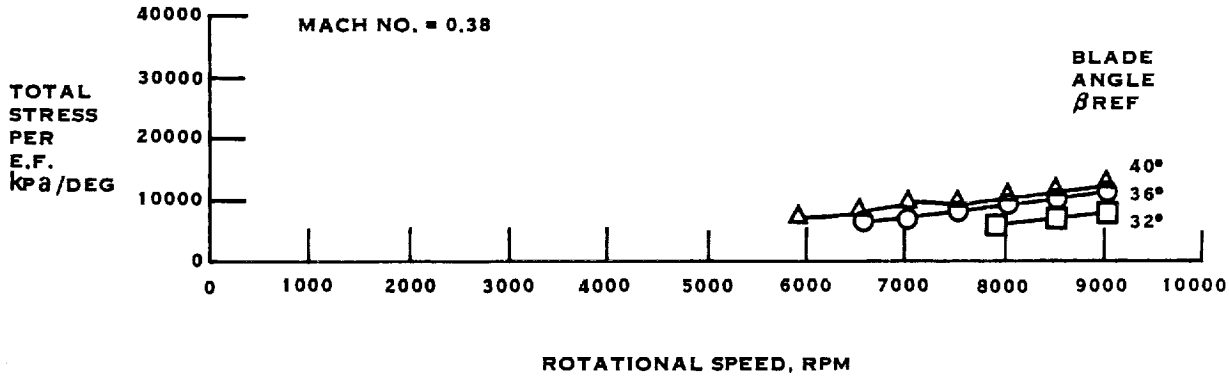

(FIGURE4-24.CONTINUED) SR-2 MODEL BLADE

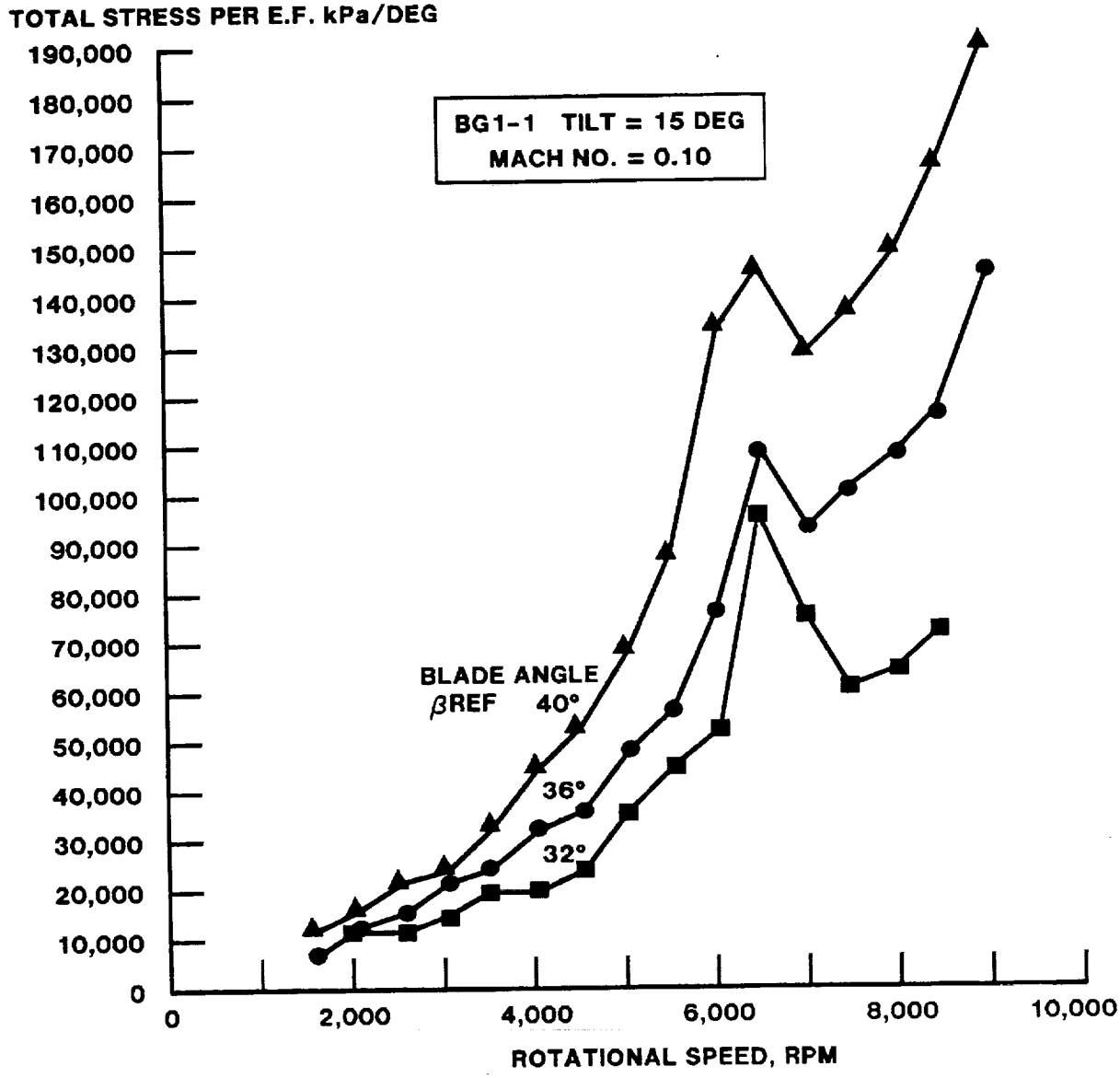

FIGURE 4-25. SR-3 MODEL BLADE 10 X 10 LOW SPEED WIND TUNNEL TESTS AT NASA LEWIS

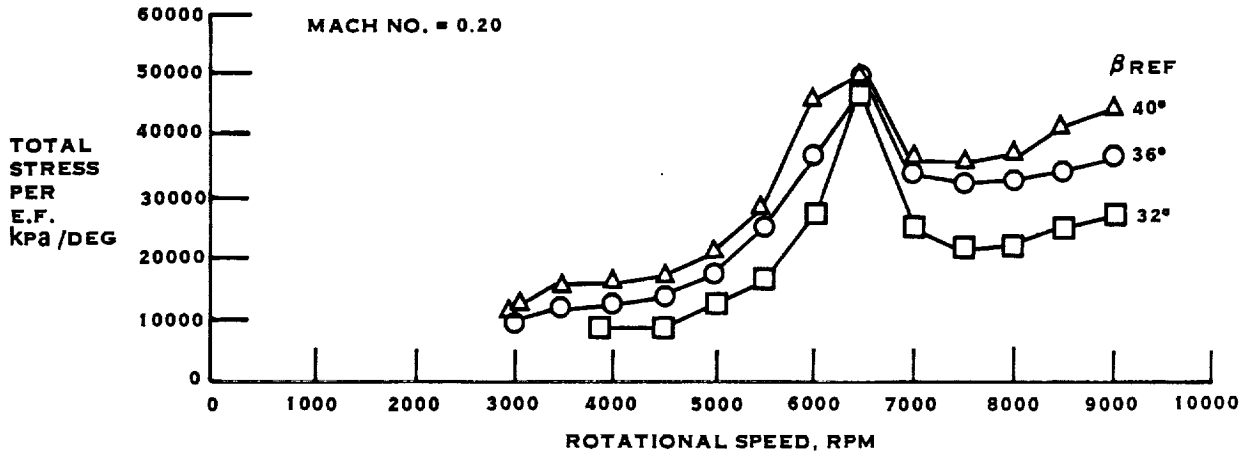

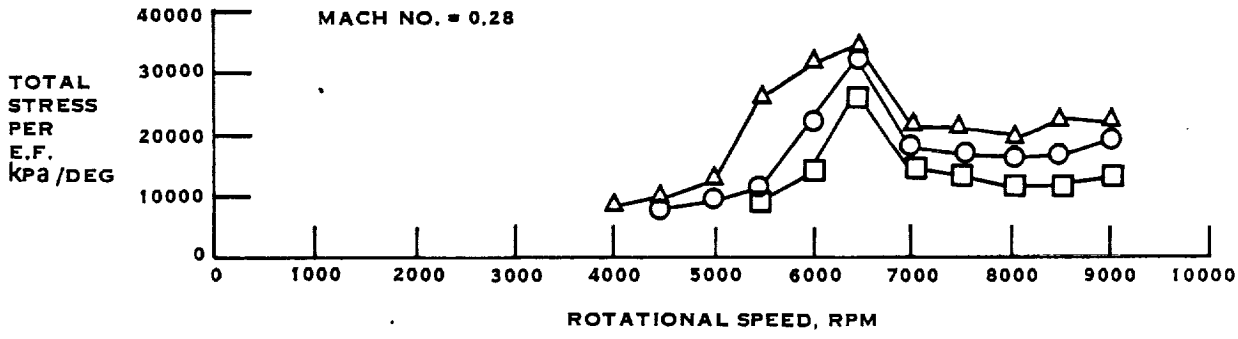

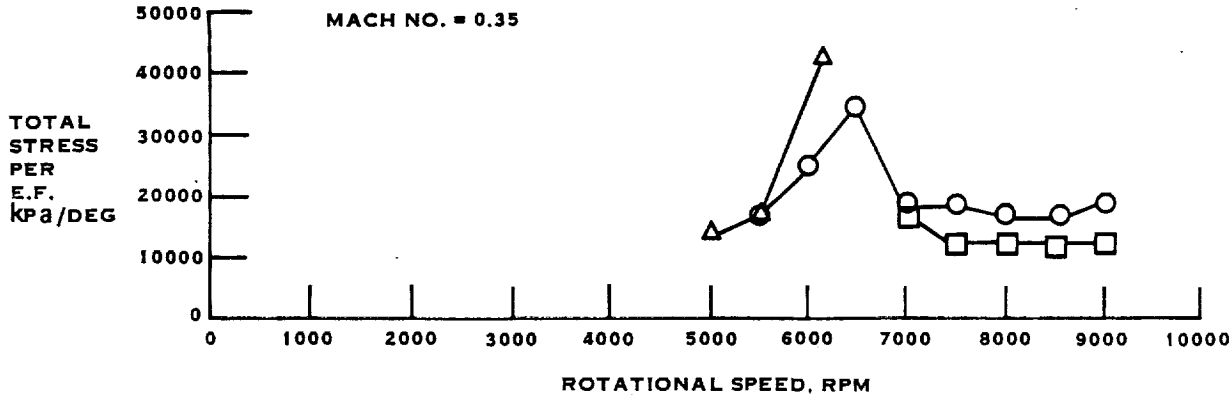

FIGURE 4-25. SR-3 (CONTINUED)

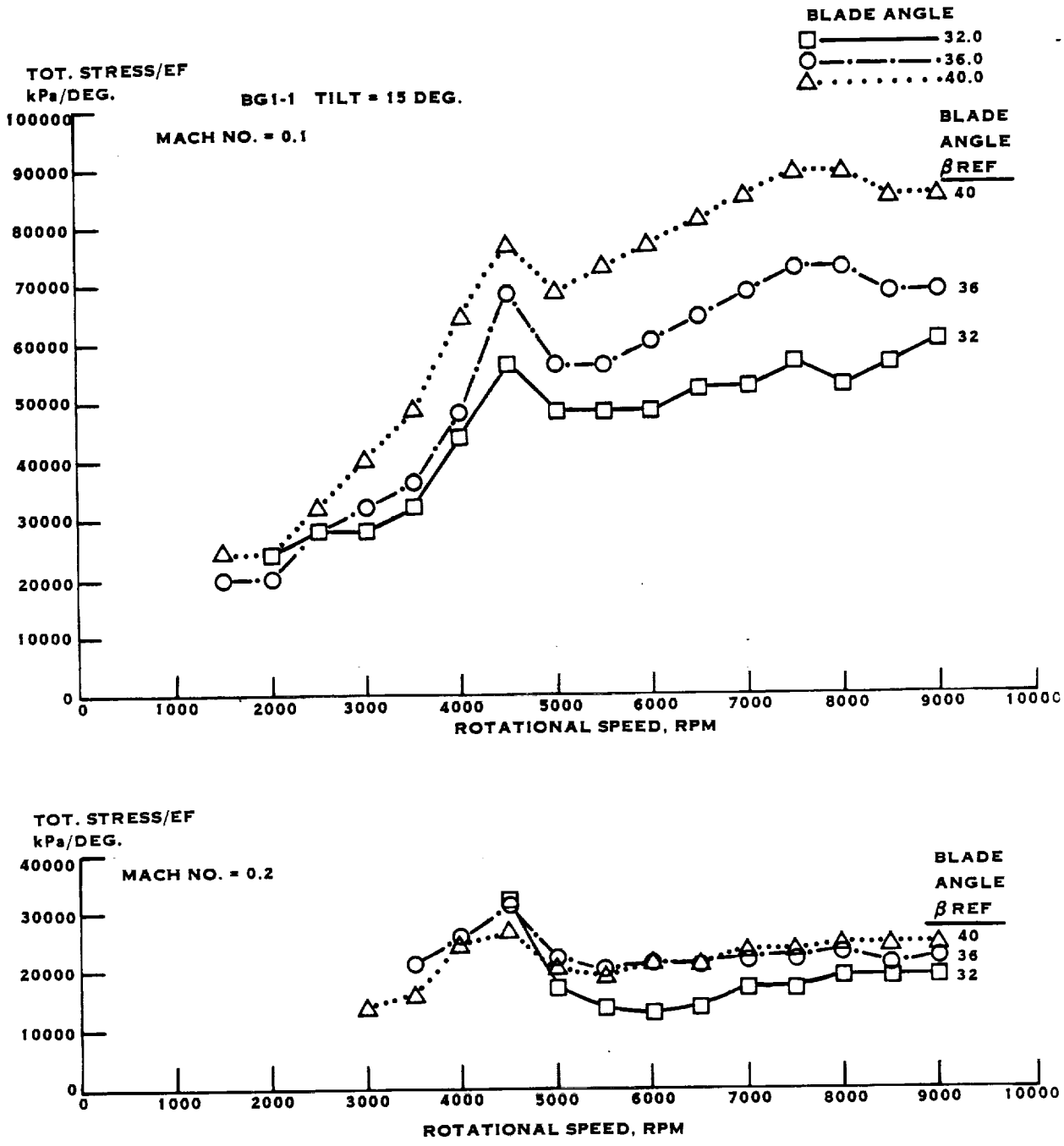

FIGURE 4-26. SR-5 MODEL BLADE 10 X 10 LOW SPEED WIND TUNNEL TESTS AT NASA LEWIS

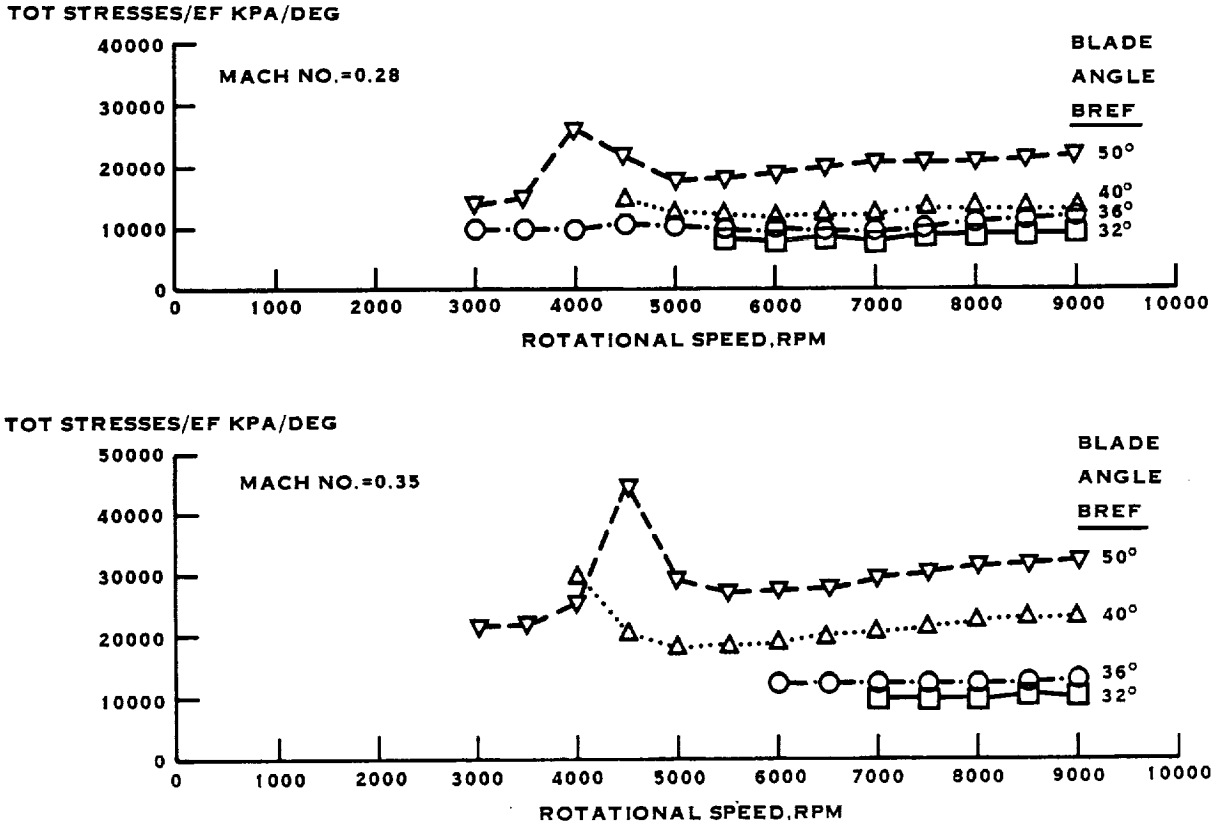

FIGURE 4-26. (CONTINUED)

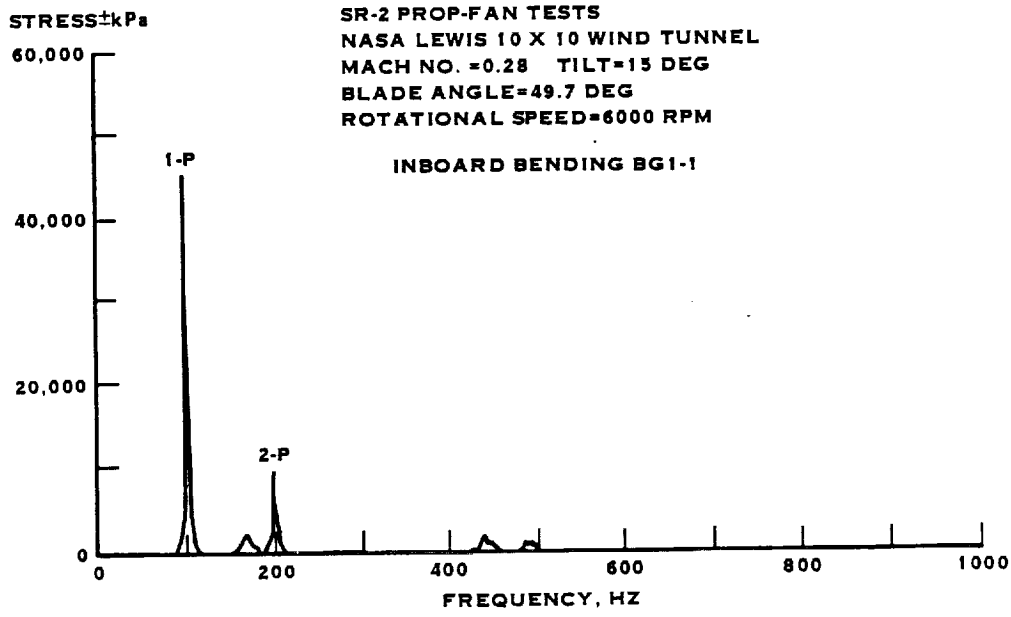

FIGURE 4-27. SR-2 SPECTRAL PLOT FOR A 15 DEGREE PROPELLER TILT

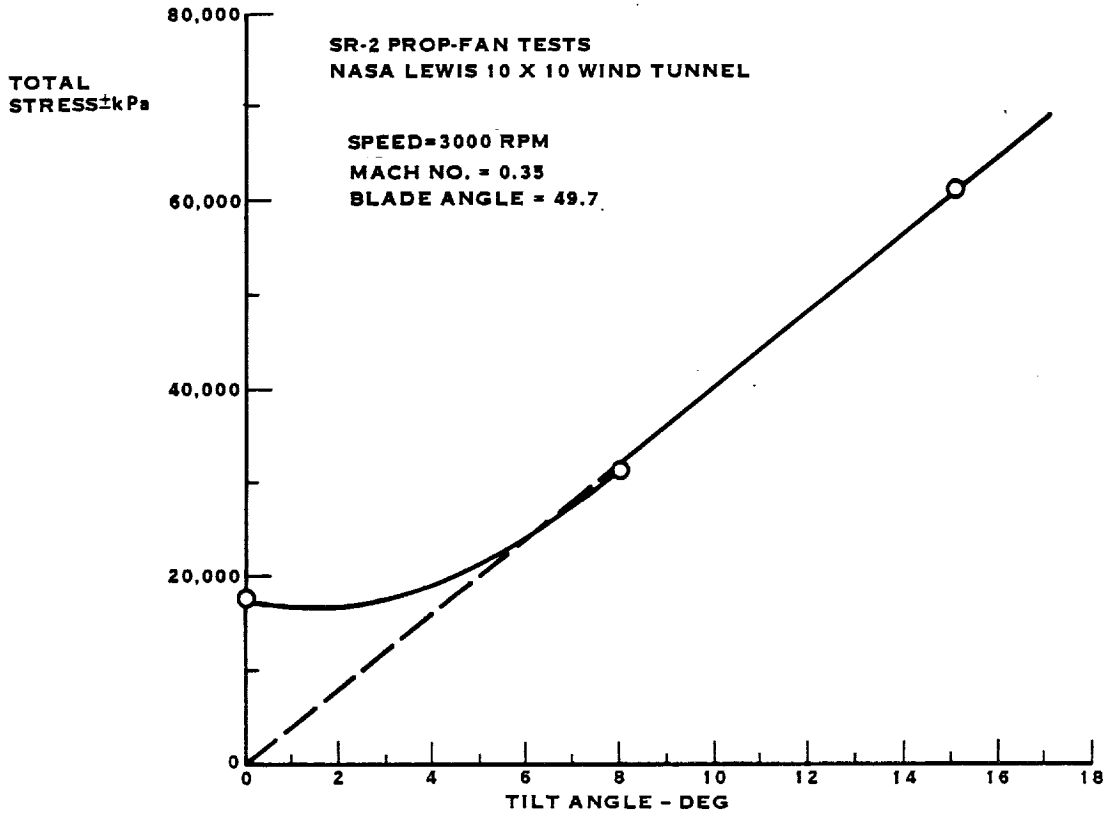

FIGURE 4-28. IN-BOARD BENDING VIBRATORY STRESS (BG1-1)

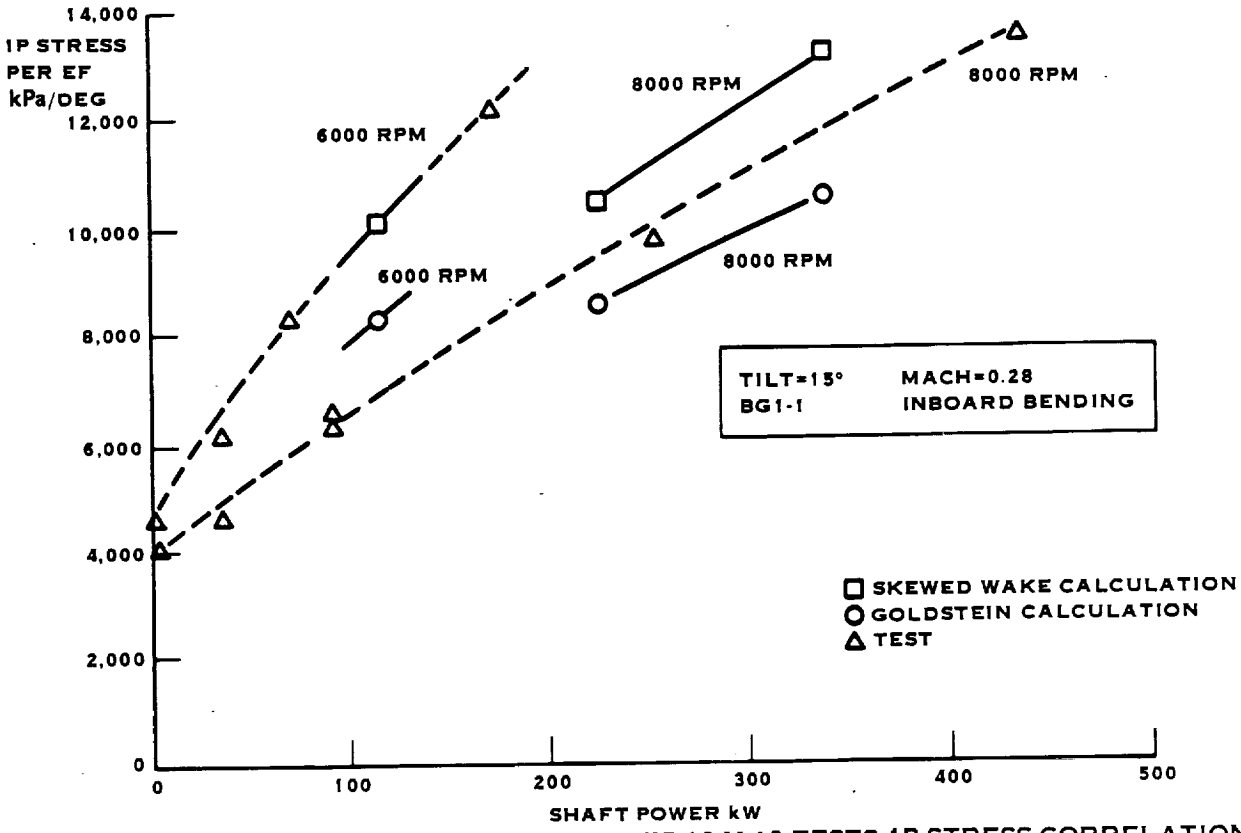

FIGURE 4-29. SR-2 PROP-FAN NASA LEWIS 10 X 10 TESTS 1P STRESS CORRELATION

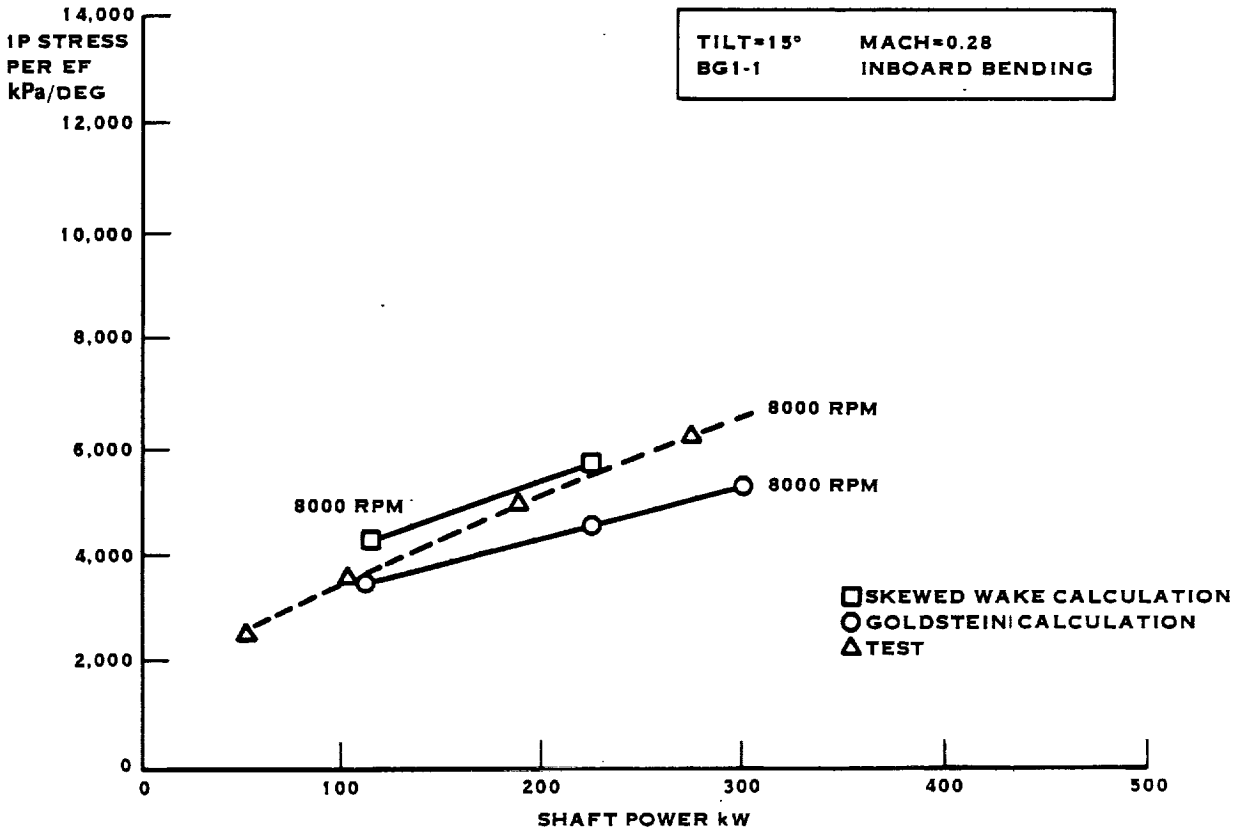

FIGURE 4-30. SR-3 PROP-FAN NASA LEWIS 10 X 10 TESTS 1P STRESS CORRELATION

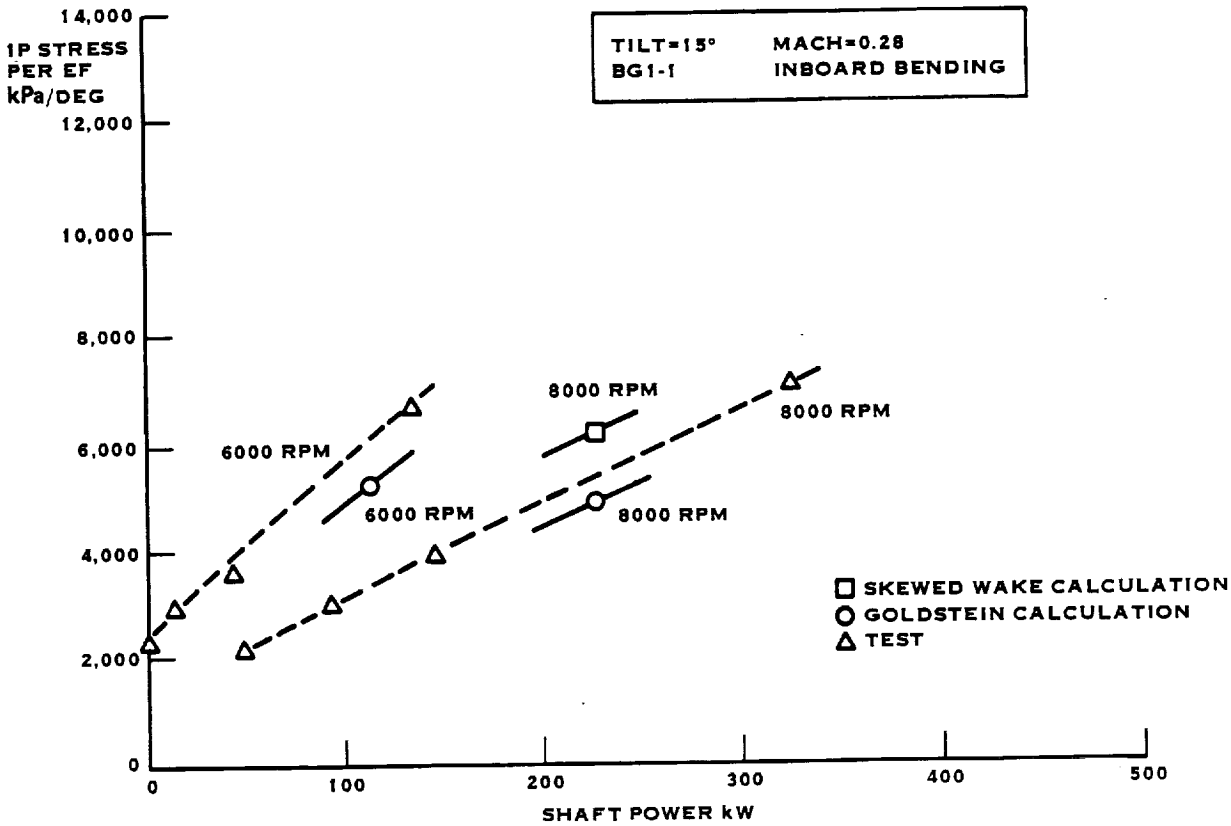

FIGURE 4-31. SR-5 PROP-FAN NASA LEWIS 10 X 10 TESTS 1P STRESS CORRELATION

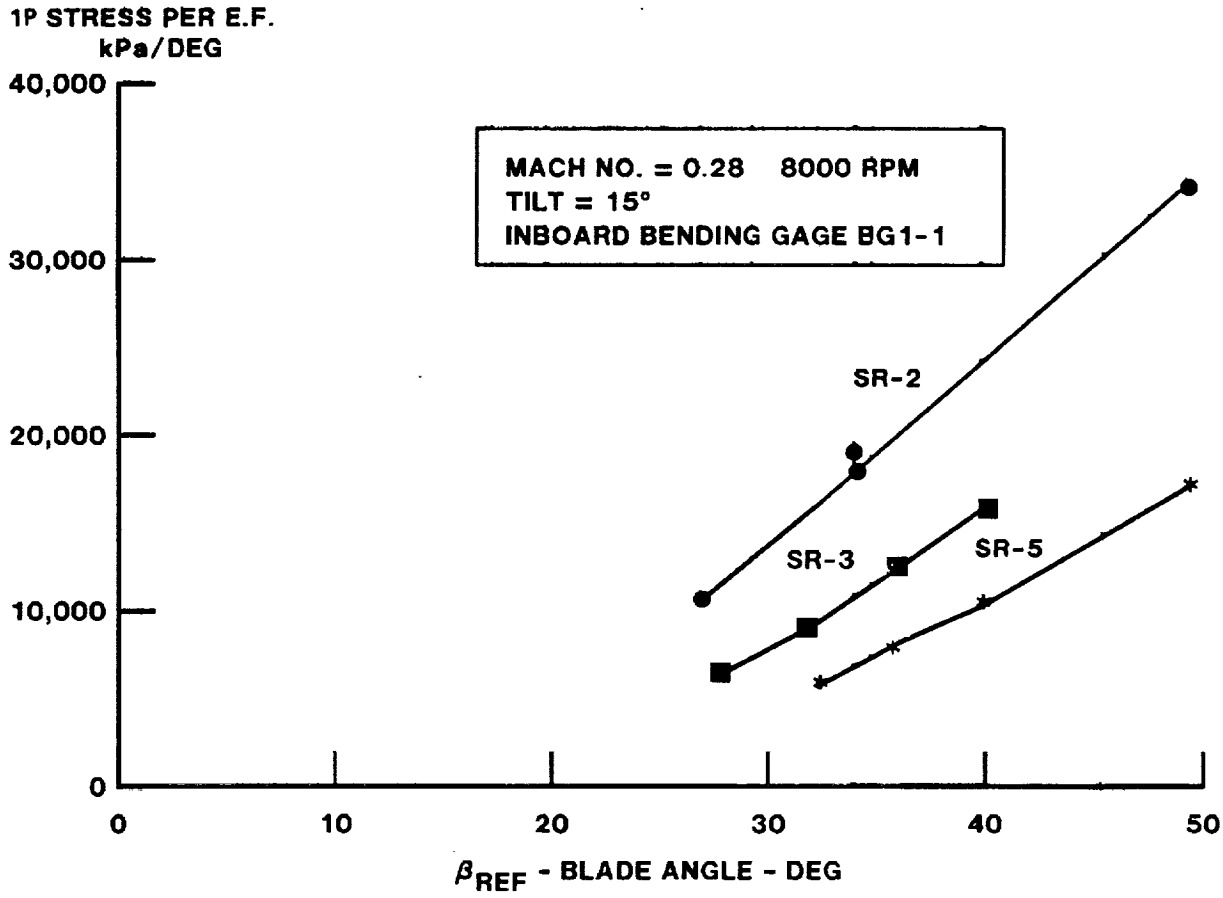

FIGURE 4-32. MODEL PROP-FAN TESTS AT NASA LEWIS IN THE 10 X 10 WIND TUNNEL

C-2

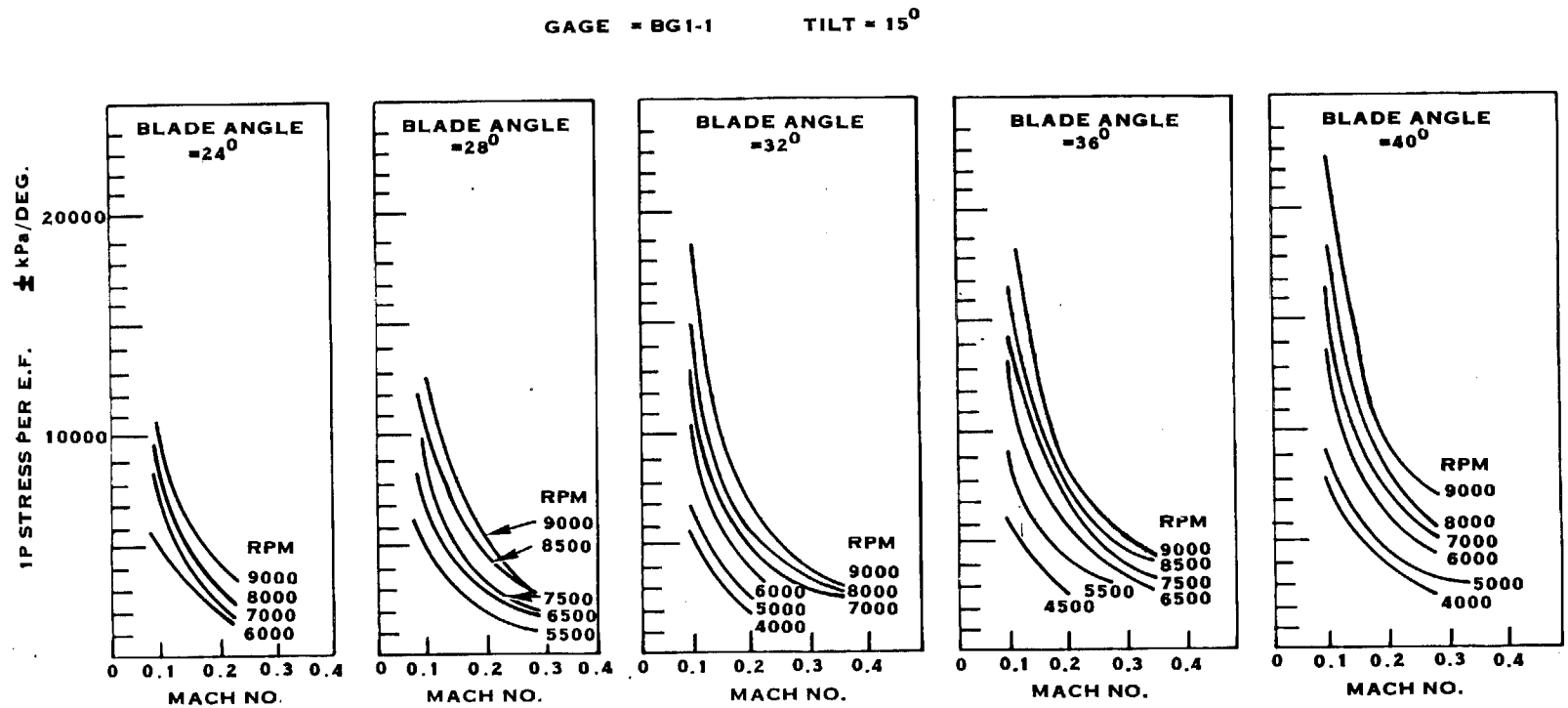

FIGURE 4-33. SR-3 PROP FAN LOW SPEED TEST
NASA/LEWIS 10 X 10 TUNNEL

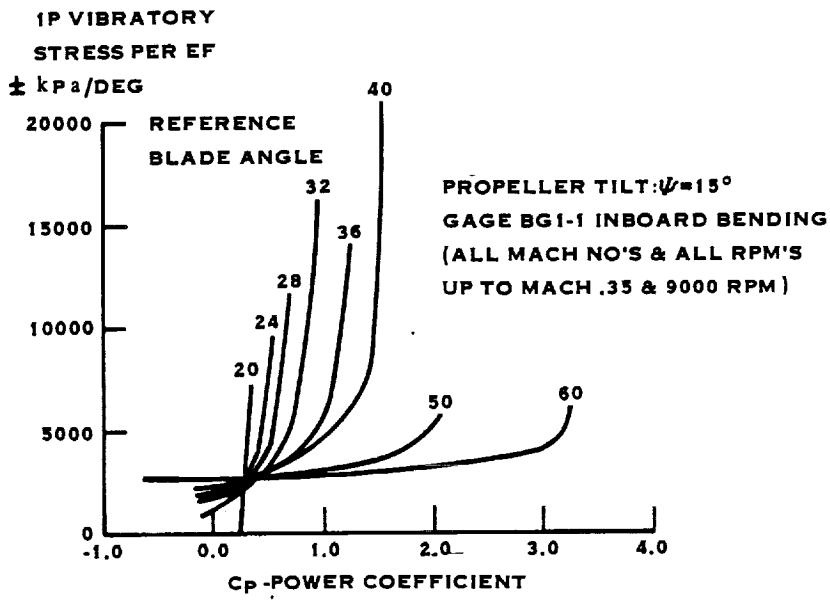

FIGURE 4-34. SR-3 PROP-FAN LOW SPEED TEST
NASA/LEWIS 10 X 10 TUNNEL

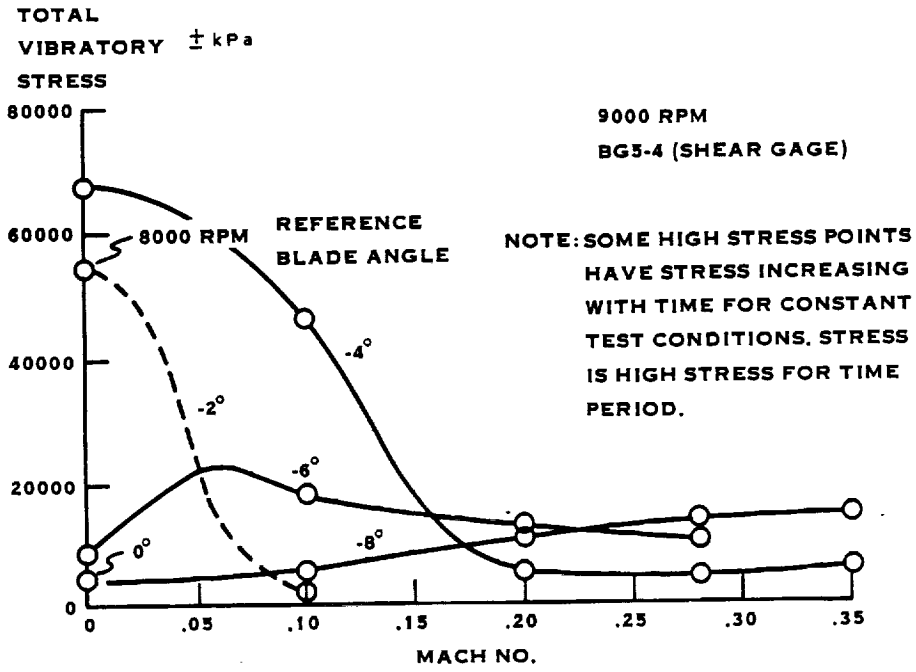

FIG 4-35. SR-3 MODEL BLADE 10 BY 10 LOW SPEED TESTS NASA-LEWIS

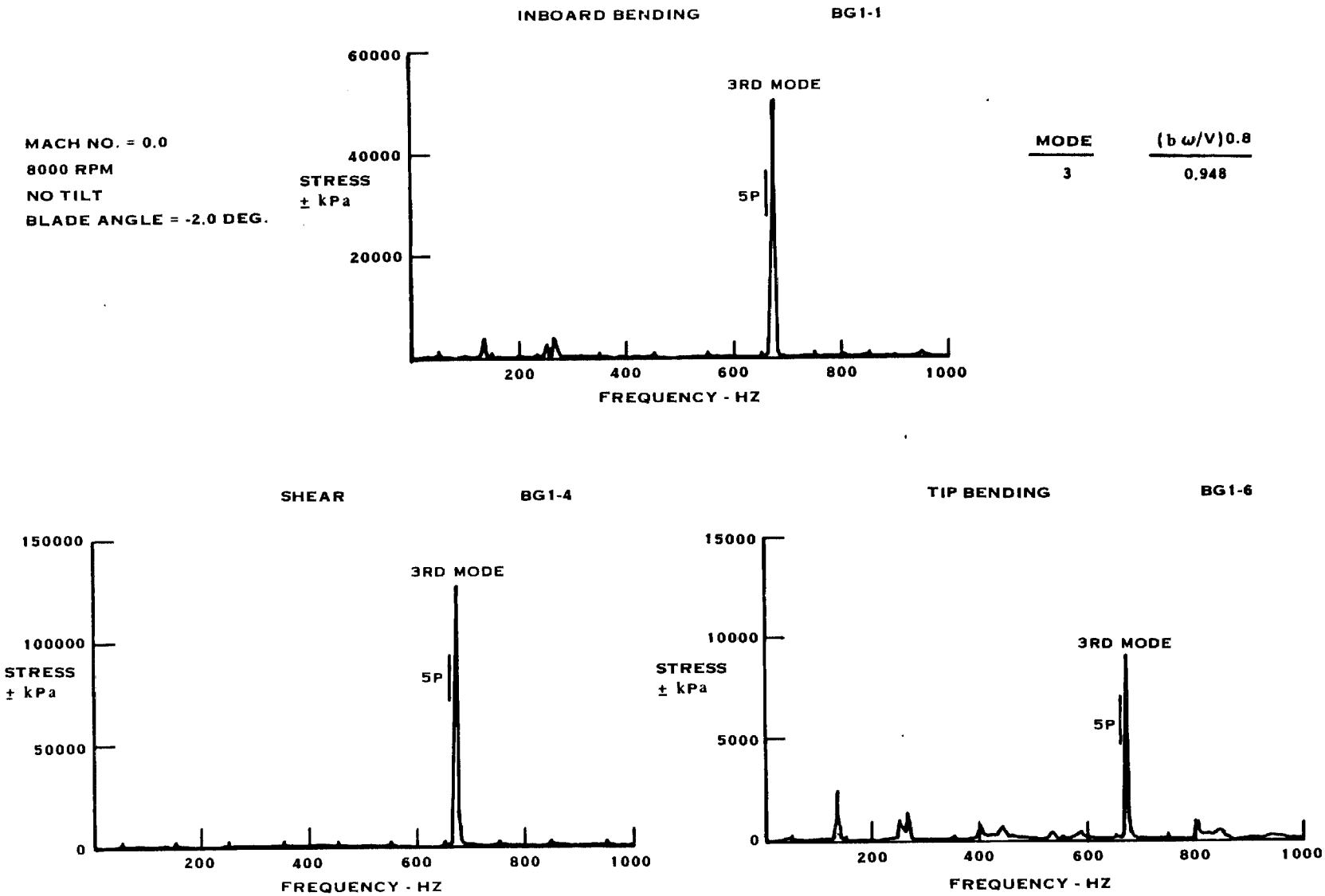

FIGURE 4-36. SR-3 PROP - FAN NASA-LEWIS 10X10 WIND TUNNEL TEST

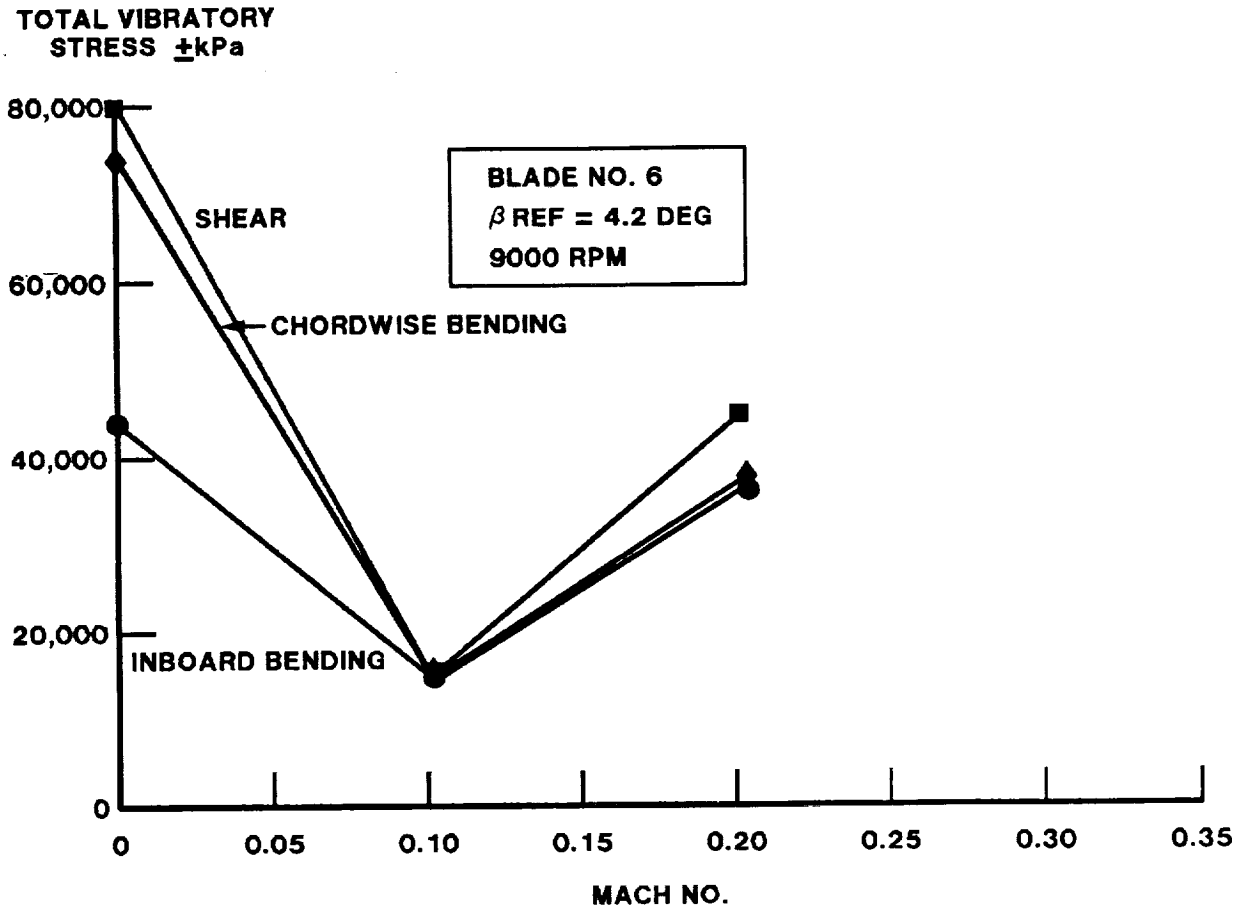

FIGURE 4-37. SR-5 MODEL PROP-FAN TESTS NASA LEWIS - 10 X 10 WIND TUNNEL

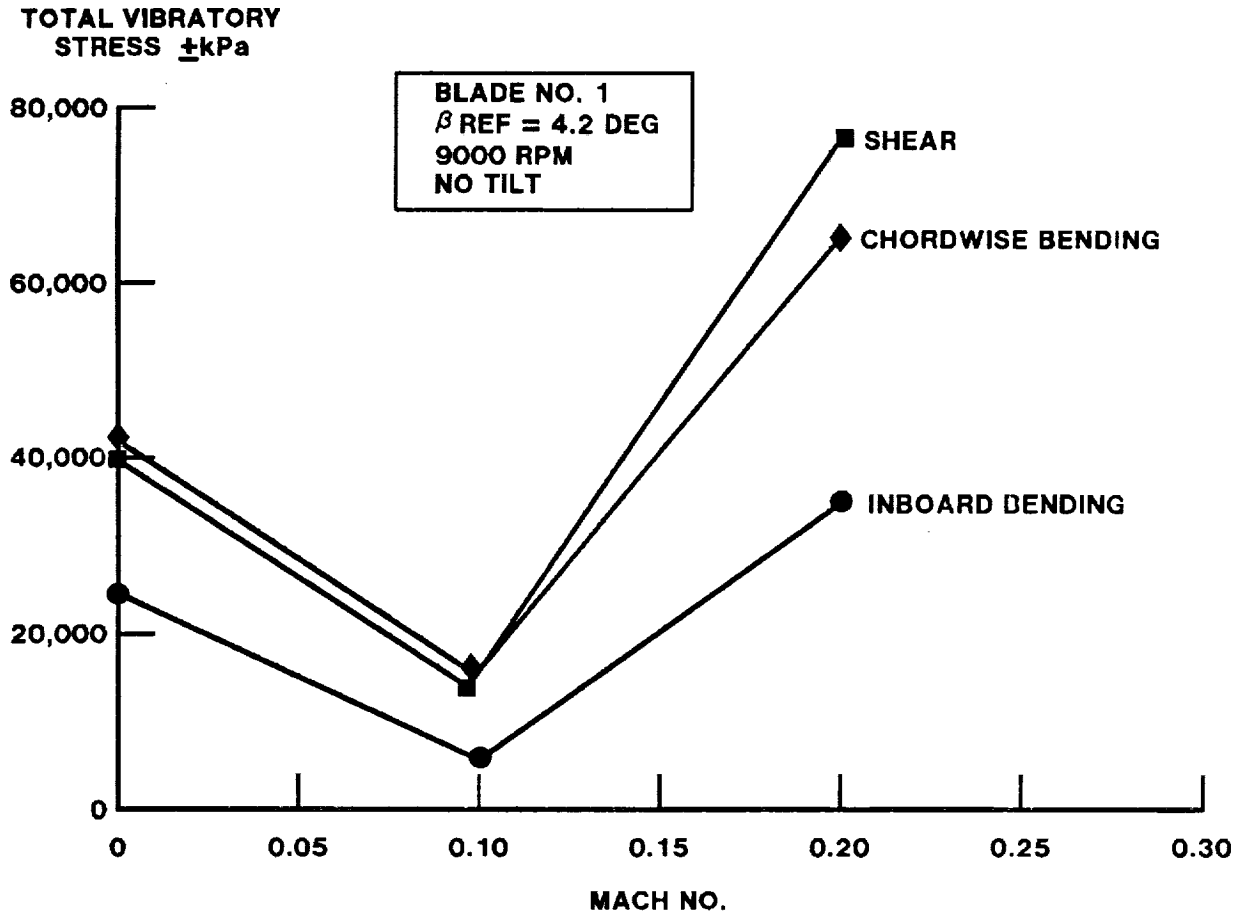

FIGURE 4-38. SR-5 MODEL PROP-FAN TESTS NASA LEWIS - 10 X 10 WIND TUNNEL

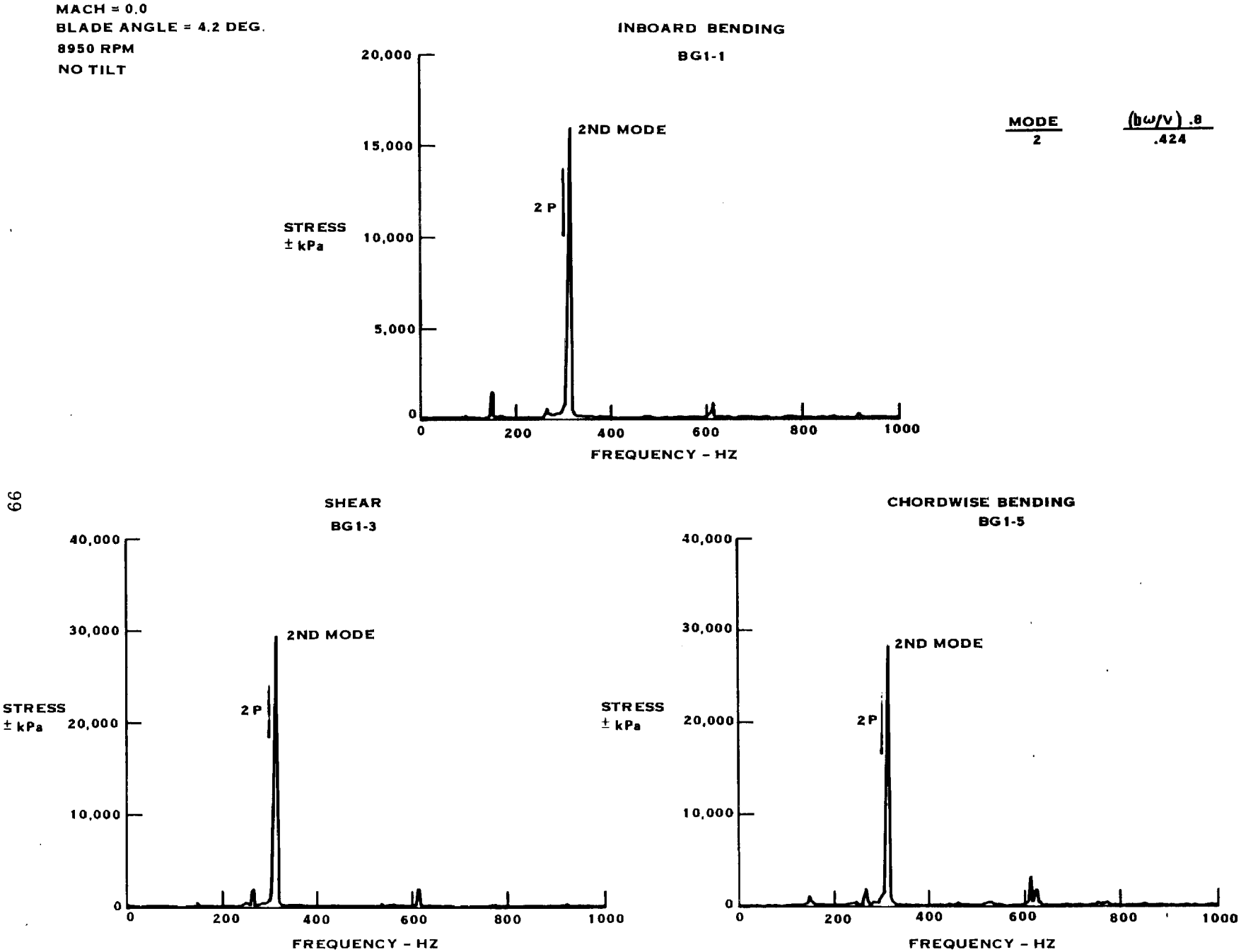

FIGURE 4-39. SR-5 PROP-FAN NASA-LEWIS 10 X 10 WIND TUNNEL TEST

MACH NO. = 0.2
BLADE ANGLE = 4.2 DEG.
8850 RPM
NO TILT

FIRST MODE MULTIPLE	(bω/V).8
1	.306
2	.615
3	.919

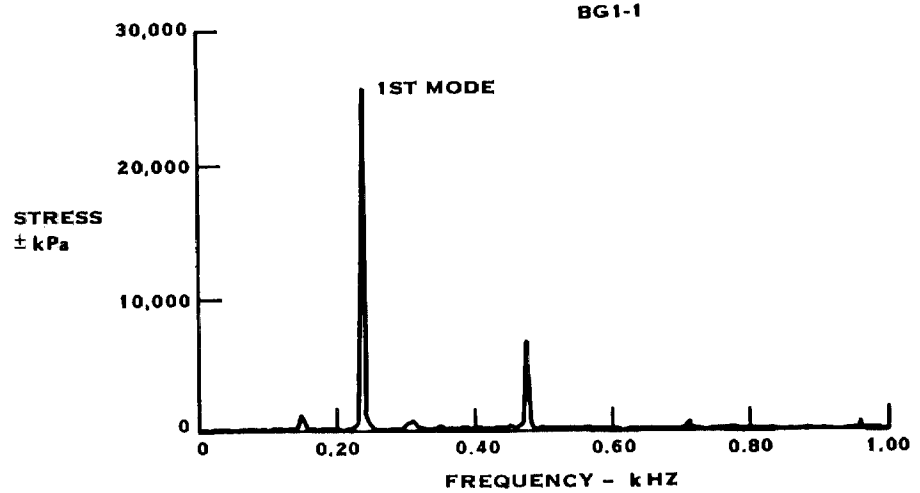

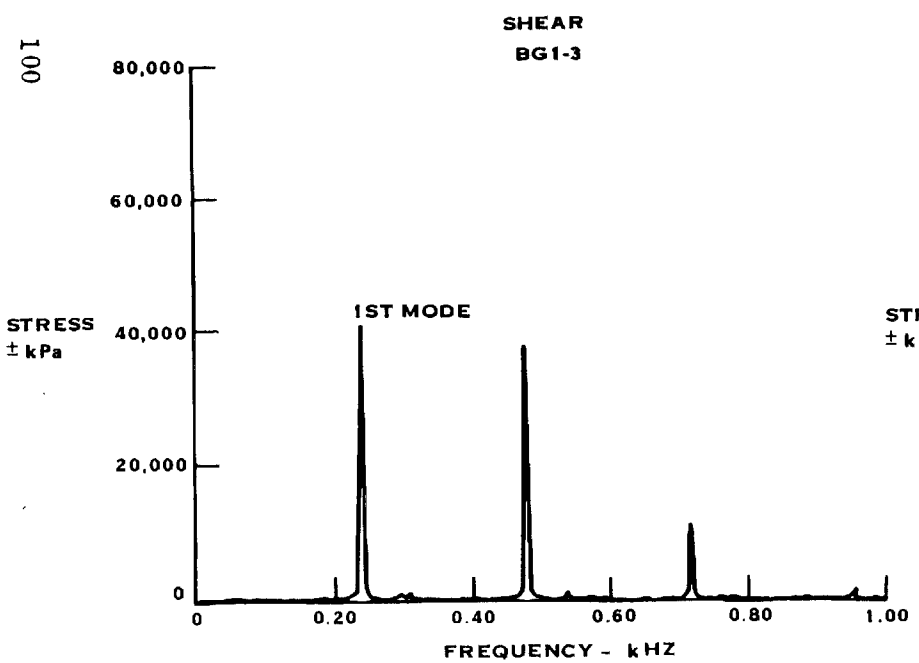

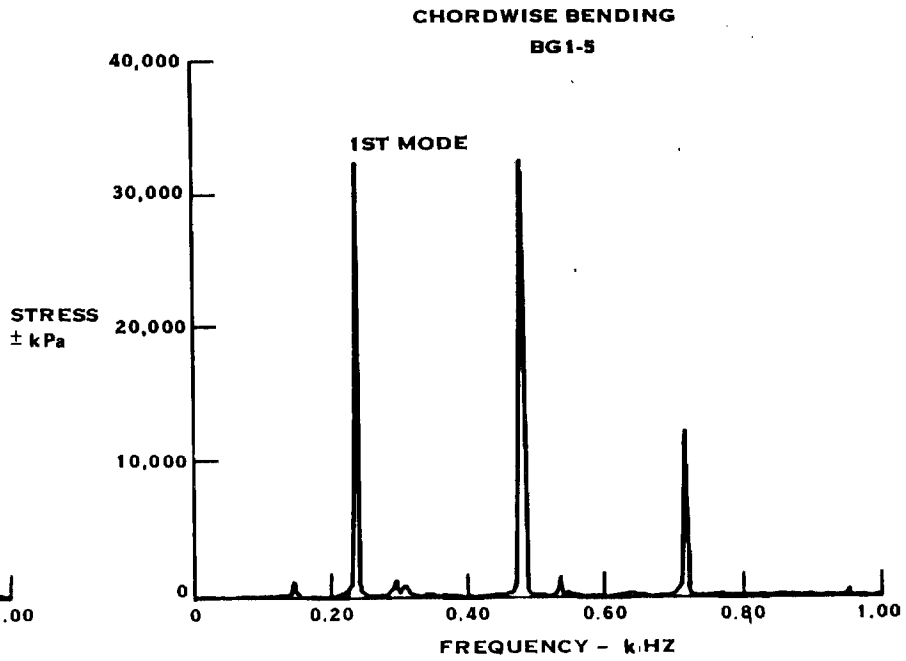

FIGURE 4-40. SR-5 PROP-FAN NASA-LEWIS WIND TUNNEL TEST

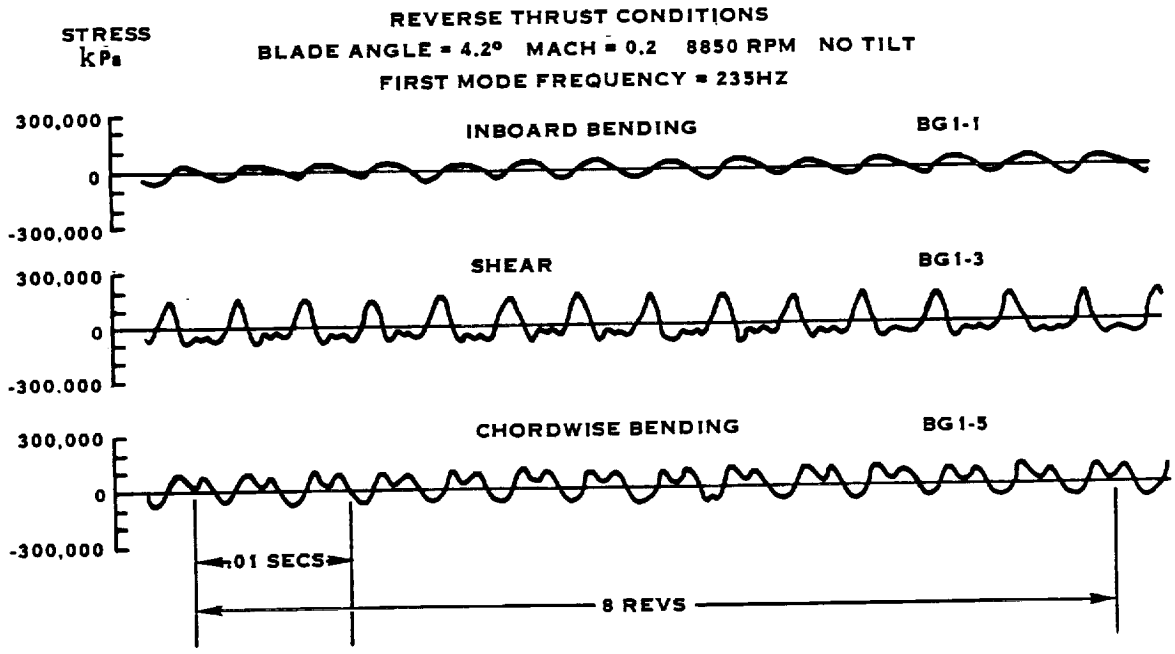

FIGURE 4-41. SR-5 PROP-FAN NASA-LEWIS WIND TUNNEL TESTS